Ocean Wave Remote Sensing System by GPS

Jian, Cui

(Degree)
博士（工学）
(Date of Degree)
2014-03-25
(Date of Publication)
2015-03-01
(Resource Type)
doctoral thesis
(Report Number)
甲第6131号
(URL)
https://hdl.handle.net/20.500.14094/D1006131

Doctoral Dissertation

Ocean Wave Remote Sensing System by GPS

（GPS 信号を用いた海洋波浪のリモートセンシングに関する研究）

January, 2014

Graduate School of Marine Sciences
Kobe University

Jian Cui
(崔　健)

SUMMARY

This dissertation presents an ocean wave remote sensing system by GPS that estimates the characteristics of ocean waves efficiently by receiving and processing the global navigation satellite system signals. This dissertation consists of five chapters in order to introduce the related theories, methods and practices.

Chapter 1 introduces the background of the ocean wave measurement and the remote sensing by the Global Positioning System (GPS). The purpose of this research is to measure ocean waves propagating from the open sea to local sea area, especially into harbor water area, since this can cause serous damages to the harbors and the vessels mooring or navigating in them. Recently developed GNSS-R techniques provide an efficient method to measure sea state by utilizing the Reflected Signals From Sea-surface (RSFS). The relative time delays of RSFS to Line-Of-Sight (LOS) signal connote much topographical information concerning the sea-surface. In order to retrieve detailed characteristics of ocean waves and provide real-time feedback to harbors and vessels for safety, the concept of ocean wave GPS remote sensing is defined.

Before the measuring of the characteristics of ocean waves, some knowledge of ocean wave is introduced. Ocean waves fluctuating with a period from 10s to 30s are targeted by the ocean wave remote sensing system. Moreover because the global navigation satellite system signals are utilized as signal sources for the ocean wave remote sensing system, its correlation property is also described. The knowledge of GPS multipath propagation and identification is introduced in chapter 2. The most important components of the GPS receiver, antenna and radio frequency (RF) front-end are also introduced. The cross-correlation and autocorrelation properties of C/A code are emphasized, from which satellite information can be acquired and the relative time delay of RSFS can be estimated. Specifically, the correlator and the Discrete Teager-Kaiser Energy Operator (TKEO) are combined to identify multipath efficiently. The wave characteristic estimator is designed and developed to estimate wave period, speed and length quantitatively. The wave characteristic estimator resolves the wave characteristics into several stages, such as the calculation of correlator and TKEO, and Fourier Transform (FT). The measurement methods of true wave characteristics are also explained.

The chapter 3 introduces in detail the system configuration. The array antenna is designed with a narrow fan beam directional pattern with which it only receives reflected signals from the objective sea-surface and suppresses signals from the side directions. Also the array antenna is constructed and its testing results are given with a narrow fan beam directional pattern. By evaluating the band-limited effects of RF front-end and the band-limited effects of TKEO, the bandwidth (BW) in the RF front-end must be determined to be 40 MHz in order to pass more reflected signal energy for the correlator and TKEO. The RF front-end based on the chip of GP2015 is used for the experimental evaluations.

The operation performance of the ocean wave remote sensing system was first of all evaluated with numerical simulation, as will be explained in chapter 4. According to a sea swell spectrum, a sea surface dominated by sea swell was generated. The amount of reflected signals arriving at an array antenna from a generated sea surface was determined by a scattering pattern. The relative time delays of RSFS are estimated successfully from output of Teager-Kaiser energy operator. It was validated that wavelength and wave period could be measured by the ocean wave remote sensing system efficiently. After that the system performance was also evaluated with a series of experiments after the construction of the whole system. The final prototype of the ocean wave remote sensing system was obtained after a series of basic testing and experiments. Finally, the GPS signals reflected from objective sea surface were detected and extracted successfully. The array antenna can receive reflected signals from specified directions and suppress reflected signals from side directions. The RSFS can be identified because of the application of 40MHz wideband RF front-end. The wave characteristic estimator yielded the wave period, wave speed and wavelength correctly.

Finally, some conclusions were draw according to the experimental evaluation of the prototype system. Moreover some considerations and proposals are also given to improve the performance of the system in the future.

With the propagation of long period gravity waves, it becomes difficult to keep and improve the harbor calmness and safety. At present, a lot of wave measurement systems have been applied but it is a hard and complicated task to measure the characteristics of long period gravity waves which might have the wave period from some ten seconds to some ten minutes and wave height less than 1 meter. The proposed ocean wave remote sensing system provides the possibility to measure the characteristics of long period gravity wave. Especially, the analysis of the characteristics of the disastrous waves only needs to observe in the time of several times the wave periods, and the ocean wave remote sensing system can work in the conditions of bad weather and low visibility. It is important to avoid the occurrence of disaster in time to protect people’s life and property.

ACKNOWLEDGEMENT

In 2007 I was admitted as a Japanese Government Scholarship student and started to study in the Graduate School of Marine Sciences of Kobe University. First of all, I would like to express my deepest gratitude to the Ministry of Education, Culture, Sports, Science and Technology (MEXT) of Japanese Government for the opportunity to pursue the advanced study and research in maritime sciences and for the financial supports during my student life.

I profoundly appreciate my supervisor, Professor Nobuyoshi Kouguchi for providing me with insight, supervision, and valuable support in every stage of this research. During the period of the research, I have received tremendous impact from his professional guidance. In particular, he can always enlighten me with new ideas. I also obliged to Mr. Akihiro Ikawa for his direction and assistance in every experiment.

I would like to thanks the help of Professors Yasuo Arai and Shigeyuki Okuda of Marine Technical College for providing with a lot of valuable advices concering this research. Thanks go to Professor Nishio Shigeru and Professor Saito Katsuhiko of Faculty of Maritime Sciences of Kobe University for their examinations and advice on the dissertation. I also wish thank the help of Mr. Y. Kobayashi, President of the Furuno Labotech International CO., LTD, and Professor Y. Arai of the Marine Technical College for the measurement of the directional pattern with the array antenna.

Special thanks goes to all members of our research laboratory for providing helpful supports with the experiments of this research.

Finally, my grateful thanks goes to my family. I thank them for their love, blessing, and encouragement during my student years.

CONTENTS

ACRONYMS

ADC	Analog-to-digital Converter
ADCPs	Doppler Current Profilers
BPSK	Binary Phase Shift Keying
BW	Bandwith
C/N0	Carrier to Noise Density Ratio
CDMA	Code Division Multiple Access
DSDD	Double Systems Double Directions
FT	Fourier Transform
FFT	Fast Fourier Transform
GNSS-R	GNSS-Reflectometry
GPS	Global Positioning System
HDD	Hard Disk Diver
IF	Intermediate Frequency
LHCP	Left-Hand Circular Polarized
LOS	Line-Of-Sight
RF	Radio Frequency
RHCP	Right-Hand Circular Polarized
RSFS	Reflected Signals From Sea-surface
SAR	Synthetic Aperture Radar
SSDD	Single System Double Directions
TKEO	Teager-Kaiser Energy Operator

TKEOt	TKEO time signals
UHF	Ultra High Frequency
ULA	Uniform Linear Array
VCO	Voltage Controlled Oscillator

NOTATIONS

α_{el}	Elevation of GPS antenna
β_{ref}	Reflection angle of RSFS
σ_l	Spectrum width
λ_S	Wave length
$\Delta\varphi$	Phase difference
d_{delay}	Delayed distance of MP channel
d_{LOS}	lengths of line-of-sight channel
d_{MP}	Lengths of multipath channel
f_0	Remarkable frequency
f_c	Center frequency
f_s	Sampling frequency / sampling rate
H_{ant}	Height of array antenna
H_s	Significant wave height
k	Wave number
k_{peak}	Number of spectral peak
P_{sv}	Position of GPS satellite
P_{ref}	Position of reflection point
P_{los}	Equivalent arriving position of LOS channel
P_{ant}	Position of array antenna / position of system
P'_{ant}	Projection of array antenna on sea-level

P_{spec}	Specular reflection point
t_{delay}	Relative time delay of reflected signal
T_s	Wave period
V_s	Wave speed

LIST OF FIGURES AND TABLES

CHAPTER 1

INTRODUCTION

1.1 Background

Ocean waves propagate in many forms. Surface waves fluctuating with a long period and containing tremendous energy threaten the safety of harbors and vessels navigating or mooring in them. Harbors are buried gradually by drifting sea-bottom sand driven by long water particle exercise orbit around harbor entrance neighborhood, and vessels also experience serious pitching and rolling movements once wave energy enters a harbor. The measurements of long period waves inside and outside of harbors have become an important research field of marine engineering.

At present, a lot of wave measurement instruments have been invented and developed to measure the ocean wave characteristics, such as high frequency radar, wave rider buoy and acoustic Doppler current profilers (ADCPs). Shore-based high frequency radar receives backscattered signals to retrieve sea surface waves for coastal monitoring, and high frequency radar system is usually built as a large-scale system operating on a wide coastal area over hundreds of square kilometers [1, 2, 3]. Wave rider buoys have been extensively applied in ocean observation to collect wave characteristics (e.g. National Data Buoy Center of U.S.A. and Nationwide Ocean Wave Information Network for Ports and Harbors of Japan) [4, 5, 6]. Doppler current profilers are deployed beneath the sea-surface to measure waves and the currents [7, 8]. Buoy system and ADCPs, however, suffer damage from floating debris or large waves, and maintenance always takes a lot of troubles.

With the developments of GPS technologies, GPS signals have already been considered to measure characteristics of ocean waves. It is known that GPS signal is usually used in positioning and navigation. However the LOS signal is always disturbed by multipath so that positioning accuracy decreases. There is much related research about how to immigrate multipath effects [9, 10]. On the contrary, the signals reflected from the Earth can be utilized for remote sensing. GNSS-Reflectometry is a kind of remote sensing technique that takes advantage of GPS signals reflection from the sea surface to retrieve wave height, wind speed and so on [11, 12, 13]. However, it is not easy to measure detailed characteristics for wave in a local area, such as wave length, wave period and wave direction.

Multipath features relative time delays to LOS signal. The relative time delays of the RSFS contain wave propagation information with which wave characteristics can be estimated. Therefore, this research focuses on identifying the signals reflected from the objective sea surface especially inside and outside of harbors to extract detailed characteristics for ocean waves.

1.2 GPS Remote Sensing

Usually GPS receiver's position can be measured by the time required for the GPS signal to travel from the satellites to the receivers in its direct path. GPS signals also arrive at receivers in multipath channel reflected from nearby surface, which is considered as interference signals to the LOS signals. However, the signals reflected from ocean and land are used as a signal sources to measure characteristics of sea state, atmosphere, soil moisture and ice [14,15,16], known as GNSS- Reflectometry. Figure 1-1 shows one case of the GNSS-Reflectometry.

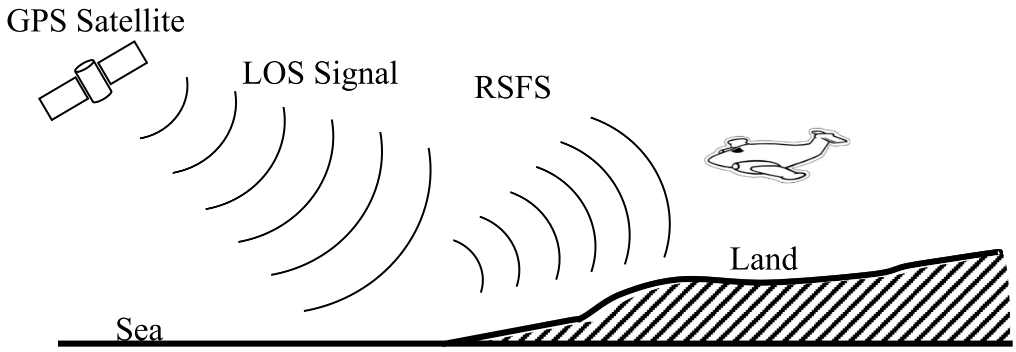

Figure 1-1 One case of GNSS-Reflectometry

In the research field of ocean remote sensing, GNSS-Reflectometry (GNSS-R) is used to measure sea-surface height and sea surface roughness to obtain characteristics of surface wind. GNSS-R is a kind of passive sensing technique that needs separate active signal sources. Fortunately, the Global Positioning System is a free source of radio waves which can be utilized all the time on the planet. For example, sea-surface height can be measured using GPS reflected signals. The two antennae are installed in an airplane to receive L1 signals, one is an up-looking Right-Hand Circular Polarized (RHCP) antenna to receive direct signal and the other is a down-looking Left-Hand Circular Polarized (LHCP) one to receive signals mainly reflected from the specular area on sea-surface. The aircraft flies at height of several kilometers. Using a complex correlation function, relative time delays of RSFS can be extracted. Based on the altimetric model composed of geometrical delay, scatteromeric delay and noise delay, variations of the sea surface height over several kilometers can be obtained.

1.3 Ocean Wave Remote Sensing System

We are devoted in the research of the ocean wave remote sensing system which possesses the following features and merits:

(1) Be able to work in the conditions of bad weather and low visibility. Especially the ocean wave remote sensing system should not be affected by powerful winds and waves.

(2) Be easy to build. It implys that the ocean wave remote sensing system is simple in structure and inexpensive in price.

(3) Be easy to install and maintain. It is not necessary to conduct surface or under-water operations of installation and maintainance.

Naturally we choose the remote sensing techniques to measure wave characteristics. The goal of the research is to provide a new way to measure the characteristics of ocean waves and find the ones harmful to harbors and navigation and mooring of vessels. In accordance with the GPS remote sensing techniques mentioned in above, a new ocean wave remote sensing system is designed and built to measure the detailed characteristics of ocean waves falling within a certain period range to improve the safety of harbors and vessels.

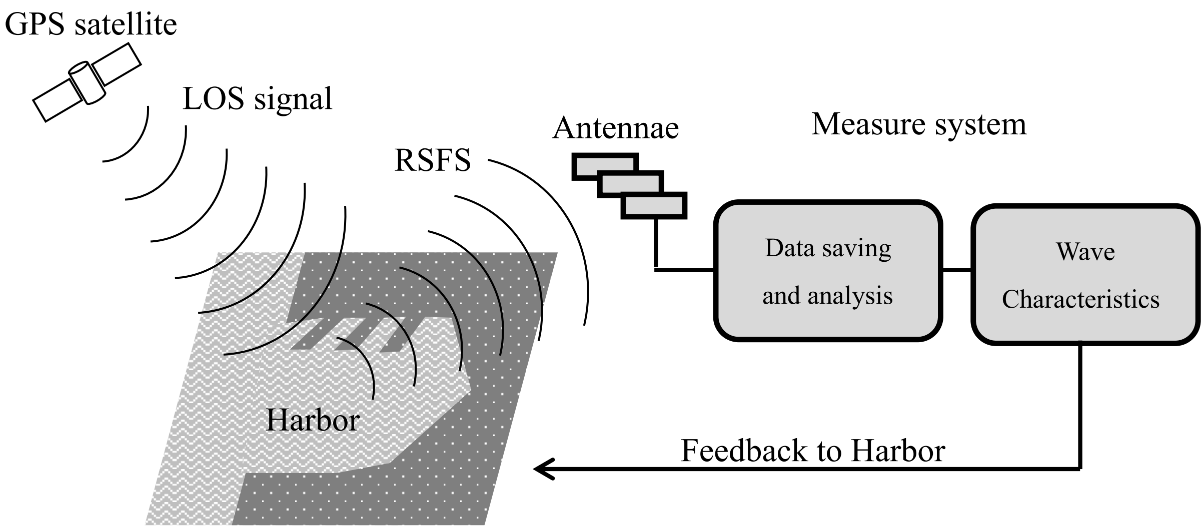

Figure 1-2 Ocean wave measurement using GPS signal.

Figure 1-2 shows the diagram of utilizing GPS signals to measure wave characteristics at the sea area of a harbor. In this figure, we can understand the information flow. In the upper-left corner, the GPS satellite is transmitting signals to the sea-surface. These signals can be used all-weather and all time and they are definitely reflected to be multipath. The antennae receive GPS signals from not only the LOS channel but also the multipath channels. The RSFS in the multipath channel must contain the information of the ocean wave. The received RSFS are then saved and analyzed to extract wave characteristics, such as wave period, wave length and wave direction. The resultant wave characteristics are sent to harbors and vessels. Once dangerous waves occur, some countermeasures will be taken out to mitigate risks and damage.

Now we try to develop the ocean wave remote sensing system in this figure. Simply the system is divided into the signal receiving part and the signal processing part. The antennae are used to receive the LOS signal and the RSFS. The received RSFS should be from the objective sea-surface. Besides, the GPS front-end in which the received signals are transformed is considered as a component of the receiving part. The main task of the signal processing part is to analyze the received signals and estimate the characteristics of ocean waves.

One of the differences between the LOS signal and the RSFS is the arrival times to the antennae. It is known that the RSFS have relative time delays to the LOS signal because of its long propagation distance. The relative time delays of the RSFS are only decided by the geometrical relationships between antennae, satellites and reflection points on the objective sea-surface. On the other hand, the geometrical relationships are known if the relative time delays are given. Therefore, it is possible to obtain the positions of the reflection points by estimating the relative time delays of the RSFS. When big waves occur, the intensities of the RSFS will change with the propagation of the waves. Consequently, the characteristics of the wave propagation can be estimated when the intensity variation of the RSFS in a certain area of the objective sea-surface is obtained. As discussed above, the signal processing part should be able to calculate the relative time delays and the intensity variations of the RSFS to estimate the characteristics of ocean waves.

Based on this idea, we proposed the ocean wave remote sensing system [17, 18]. Figures 1-3 and 1-4 respectively show the outline and the signal flow diagrams of the ocean wave remote sensing system.

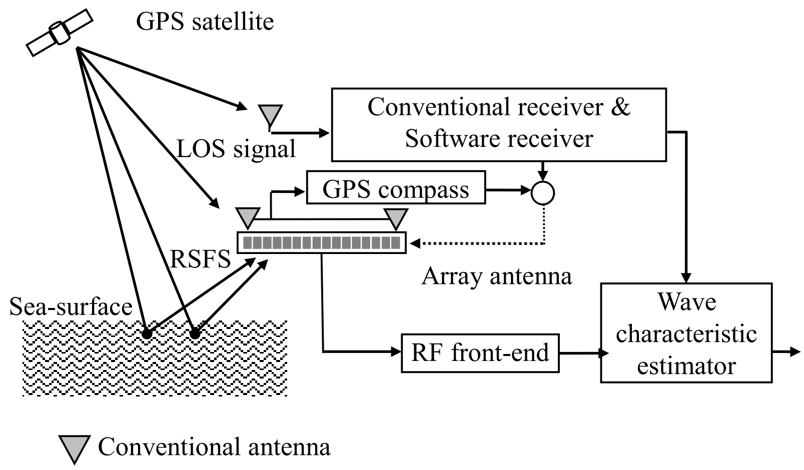

Figure 1-3 Outline of the ocean wave remote sensing system.

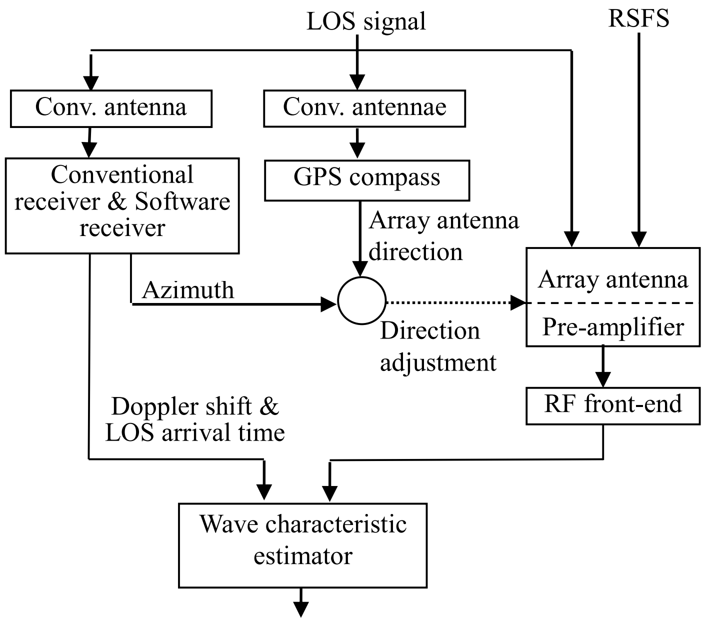

Figure 1-4 Signal flow diagram of the prototype system.

There are four GPS antennae in Figure 1-3. The upper conventional antenna receive the LOS signal from the objective GPS satellite to obtain its azimuth, elevation angle, Doppler shift and the arrival time of the LOS signal. In the middle of the figure there is an array antenna mounted with two conventional GPS antennae on both ends. The array antenna is a uniform linear array which can receive RSFS from the objective sea-surface with its narrow fan beam directional pattern. The two conventional antennae are used as a GPS compass to measure the direction of the array antenna. The array antenna is set in the direction of the objective satellite using the satellite azimuth from the upper conventional GPS receiver and the directional information of the array antenna from the GPS compass.

The LOS signal and the RSFS from the objective satellite are received with the upper antenna and the array antenna simultaneously. It is very important for calculating the relative time delays of the RSFS because the arrival time of the LOS signal is used as a time reference. In Figure 1-4, the LOS signal and the RSFS signals are analyzed with a wave characteristic estimator. The wave characteristic estimator calculates the relative time delays of the RSFS to determine where they are reflected and estimates the intensity variations of the RSFS to demonstrate the propagation of the ocean waves. And the characteristics of the ocean waves are output and sent to harbor or vessels.

References

[1] L.R Wyatt, S.P Thompson and R.R Burton, "Evaluation of high frequency radar wave measurement", Coastal Engineering, Vol. 37, Issues 3-4, pp.259-282, 1999.

[2] V. Cees, A. Reniers, J. Atanga, A. Vizinho and J. Vogelzang, "Monitoring surface waves in coastal waters by integrating HF radar measurement and modeling", Coastal Engineering, Vol. 37, Issues 3-4, pp.431-453, 1999.

[3] S.B. Jonathan, L.H. Malcolm and P. Arnstein, "A Method of Swell-Wave Parameter Extraction From HF Ocean Surface Radar Spectra", IEEE Journal of Oceanic Engineering, Vol. 31, No. 4, pp.812-818, 2006.

[4] P.A. Work, "Near shore directional wave measurements by surface-following buoy and acoustic doppler current profiler", Ocean Engineering 35, pp.727-737, 2008.

[5] J.C. McCall, "Advances in National Data Buoy Center technology", OCEANS '98 Conference Proceedings, pp.544-548, 1998.

[6] K. Kawaguchi, M. Satoh, K. Seki and Hiroyasu KAWAI, "Annual Report on Nationwide Ocean Wave Information Network for Ports and Harbors (NOWPHAS 2010)", PARI Technical Note, 2012.

[7] E.A.Terray, B.H. Brumley and B. Strong, "Measuring Waves and Currents with an Upward-Looking ADCP", Current Measurement, Proceedings of the IEEE Sixth Working Conference, pp.66-71, 1999.

[8] R. Pinkel and J.A. Smith, "Open Ocean Surface Wave Measurement Using Doppler Sonar", Journal of Geophysical Research, Vol.92, pp.12967-12973, 1987.

[9] Z. Zhang, C.L. Law and E. Gunawan, "Multipath Mitigation Technique Based on Partial Autocorrelation Function", Wireless Personal Communications, Vol. 41, No. 1, pp145-154, 2007.

[10] C.L. Chang and J.C. Juang, "An Adaptive MultipathMitigation Filter for GNSS Applications", Hindawi Publishing Corporation, EURASIP Journal on Advances in Signal Processing, Vol. 2008, No. 44, pp1-10, 2008.

[11] Y. Kegen, R. Chris and D. Andrew, "Sea Surface Altimetry Based on Airborne GNSS Signal Measurements", ISPRS Ann. Photogram. Remote Sens. Spatial Inf. Sci., I-7, pp.347-352, 2012.

[12] A. Komjathy, M. Armatys, D. Masters and P. Axelrad, "Retrieval of Ocean Surface Wind Speed and Wind Direction Using Reflected GPS Signals", Journal of Atmospheric and Oceanic Technology, Vol. 21, pp.515-526, Mar. 2004.

[13] M. N. Manuel, C. Marco, J. Font-Rossello, S. Lannelongue, and C. S. Vallmitjana, “The PARIS concept: an experimental demonstration of sea surface altimetry using GPS reflected signals”, Geoscience and Remote Sensing, IEEE Transactions, Vol.39, No.1, pp.142-145, Aug. 2002.

[14] M. Armatys, A. Komjathy, P. Axelrad, S.J. Katzberg, “A Comparison of GPS and Scatterometry Sensing of Ocean Wind Speed and Direction”, Geoscience and Remote Sensing Symposium, Proceedings. IGARSS 2000, IEEE 2000 International, Vol.7, pp2861-2863, 2000.

[15] M. Bevis, S. Businger, T. A. Herring, C. Rocken, “GPS Meteorology' Remote Sensing of Atmospheric Water Vapor Using the Global Positioning System”, Journal of Geophysical Research, Vol.97, No. D14, pp.15,787-15,801, 1992.

[16] S. J. Katzberg, O. Torres, M. S. Grant ，D. Masters, “Utilizing calibrated GPS reflected signals to estimate soil reflectivity and dielectric constant: results from SMEX02”, Remote Sens. Environ., Vol. 100, No. 1, pp. 17–28, 2006.

[17] J. Cui and N. Kouguchi, “Bistatic ocean wave remote sensing system by GPS”, IEICE, Vol.E96-B, No.06, pp.1625-1632, Jun. 2013.

[18] J. Cui and N. Kouguchi, “Experimental Evaluation of Bistatic Ocean Wave Remote Sensing System by GPS”, Vol.E97-B, No.02, pp.519-527, Feb. 2014.

CHAPTER 2

METHODOLOGY

2.1 Ocean Wave

2.1.1 Characteristics of Ocean Wave

As we all know, oceans cover more than 70 percent of the earth. Ocean water is permanently in coexistence with various forces of nature so that many types of ocean waves are generated. Ocean waves oscillate not only on the sea surface but also in deep water. In general, ocean surface waves can be classified into capillary ripples, wind waves, sea swell, tsunamis, and tides. Any type of wave involves certain physical factors. Capillary ripples result from sea surface tension. Wind wave results from the wind blowing over sea surface. Sea swell is usually generated by distant storms. Tsunamis are long period oscillation caused by submarine earthquakes or landslides. Tides are caused by astronomical rotation. In this paper, sea swell that impacts the safety of harbor and ship navigation will be discussed and measured with the proposed measurement method. In this section, we will introduce the characteristics of ocean wave and the classic wave modelling.

Ocean waves have many characteristics. The characteristics of an ocean wave can be measured and used to describe that wave, as shown in Figure 2-1.

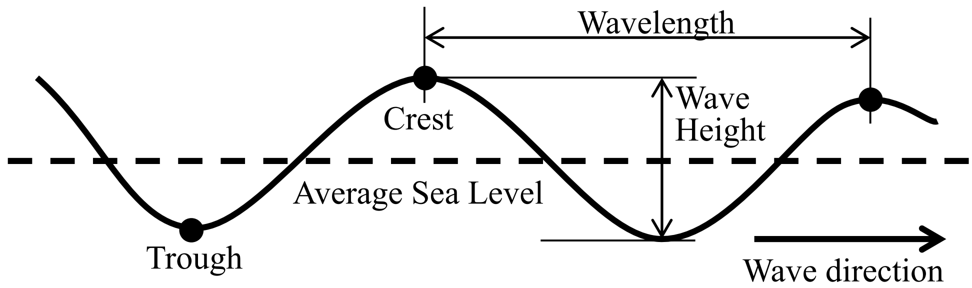

Figure 2-1 Primary characteristics of ocean wave.

The highest point of a wave is referred to as the crest and the lowest point of a wave is referred to as the trough. Wave height H_w is the vertical distance between crest and trough of wave. Wavelength λ_w is defined as the horizontal distance between two successive wave crests or wave troughs. Addition to wave height and wavelength, a wave is also described by the wave period T_w and the wave speed V_w. Wave period T_w is the time that two successive wave crests pass a fixed point, and wave speed V_w can be determined by dividing wavelength by wave period. Wave direction is the direction of wave propagation. The relationship between the wave period T_w, the wave speed V_w and wave length λ_w is well-known as follows,

$$\lambda_{\mathrm{w}} = V_w \times T_w \tag{2.1}$$

The wave speed V_w and wave length λ_w can also be estimated with the dispersion relation [1, 2] in which

$$V_w = \frac{gT_w}{2\pi}\tanh(kz) \tag{2.2}$$

$$\lambda_w = \frac{gT_w^{\ 2}}{2\pi}\tanh(kz) \tag{2.3}$$

where g is the gravitational acceleration, k is the wave number (k = $2\pi/\lambda_w$), and z is the water depth. From the dispersion relation, it is known that ocean waves of different wavelengths propagate at different wave speeds, and the wave speed V_w and wave length λ_w depend on the wave depth.

However sea-surface waves are not composed of a single sinusoidal wave. The sea-surface is always composed of various waves with different frequencies and lengths. Therefore it is not suitable to describe the sea-surface by a single wave. The ocean waves on the sea-surface can be represented with an infinite sum of sine and cosine waves of different frequencies

$$\xi(t) = \sum_{n=1}^{\infty}(a_n \cos(2\pi nft) + b_n \sin(2\pi nft)) \tag{2.4}$$

where f is the fundamental frequency, a_n and b_n are amplitudes of different wave components.

We can obtain the spectrum of an ocean wave with the following computation [3],

$$S(nf) = Z_n Z_n^* \tag{2.5}$$

where

$$Z_n = \int_{-\infty}^{\infty} \xi(t) e^{-i2\pi nft} dt \tag{2.6}$$

and Z^* is the complex conjugate of Z. Here the equation of Z_n is called the Fourier transform which will be introduced in section 2.4.2 in detail.

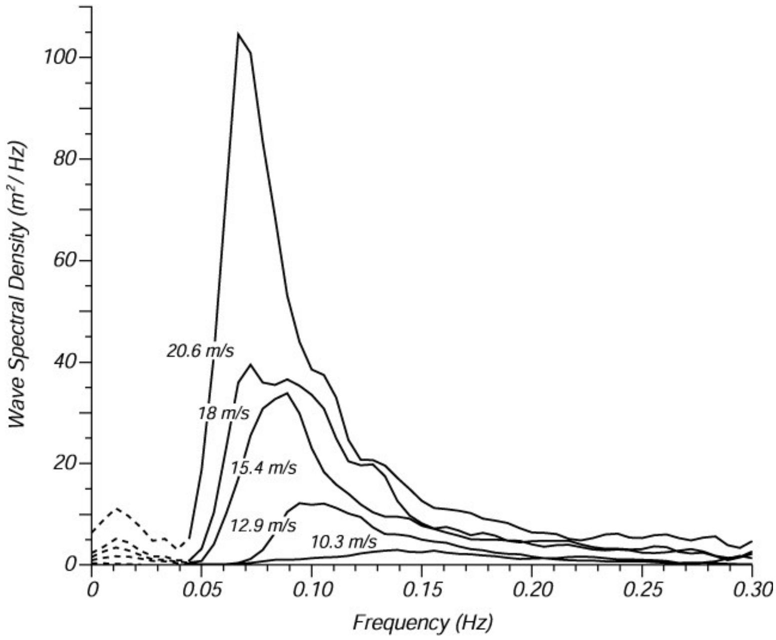

Figure 2-2 Wave spectra of a fully developed sea for different wind speeds.

The Pierson-Moskowitz Spectrum is a simplest spectrum of ocean waves on a fully developed sea on which the wind blows steadily for a long time over a large area so thus the waves could come into equilibrium with the wind. Figure 2-2 shows the wave spectra of a fully developed sea for different wind speeds found by Moskowitz. The empirical relationship that defines the ocean wave energy distribution with frequency is given by

$$S(\omega) = \frac{\alpha g^2}{\omega^5} \exp[-\beta(\frac{\omega 0}{\omega})^4] \tag{2.7}$$

where ω=2πf and α = 8.1×10-3, β = 0.74, ω0 = *g*/U19.5 and U19.5 is the wind speed at a height of 19.5 m above the sea surface.

2.1.2 Sea swell

There are various ways to classify the ocean waves, such as the wave period and the force which generates the ocean waves. The sea swell wave discussed here is classified by wave period range from 10 to 30 seconds. We propose the ocean wave remote sensing system to measure the ocean wave possessing the wave period from tens of seconds to minutes and the wave length from hundreds of meters to kilometers, especially the sea swell.

A swell is a train of waves of similar wavelengths, moving across the ocean in the same direction [4]. Sea swell occurs frequently and can be observed easily near a coast. Sea swell is generated by storms kilometers or even hundreds of kilometers away. The stronger the storm at the source area, the bigger will be the swell and the further it will travel. The wave period of swells ranges from 10 seconds to 30 seconds. The wavelength will be over 200 meters and the wave height will be over 4 meters for long and heavy swell. The wavelength increases but the wave height decreases relatively slowly correlated with the distance away from the source area. Sea swell propagation features relatively regular wave motion. Also the wave spectrum of swell has been defined and we will use wave spectrum to generate sea-surface for the numerical simulation of the ocean wave remote sensing system.

Sea swells cause great disturbance of vessel motion and even cause unstable course deviation to vessels navigating along harbor entrance channels. Moreover the effectiveness of breakwaters and jetties to sea swell progressively decreases. Sea wells have seriously hampered the secure and efficient use of harbors. Therefore, various devices and instruments were invented to measure the characteristics of sea swells.

Modelling

The sea-surface with swell can be modelled as a narrow-band Gaussian process with the following spectrum [5]:

$$F(Kx,Ky)=\frac{<h^2>}{2\pi\sigma_{kx}\sigma_{ky}}\exp\{-\frac{1}{2}[(\frac{Kx-Kxm}{\sigma_{kx}})^2-(\frac{Ky-Kym}{\sigma_{ky}})^2]\} \quad (2.8)$$

where $<h^2>$ is the variance due to swell, K_{xm} and K_{ym} are the wavenumbers of the spectral peak, and σ_{kx} and σ_{ky} are the spectrum widths in the x and y directions respectively. The wave spectrum widths σ_{kx} and σ_{ky} are very small values to ensure that the sea-surface waves are regular and rounded but not monochromatic. In chapter 4, a sea-surface is generated with reference to this swell model.

Propagation in shallow water

The proposed ocean wave remote sensing system usually measures the sea swell near a harbor. It implies that the objective sea swell propagates in relatively shallow water. When sea swells travel from deep water to shallow water, wave characteristics will change. The wave speed is reduced because of the influence of the water bottom, and the wavelength is shortened correspondingly. However the wave period remains unchanged. Moreover, some phenomena will occur in the shallow water, such as refraction, diffraction [6].

The refraction occurs because of the inhomogeneous water depth in shallow water. A wave will bend when its different parts move in different water depth. One part in deeper water than the adjacent parts will move rapidly. Therefore the wave trends to be aligned with the bottom contour. Figure 2-3 shows the refraction of swell waves.

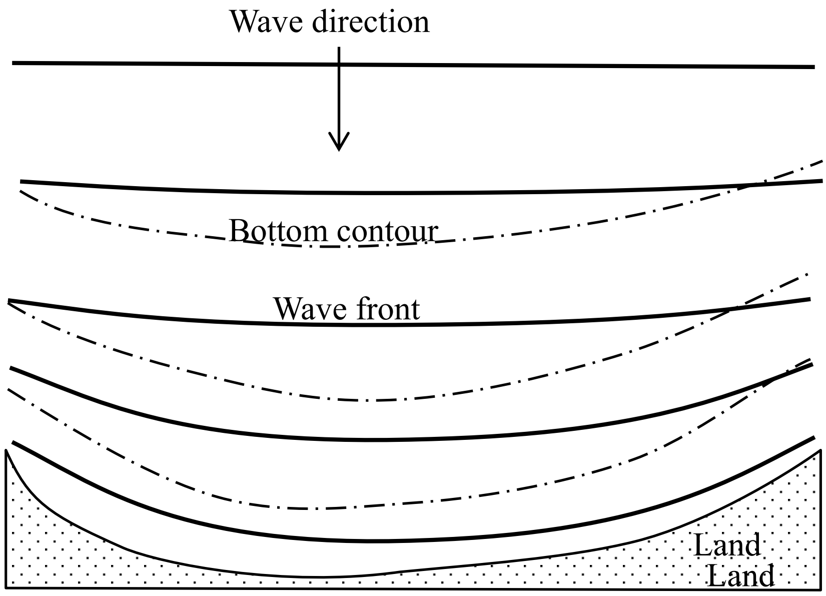

Figure 2-3 The refraction of swell waves.

The diffraction happens when the waves encounter an obstacle such as a jetty, breakwater and island. The waves will enter the shadow zone when they pass the obstacles.

It means the wave energy will be carried into the shadow zone. However the waves entering the shadow zone have relatively low wave height. The refraction will also occur if the bottom around the obstacle is sloping. Figure 2-4 shows the diffraction of swell waves. The numbers near the broken lines indicate how much the wave height can be remained after the wave diffraction occurs.

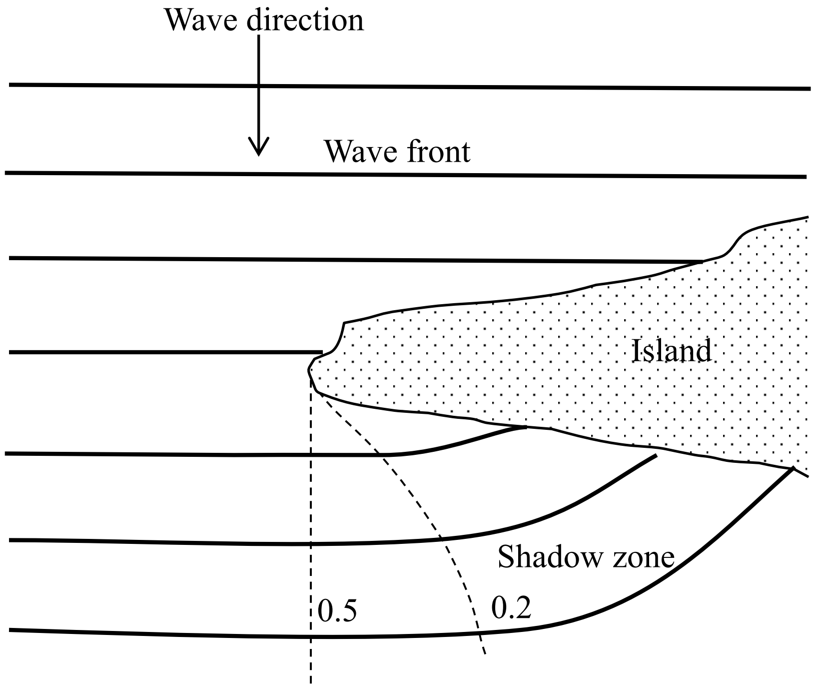

Figure 2-4 The diffraction of swell waves.

It is obvious that the refraction and the diffraction can change the direction and the height of swell waves severely and can affect the results of wave measurements. Besides the refraction and the diffraction of ocean waves, some other phenomena also happen such as reflection and breaking. The reflection means that the waves can be bounded back by solid obstacle and the reflected waves interfere with the coming waves; and the breaking means the wave crest collapses because the wave steepness increases so that the wave can no longer support its own weight or the crest speed exceeds the speed of the wave.

Scattering Pattern of sea-surface

The proposed wave ocean wave remote sensing system is based on the bistatic reflection of the GPS signals off sea swell. Some scattering patterns of random rough surfaces have been studied [7], such as Kirchhoff approximation, small perturbation method and two-scale composite model and so on. Each point on sea-surface is approximated by an infinitely extended tangent plane in the Kirchhoff approximation, but this approximation is only valid for a surface with an important horizontal roughness scale and average curvature radius compared to the electromagnetic wavelength [8]; for small slopes or small roughness scales, the small perturbation method is appropriate and accurate to estimate the diffuse components of the electromagnetic scattered waves; the two-scale model is a composite one that considers the large scale roughness and small scale effect. Because the scale of the swell waves is much larger than the wavelength of GPS signals, the bi-directional reflectance distribution function based on the Kirchhoff approximation will be used in the numerical simulation.

2.1.3 Ocean Wave Measurement

There are a lot of ocean wave measurement instruments and techniques such as wave rider buoy, high frequency radar, acoustic Doppler current profilers and the recently developed Global navigation satellite system Reflecmetery. All the techniques can be divided into two categories: in situ techniques and remote sensing techniques [9]. The in situ instruments are positioned at sea-surface or below sea-surface, such as floating surface buoy and pressure transducer. They try to measure the motions of the sea-surface but they are sensitive to aggressive marine environment. The remote sensing instruments are mounted above sea-surface on a fixed or a moving platform such as a tower at sea, a ship, an airplane or a satellite. They receive the visible or infra-red light or radar wave reflected from the sea-surface. They can cover a larger area or measure in a short period of time than the in situ instruments. The remote sensing instruments are not sensitive to the marine environment but sensitive to the atmospheric environment.

Here some examples of the applications are introduced. Figure 2-5 shows an arrayed buoy system developed by our Laboratory. A group of four-ball buoys are placed onto the several positions on the objective sea-surface to measure the wave movements by GPS. The 3-D movement of each four-ball buoy is resolved and reordered. We consider the movement of buoy equivalent to the movement of water particles. The GPS data is sent to the land station through wireless transmission to be analyzed. The wave height, wave period, wavelength and direction can be estimated with the data of buoy movements [10]. In particular, the long period wave can be measured well. However, because the precise wavelength could not be measured, we used a wavelength that was estimated by dispersion relation.

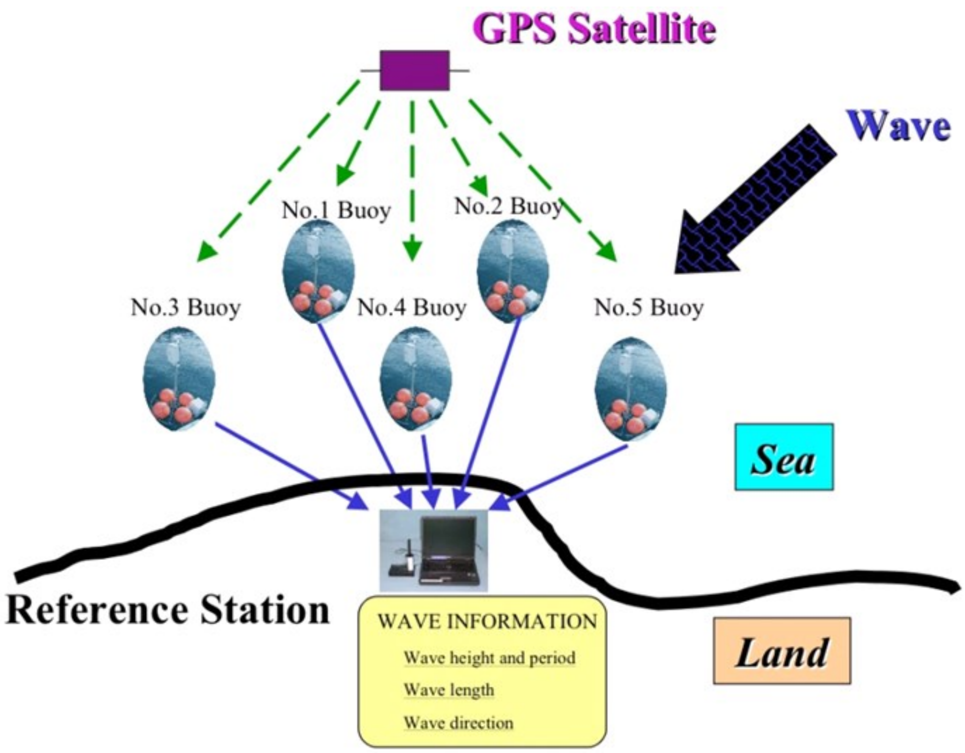

Figure 2-5 Arrayed GPS buoy system.

High frequency Radar has been used to measure sea-surface for quite a long time to measure sea-surface currents and waves of the coastal ocean. The high frequency radar ocean wave measurement system usually consists of transmitters and receivers. The transmitters send electromagnetic waves in the high frequency band. If the currents or ocean waves occur on the sea-surface, the high frequency electromagnetic waves are scattered back towards the receiver. The transmitted electromagnetic wave is single-frequency but the backscattered waves possess a wider spectrum because the propagations of the currents and ocean waves change the frequencies of the backscattered waves, known as Doppler shift. Meanwhile, it is known that the Doppler shift is positive or negative when the wave is approaching the receiver or moving away from the receiver respectively. Consequently, the velocity of the sea-surface currents and waves can be resolved with the measured Doppler shift. Usually, two high frequency radar ocean wave measurement systems are used to estimate true parameters of currents and waves. The high frequency Radar is also used to measure parameters of sea swell [11]. Figure 2-6 shows an example of sea swell measurement with two high frequency Radar systems. In Figure 2-6, the researchers used two stations deployed at Tweed Heads (Qld., Australia). The bore sights of the two stations at intersect almost orthogonally.

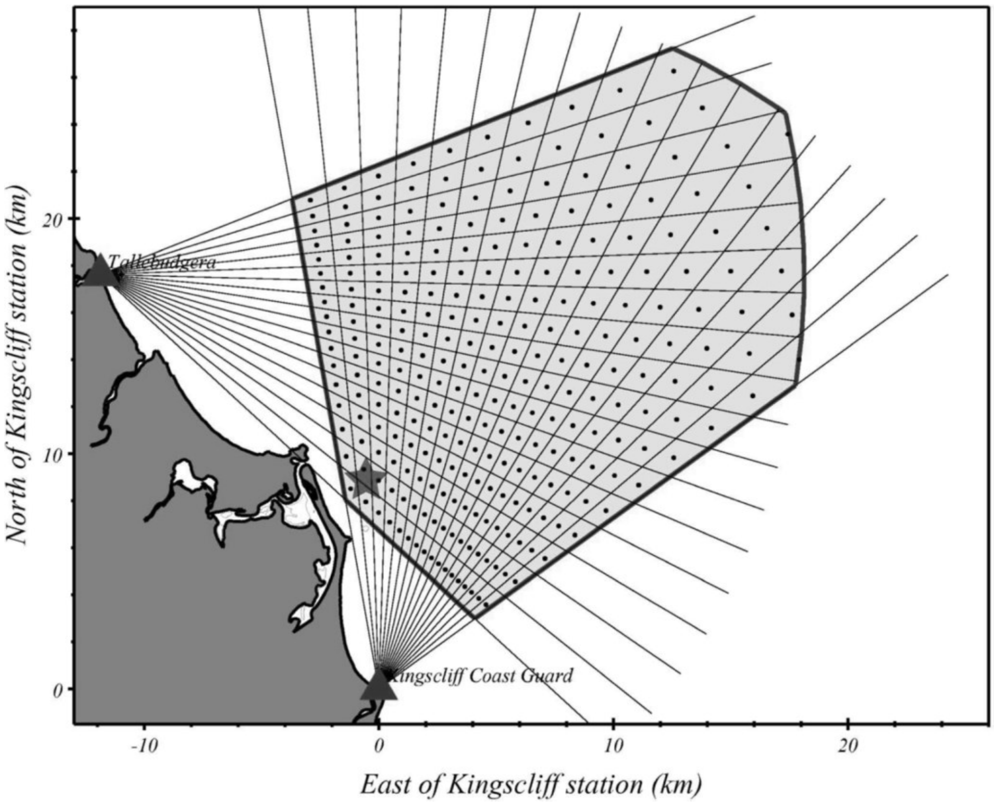

Figure 2-6 Sea swell measurements with two high frequency Radar systems.

Synthetic Aperture Radar (SAR) [12] is mounted on an aircraft or spacecraft to generate high resolution remote sensing image which can be used to measure ocean waves. The antenna transmits a series of pulse to the objective area in a certain time interval. All the backscattered echoes are received in turn with the same antenna, and the magnitudes and phases are recorded during the objective area locating within the antenna beam. The objective area can be detected by summing the backscattered echoes from it and the image processing system of the SAR will illustrate the objective area. Therefore the SAR moving with a platform works as a synthesized antenna. SAR is a unique sensor for the ocean surface wave measurement since SAR is the only sensor that can provide images from space with high enough resolution, independent of cloud cover and light conditions, to detect ocean surface wave scales of interest. Figure 2-7 shows a SAR image of the sea-surface waves at Point Reyes National Seashore. The wave propagation on the sea-surface can be obtained from this image.

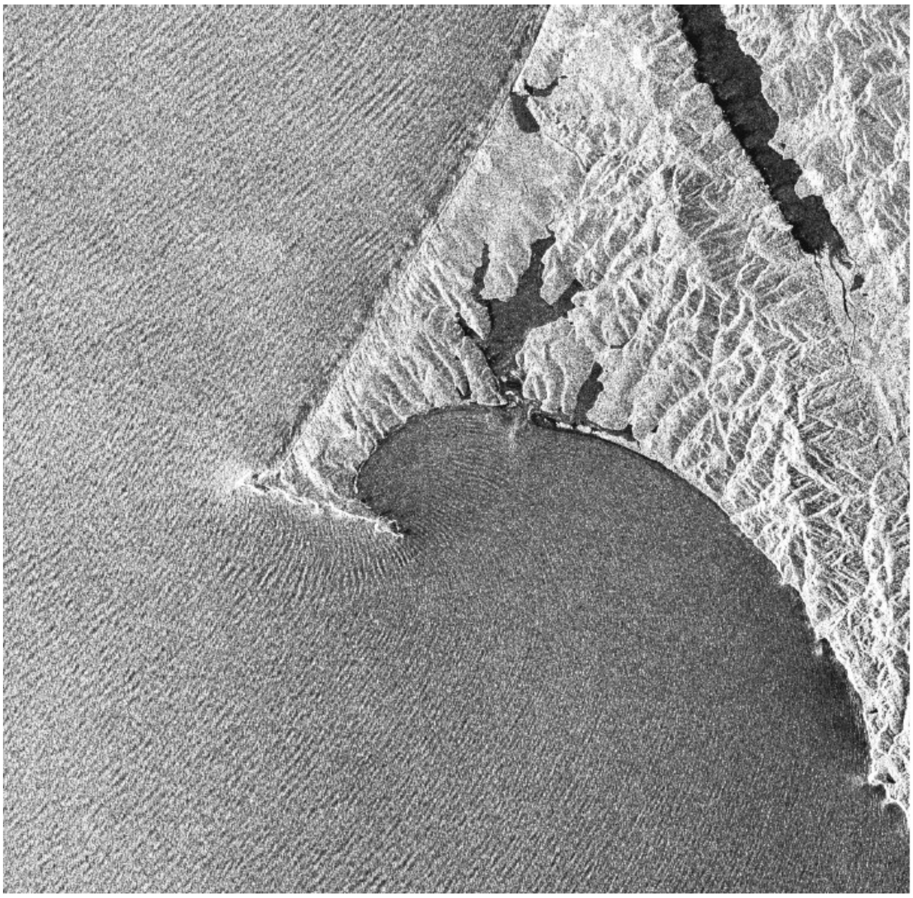

Figure 2-7 An SAR image of sea-surface waves (31.5km×31.5km).

2.2 GPS Signal

2.2.1 Global Position System

From the moment of its birth, GPS has gradually become an indispensable part of engineering and scientific researches in which positioning, surveying and real-time navigation are fundamental assignments. GPS is abbreviation of Global Positioning System [13] , and it consists of three parts: in the space, there is a constellation of 24 satellites and each satellite sends the universal time and navigation data using a spread spectrum Code Division Multiple Access (CDMA) technique; on the earth, five ground-based monitoring stations and one master control station are controlling the space part continuously; the third part is the user device; signal receiver, which can process GPS signals and calculate the receiver's location. For receivers on earth, high quality GPS signals from three satellites are required to determine the current time, latitude, and longitude, and four satellites to determine the current altitude. More GPS signals will increase the accuracy of positioning and navigation.

In the ocean wave remote sensing system, the GPS signal is utilized as an indirect tool to obtain wave characteristics. Here, the GPS signal and its components and prosperities will be introduced in detail.

2.2.2 Signal Generation

Every satellite is transmitting GPS signals continuously on two different radio frequencies in the Ultra High Frequency (UHF) band. These frequencies are known as L1 (1575.42MHz) and L2 (1227.60MHz). L1 carries two unique spreading sequences or codes, including C/A code and an encrypted precision code (P(Y)). L2 only carries P code. The C/A code and P code carried on these two frequencies can be considered as pseudo random noises, which are modulated with navigation data. Thus GPS signals are also referred to as pseudo random noise spread spectrum signals.

During the generation of GPS signal, the C/A code and the P(Y) code should firstly be combined respectively with navigation data through modulo-2 adders. Then all the combined signals, C/A code ⊕ data and P(Y) code ⊕ data, are modulated into the carrier signal using the Binary Phase Shift Keying (BPSK) method. The BPSK is the simplest form of phase modulation where the carrier is instantaneously phase shifted by 180 degrees at the time of a bit change. Adding the two combined signals generates the resulting GPS signal. Consequently, the signal transmitted from satellite *k* can be described as

$$\begin{aligned} s^k(t) &= \sqrt{2P_C}(C^k(t) \oplus D^k(t))\cos(2\pi f_{L1}t) \\ \vdots \quad &+ \sqrt{2P_{PL1}}(P^k(t) \oplus D^k(t))\sin(2\pi f_{L1}t) \\ &+ \sqrt{2P_{PL2}}(P^k(t) \oplus D^k(t))\sin(2\pi f_{L2}t) \end{aligned} \tag{2.9}$$

P_C, P_{PL1}, P_{PL1} : Powers of signals with C/A or P(Y) code;

C^k : C/A code sequence assigned to satellite *k*;

P^k : P(Y) code sequence assigned to satellite *k*;

D^k : Navigation data sequence;

f_{L1}, f_{L2} : Carrier frequencies of L1 and L2.

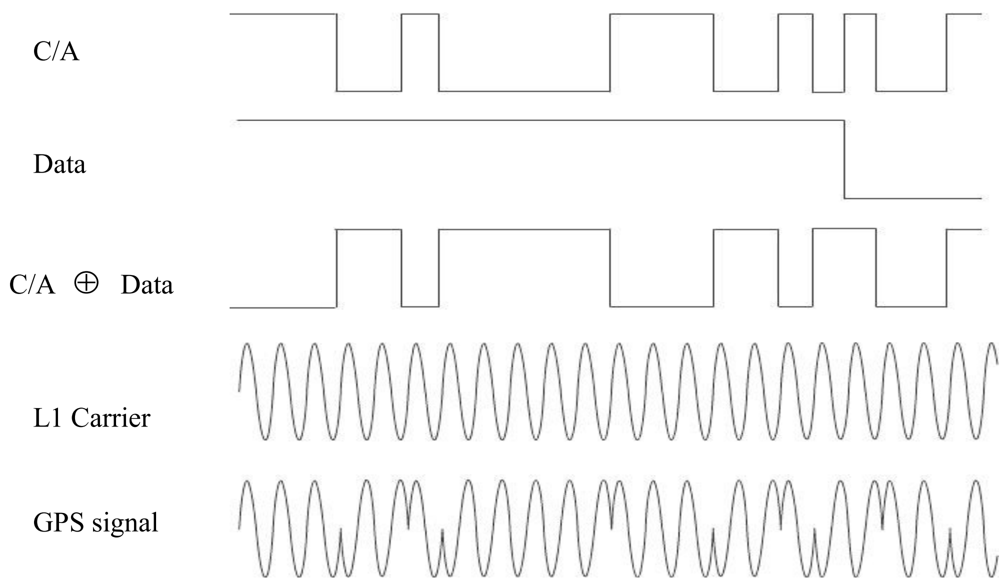

Figure 2-8 Generation of GPS signal by BPSK modulation

In our research, we only discuss the L1 signal. Figure 2-8 describes the final GPS signal which is the product of the C/A code, navigation data and carrier signals. The carrier is instantaneously phase shifted by 180 degrees at the time of chip change. Also the phase of the GPS signal is also occurs phase shifted 180 degrees when a navigation data bit transition occurs.

Propagation of electromagnetic wave

GPS signal is a kind of electromagnetic wave generated and transmitted by GPS satellite. As shown in Figure 2-9, the electromagnetic wave has two components: electric field (E) and magnetic field (M). They are perpendicular to each other and in phase. The dotted-line is variation of the magnetic field vector and the heavy line is variation of the electric field vector. The propagation direction of the electromagnetic wave is indicated with the arrow x. The electromagnetic wave propagates through a vacuum at a speed of 3×10^{8}m/s. The right-hand rule can be applied to the electromagnetic wave: Pointing your right thumb along the arrow x and pointing your right index finger in the direction of the electric field vector, your middle finger ought to point along the direction of the magnetic field vector. The energy of the electromagnetic wave propagate alone the direction x, therefore, the largest energy can be received in this direction and the no energy can be received in its vertical directions.

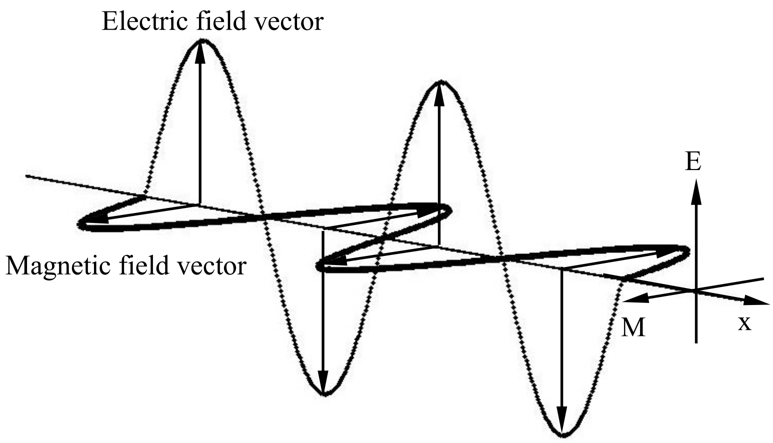

Figure 2-9 Propagation of Electromagnetic wave.

Polarization

The electromagnetic wave does not always propagate in a sinusoidal manner in a plane, as shown in Figure 2-9. The direction of the electric field vector defines the polarization of the electromagnetic wave. In Figure 2-10, linear, circular and elliptical polarizations are shown.

Given a plane perpendicular to the diction of the propagation, the traces of the electric filed vectors on the plane are different. The linear polarization has a straight line on the plane (a); the circular polarization has a circular trance on the plane (b); and the elliptical polarization has an elliptical trance (c). The three electromagnetic waves have different polarizations but each of the electric field vectors can be resolved into two orthogonal sinusoidal components with equal frequency.

Circular polarization is most often employed in satellite communication, since circular polarized antennae transmit and receive radio waves in all directions, circularly polarized radio waves can be received regardless of the direction of the antenna [14]. The electric field vector rotates with the circular polarization. Form the point of the receiver, the circularly polarized electromagnetic wave is considered right-handed circular polarization if the rotation is counter-clockwise. Conversely, it is left-handed circular polarization if the rotation is clockwise. The GPS signal has right-hand circular polarization. The receivers on Earth should have same polarization with the signals.

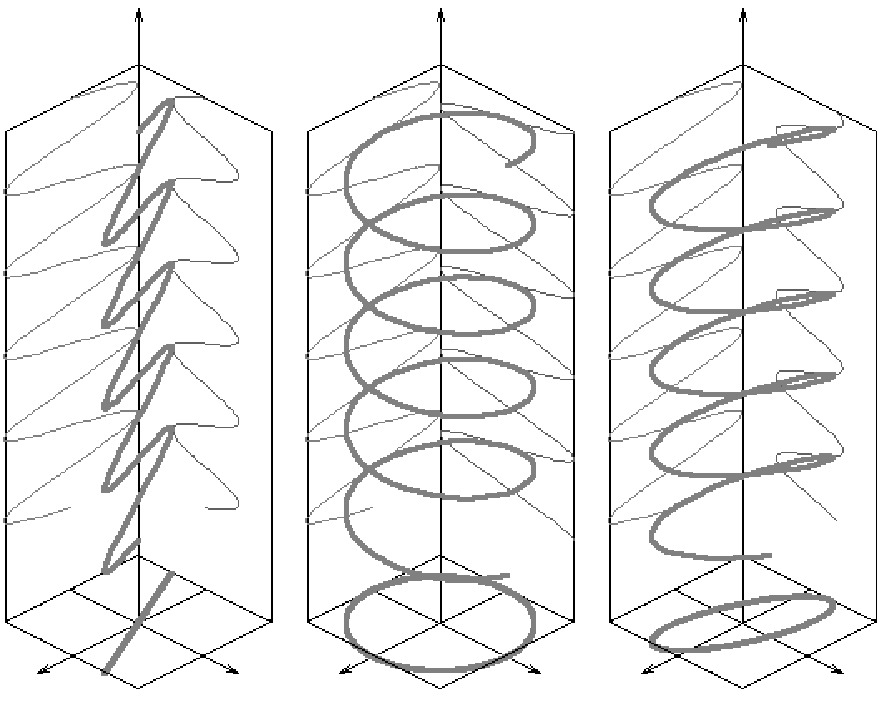

(a) (b) (c)

Figure 2-10 Linear, circular and elliptical polarizations.

2.2.3 C/A Code and Correlation Properties

The C/A code is also referred to as the PRN code or as the Gold codes; the non-encrypted portion of the GPS signal. It is a sequence of 1023 chips and repeats in 1ms. Each satellite has its own unique C/A code to be differentiated from others for coarse acquisition.

Here, two properties of C/A should be emphasized because they will be used in the ocean wave remote sensing system. One of the properties is that of nearly no cross correlation, meaning that all the C/A codes are nearly uncorrelated with each other. The other is that there is nearly no correlation except for zero lag, that is to say all C/A codes are nearly uncorrelated with themselves, except for zero lag. If given two C/A codes C^i and C^k for satellites *i* and *k*, these two properties can be expressed as follows [15, 16]:

cross correlation: $r_{ik} = \sum_{l=0}^{1022} C^i(l)C^k(l+m) \approx 0$ for all *m*;

autocorrelation: $r_{kk} = \sum_{l=0}^{1022} C^k(l)C^k(l+m) \approx 0$ for $|m| \geq 1$.

The autocorrelation property makes it easy to find out when two similar codes are perfectly aligned. It means that a C/A code will be nearly uncorrelated with itself, unless two identical C/A codes are perfectly aligned. This property enables us to find out the code phase of a C/A code, which denotes the arrival time of the code sequence. Therefore, by searching and determining the time delays of the transmission of reflected signals from one satellite, we can take advantage of this autocorrelation property to calculate the code phase of C/A code modulated within each reflected signal. The autocorrelation function of one GPS C/A code sequence is given as:

$$\mathrm{ACF}(m) = \frac{1}{1023}\sum_{l=0}^{1022} C(l)C(l+m), \quad and \quad \begin{cases} R_i(m) \approx 0, & |m| \geq 1 \\ R_i(m) = 1, & m = 0 \end{cases} \tag{2.10}$$

where, $\mathrm{ACF}(m)$ is the autocorrelation value for satellite *i* at m code phase difference; C(*l*) is C/A Code.

One C/A code is a repeating sequence with period of 1ms, and Figure 2-11 illustrates all the autocorrelation values if we calculate its C/A Code autocorrelations by each code phase.

As seen from Figure 2-11, only on the points where two similar C/A codes aligned perfectly will the autocorrelation calculation show obvious peaks. Therefore the autocorrelation property of C/A code is used to identify code phase of GPS signal.

Figure 2-11 C/A code autocorrelation with different code phases

2.2.4 Multipath Propagation

A GPS antenna can receive not only LOS signal directly from satellite but also the reflected or diffracted signals from its surrounding environment [17]. It means that the GPS signals can arrival at the receiving antenna from more than one propagation path, referred to as multipath. The multipath has longer distance than the path of LOS signal so that the signals transmitted in multipath channels have relative time delays to the LOS signals. The signals in multipath channels feature different intensities and phases with the LOS signals. The intensities are related to the nature of the reflection surface.

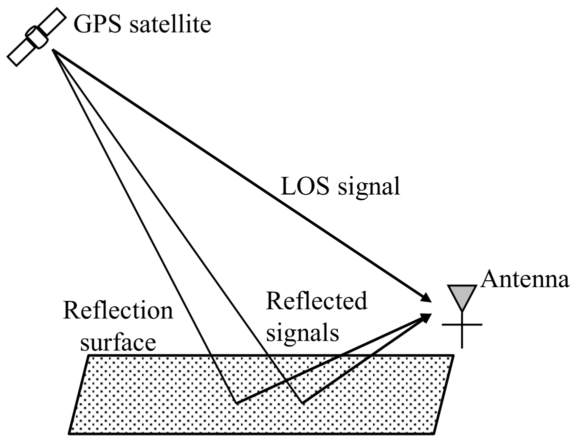

Figure 2-12 Multipath propagation from reflection.

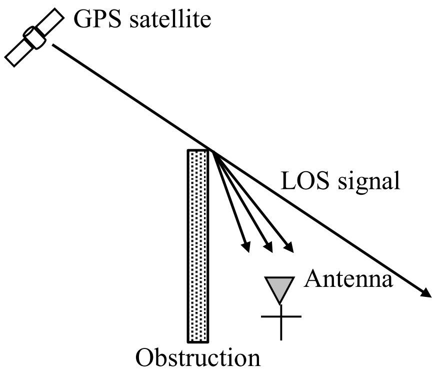

Figure 2-13 Multipath propagation from diffraction.

Figure 2-12 and Figure 2-13 show the examples of multipath propagations. In Figure 2-12, if the reflection surface is smooth, the antenna can only receive one reflected signal, i.e. specular reflection. However, in most cases, the reflection surfaces are rough so that the signals are scattered. In Figure 2-13, the signal cannot arrive at the antenna directly because of the obstructing object but the signal is diffracted to the area behind of the obstructing object in multipath channel and received by the antenna. In our search, we only study the signal multipath propagations caused by the scattering because the array antenna of the ocean wave remote sensing system mainly receives the reflected signals from sea-surface.

signal phase

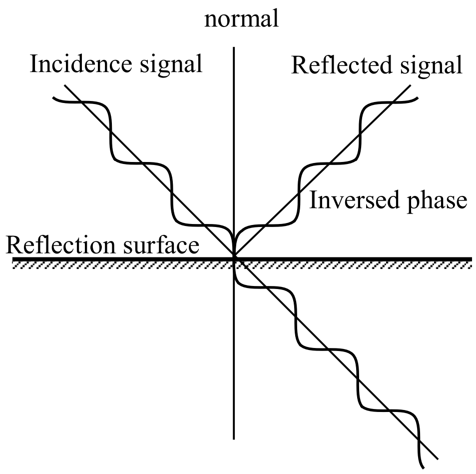

Figure 2-14 Phase shift in the multipath propagation.

Usually the signals in multipath channels have different polarities with the LOS signal. The LOS signal is right hand circularly polarized and the reflected signals may have reversed polarity which also induces phase to reverse. Figure 2-14 shows the simple example of the phase reversal of GPS signal with specular reflection. If the incidence signal is not reflected with the reflection surface, its phase is kept. However, with the specular reflection, the reflected signal has phase shift of 180 degrees which can be manifested with the opposite phases of two sinusoidal waves in the left of the normal.

Multipath Correlation

It is necessary to examine the correlation of the signals transmitted in the multipath channel because the correlation is the method to detect the RSFS. The correlation is a triangular peak as shown in Figure 2-11. But there are the constructive interference if the multipath is in-phase and destructive interference if the multipath is out-of-phase.

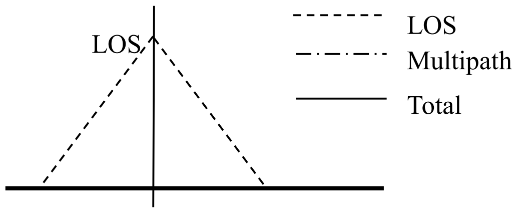

(a) Correlation without multipath

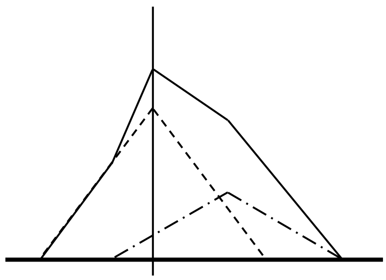

(b) Correlation with in-phase multipath

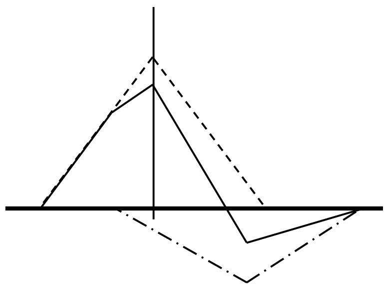

(c) Correlation with out-of-phase multipath

Figure 2-15 Constructive interference and destructive interference of multipath.

Figure 2-15 shows the constructive interference and the destructive interference of multipath. Sub-figure (a) is the correlation peak without any multipath and it is an isosceles triangular. Sub-figure (b) shows the correlation with in-phase multipath, and the total correlation is the sum of the two individual correlations. The constructive interference amplifies the LOS signal equivalently. Sub-figure (c) shows the correlation with out-of-phase multipath and the total correlation is the difference of the two individual correlations. The deconstructive interference reduces the LOS signal. In a complex multipath environment, the antenna will receive much reflected signals including in-phase and out-of-phase. Especially the phases and the intensities of the reflected signal are varying relative to the LOS signal. Therefore the total correlation will be constructed and deconstructed severely, referred to as signal fading.

Geometry

The reflected signals travel longer distance than the LOS signal and have relative time delays. We discuss the geometry of multipath using the case of the ocean wave remote sensing system. When the ocean wave remote sensing system is installed near a harbor and its array antenna is adjusted to face the objective sea-surface, almost any point on the objective sea-surface can theoretically reflect GPS signal to ocean wave remote sensing system. Also the relative time delay t_{delay} of reflected GPS signal transmitted in multipath channel is determined by the geometrical relationship of reflection.

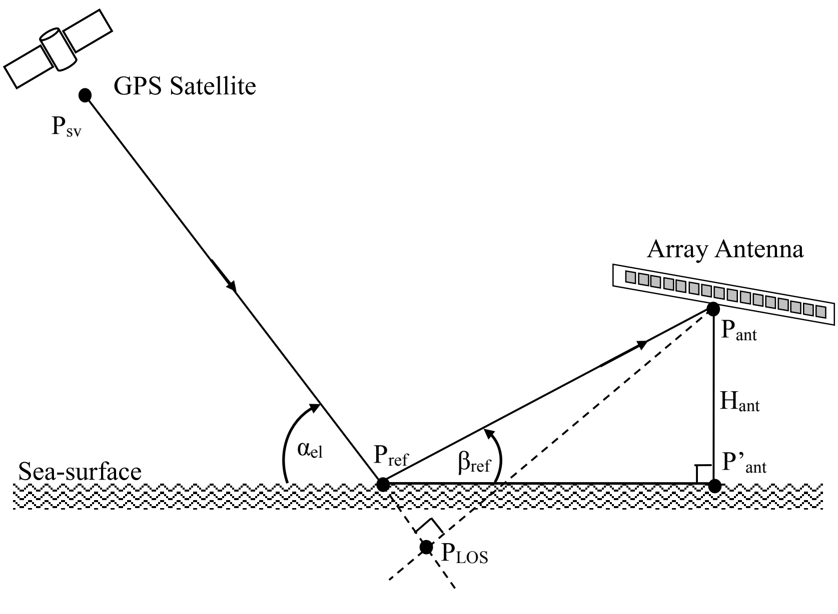

Figure 2-16 Geometrical relationship of reflection.

P_{sv}: position of GPS satellite;

P_{ref}: position of reflection point;

P_{LOS}: equivalent arriving position of LOS;

P_{ant}: position of array antenna / position of system;

P'_{ant}: projection of array antenna on sea-level;

H_{ant}: height of array antenna;

α_{el}: elevation of GPS satellite;

β_{ref}: reflection angle of multipath.

Figure 2-16 gives an example of the geometrical relationship of one signal reflected from point P_{ref} on target sea-surface. Generally, the geometry of RSFS is determined by the antenna height and satellite elevation angle. The geometrical relationship of reflection is explained with Figure 2-16.

In Figure 2-16, the lengths of LOS propagation and RSFS propagation from satellite to array antenna are defined as

$$d_{LOS} = |P_{sv}P_{LOS}| = |P_{sv}P_{ref}| + |P_{ref}P_{LOS}| \tag{2.11}$$

$$d_{RSFS} = |P_{sv}P_{ref}| + |P_{ref}P_{ant}| \tag{2.12}$$

Therefore, the delayed distance d_{delay} of RSFS propagation comparing with LOS signal is the difference of d_{LOS} and d_{RSFS}

$$d_{delay} = d_{RSFS} - d_{LOS} = |P_{ref}P_{ant}| - |P_{ref}P_{LOS}| \tag{2.13}$$

d_{delay} is always larger than zero because hypotenuse $|P_{ref}P_{ant}|$ is longer than right-angle side $|P_{ref}P_{LOS}|$ in the right triangle $\Delta P_{ref}P_{LOS}P_{ant}$. If c is speed of light, then time delay t_{delay} is expressed as

$$t_{delay} = \frac{d_{delay}}{c} = \frac{d_{MP} - d_{LOS}}{c} = \frac{|P_{ref}P_{ant}| - |P_{ref}P_{LOS}|}{c} \tag{2.14}$$

During a long-term measurement for the objective sea-surface, the position of ocean wave remote sensing system is fixed, i.e. the height of array antenna H_{ant} is a constant value.

$$\left|P_{ref}P_{ant}\right| = \frac{H_{ant}}{\sin(\beta_{ref})} \tag{2.15}$$

$$\left|P_{ref}P_{LOS}\right| = \left|P_{ref}P_{ant}\right|\cos(\alpha_{el}+\beta_{ref}) = \frac{H_{ant}}{\sin(\beta_{ref})}\cos(\alpha_{el}+\beta_{ref}) \tag{2.16}$$

$$t_{delay} = \frac{\left|P_{ref}P_{ant}\right| - \left|P_{ref}P_{LOS}\right|}{c} = \frac{H_{ant}}{c\sin(\beta_{ref})}\left[1-\cos(\alpha_{el}+\beta_{ref})\right] \tag{2.17}$$

It can be shown that the time delay of the RSFS is based on three parameters, namely, antenna height H_{ant}, elevation of GPS antenna α_{el} and reflection angle β_{ref}. Meanwhile, β_{ref} is also decided by antenna height H_{ant} and the horizontal distance of reflection point P_{ref} to ocean wave remote sensing system $|P_{ref}P'_{ant}|$. For this reason, the time delay of the RSFS is reformulated as

$$t_{delay} = \frac{(\sqrt{{H_{ant}}^2 + \left|P_{ref}P'_{ant}\right|^2}\left[1-\cos(\alpha_{el}+\operatorname{atan}(\frac{H_{ant}}{\left|P_{ref}P'_{ant}\right|}))\right])}{c} \tag{2.18}$$

Conversely, if the relative time delay of the RSFS is given, the horizontal distance of reflection point P_{ref} can be calculated with the following equation.

$$d = H_{ant}\tan\left(2\arctan\left(\frac{\frac{mc}{f_s H_{ant}} - \sin\alpha_{el} - \sqrt{\rho}}{1+\cos\alpha_{el}}\right)\right)^{-1} \tag{2.19}$$

where, $\rho = (\frac{mc}{f_s h})^2 - \frac{2mc}{f_s h}\sin E$, f_s is sampling frequency, m is the number of samples for relative time delay to LOS, $m = t_{delay}/f_s$.

2.3 GPS Receiver

2.3.1 GPS Antenna

Antennae are the first components of a GPS receiver to tune the frequencies transmitted from the GPS satellites and pass the received signal energy to the subsequent components. The GPS antenna can be designed as a single-frequency (L1) or a double-frequency (L1/L2). It is best placed at position with an unobstructed view of the sky over the antenna for acquiring and tracking more satellites.

There are many types of GPS antennae such as monopole, dipole, quadrifilar helix, spiral helix, and microstrip antennae [18]. The rectangular microstrip antenna [19] referred to as the patch antenna is used as the element of the array antenna in the ocean wave remote sensing system.

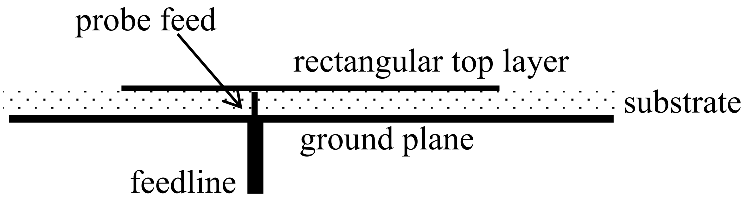

Figure 2-17 Side view of a patch antenna.

Figure 2-17 shows the basic design of a patch antenna. The top layer is a rectangular patch of metal (usually copper), and its length is approximately one-half of the wavelength of GPS signal. The substrate is dielectric and the ground plane is set on other side of it.

The center frequency (f_c) of the patch antenna is approximately determined by its length (L) and permittivity (ε).

$$f_c \approx \frac{c}{2L\sqrt{\varepsilon}} \tag{2.20}$$

where c is the velocity of light in vacuum.

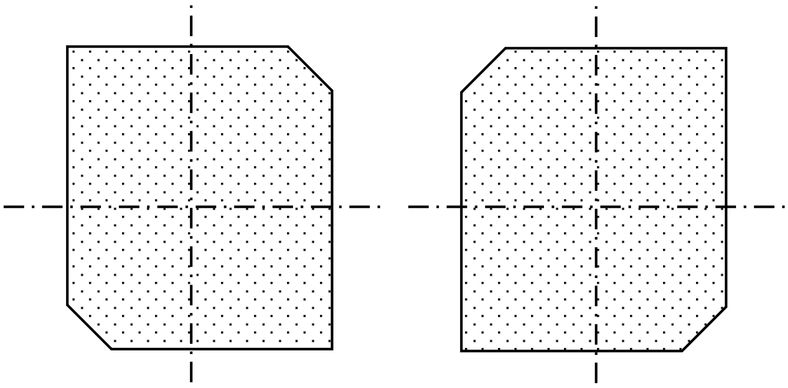

Figure 2-18 One of the polarization techniques of patch antennae.

A conventional GPS antenna has right-hand circular polarization because the signals transmitted by GPS satellites are right-hand circularly polarized. While the signal polarization is changed after the reflection, the GPS antenna used to receive reflected signals has to be designed with left-hand circular polarization. The received signal power will be attenuated significantly if the polarizations of an antenna and a signal are opposites. The polarization of patch antennae can be achieved using truncated corners in the patch. Figure 2-18 shows the rectangular top layer reshaped to achieve two kinds of polarization, RHCP and LHCP.

Combining the directivity of the patch antenna, we can obtain the gain of the patch antenna. The maximum gain of a patch antenna ranges from 6 dBi to 9 dBi and the beam width of them main lobe is over 60 degrees. In practical applications of the proposed ocean wave remote sensing system, the signal intensity reflected from sea-surface is weak and the signals reflected from side directions are undesirable. As a result, single patch antenna cannot be used to receive reflected signals from a specified sea-surface because of its low gain and wide beam width. Consequently, the antenna array composed of a series of patch antennae is used to obtain a high gain and a narrow beam width. The detailed configuration of array antenna will be described in the next chapter.

2.3.2 RF Front-end

The output of antennae are passed to a RF front-end [20, 21] to be processed for extracting and computing more information such as the visible satellite number, ephemeris data, pseudoranges, positions of satellites, and the position of the receiver. The basic processing stages of a RF front-end are amplification, frequency down-conversion, and analog-to-digital conversion. Figure 2-19 shows the basic processing stages of a RF front-end.

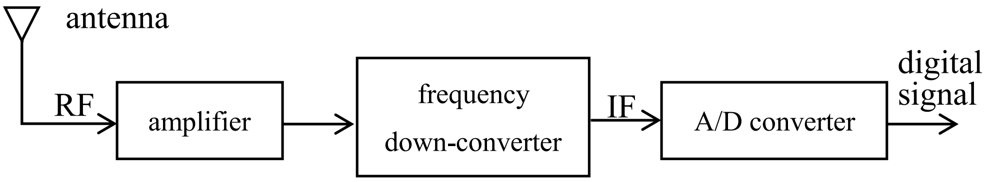

Figure 2-19 Basic processing stages of a RF front-end

The magnitude of the incoming signals of the RF front-end has to be increased because it is so weak that the following components cannot work properly. Therefore the gain of amplifier should be considered. 50 dB gain is usually selected to improve the incoming signal to an appropriate level for the frequency down-converter and Analog-to-Digital Converter (ADC). Then the amplified RF signal is down-converted into Intermediate Frequency (IF) signals. The down-converted IF signal can be sampled with the analog-to-digital converter with a low sampling frequency. The frequency down-conversion is usually handled with mixer and a crystal oscillator, and its processing can be expressed simply with the following equation.

$$\begin{aligned} &\mathrm{A}(t)\mathrm{C}(t)\mathrm{D}(t)\cos(2\pi f_c t)\cos(2\pi f_{co} t) \\ &= \frac{1}{2}\mathrm{A}(t)\mathrm{C}(t)\mathrm{D}(t)[\cos(2\pi(f_c - f_{co})t) - \cos(2\pi(f_c + f_{co})t] \end{aligned} \tag{2.21}$$

where, A, C and D are the amplified signal amplitude, C/A code and navigation date respectively, f_c is the center frequency of GPS signal and f_{co} is the oscillator frequency. The difference frequency f_c - f_{co} is the resultant IF frequency which will be sampled with the analog-to-digital converter. The sampled signals will be processed by several channels of the GPS receiver to acquire and track the visible satellites. According to the sampling theorem, half of the sampling frequency should be larger than bandwidth of the GPS signal. Generally, the bandwidth of GPS signals is about 2 MHz [22, 23], so the sampling frequency is over 4 MHz. However, a 2 MHz bandwidth may not enough for identification of RSFS by the ocean wave remote sensing system. If the bandwidth of the RF front-end is broadened, the sampling frequency of the analog-to-digital converter should be raised. The proper bandwidth of RF front-end will be discussed in section 3.2. And the sampling frequency is also related to the resolution on sea-surface.

2.4 Wave Characteristic Estimation

In this section, estimation methods of wave characteristics are introduced according to the various properties of ocean wave and GPS signals. Here an estimation example is given to explain each necessary processing step. Figure 2-20 shows the situation of the signal receiving near the sea-surface.

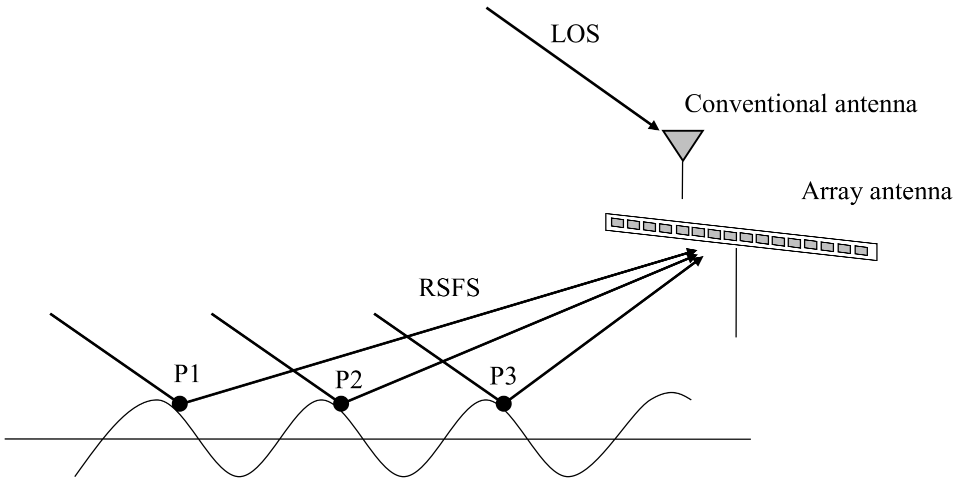

Figure 2-20 Signal receiving near sea-surface.

The array antenna is receiving three relatively strong RSFS from P1, P2 and P3 on the crest of ocean waves, and the conventional antenna is receiving the LOS signal. The received RSFS is a composite signal which can be expressed by the following equation

$$x^k(t) = \sum_{i=1}^{3} A_i(t) C^k(t-\tau_i(t)) D^k(t-\tau_i(t)) \cos(2\pi(f_0 + v_i(t))t + \varphi_i(t)) + e(t) \tag{2.22}$$

where,

x: Composite RSFS;

k: Satellite number;

A_i: Amplitude of the ith RSFS;

D: Navigation data;

C: C/A code;

f_0: L1 carrier frequency;

τ_i : Relative time delay of the i^th^ RSFS to LOS;

v_i: Frequency change of the i^th^ RSFS;

φ_i: Carrier phase offset of the i^th^ RSFS;

e: Noise.

The received signal $x(t)$ is then processed by a RF front-end. Let $y(t)$ denote the output of the mixer of the RF front-end, let B_i denote resultant amplitude of each received RSFS, then $y(t)$ is expressed as

$$\begin{aligned} y^k(t) = \sum_{i=1}^{3} B_i(t) C^k(t-\tau_i(t)) D^k(t-\tau_i(t)) \\ \cos(2\pi(f_{IF}+v_i(t))t+\varphi_i(t))+e(t) \end{aligned} \tag{2.23}$$

Then the digital output signal of the RF front-end is

$$\begin{aligned} \mathrm{y}^k(n) = \sum_{i=1}^{3} B_i(n) C^k(n-m_i(n)) D^k(n-m_i(n)) \\ \cos(2\pi(f_{IF}+v_i(n))n+\varphi_i(n))+e(n) \end{aligned} \tag{2.24}$$

with n in units of $1/fs$ seconds; n indicates the signal is discrete in time. m_i is the number of samples for relative time delay to LOS signal, $m_i = \tau_i/fs$.

If the C/A code components are demodulated, the correlations between received C/A codes and the locally generated C/A code can be calculated. Let $C^k(0)$, $C^k(m_i)$ denote a C/A code of LOS signal without time delay and a C/A code of i^th^ RSFS with relative time delay m_i respectively, and let $C^k(m)$ denote a locally generated C/A code with time delay m. According to the correlation property of C/A code, the correlation between $C^k(0)$ and $C^k(m)$ is formulated as

$$\begin{aligned} & r_0^{kk}(m) = \sum C^k(0) C^k(m), \\ & and \begin{cases} r_0^{kk}(m) \approx 0 & m \neq 0 \\ r_0^{kk}(m) = \dfrac{fs}{1000} & m = 0 \end{cases} \end{aligned} \tag{2.25}$$

and the correlations between $C^k(m_i)$ and $C^k(m)$ are

$$r_i^{kk}(m) = \sum C^k(m_i)C^k(m),$$
$$and \begin{cases} r_i^{kk}(m) \approx 0 & m \neq m_i \\ r_i^{kk}(m) = \dfrac{fs}{1000} & m = m_i \end{cases} \tag{2.26}$$

where r denotes correlation of C/A code.

A high correlation value can be obtained when the locally generated C/A code is aligned perfectly with the C/A codes of RSFS because the sampling frequency f_s is much larger than 1000.

In Figure 2-21, four broken-line equilateral triangle peaks with different magnitudes are used to illustrate the correlator outputs. Let a_0, a_1, a_2, a_3 denote coefficients to adjust the correlation values of LOS signal and the three reflected signals and $a_0 > a_1 > a_2 > a_3$. Consequently the correlation between the C/A codes of LOS signal and the locally generated C/A code is

$$r_{LOS}^{kk} = a_0 r_0^{kk}(m) \tag{2.27}$$

and the correlation between C/A codes of RSFS and locally generated C/A code is

$$r_{\mathrm{MP}}^{kk}(m) = a_1 r_1^{kk}(m_1) + a_2 r_2^{kk}(m_2) + a_3 r_3^{kk}(m_3) \tag{2.28}$$

If relative time delays to the LOS signal are shorter than the time length of one correlation peak, three correlation peaks are usually superimposed to be a polyline, shown as the solid lines in Figure 2-21. Three peak points are circled and m_1, m_2 and m_3 are considered as relative time delays of RSFS to the LOS signal.

However it is difficult to find out the peak points sometimes, especially since some noise components are included. If noise is included, many peaks occur in the correlation so that the RSFS cannot be identitied clearly. Therefore, the discrete time Teager-kaiser energy operator is utilized to identify RSFS from the outputs of correlator. The algorithm of the Teager-kaiser energy operator will be introduced in the next section.

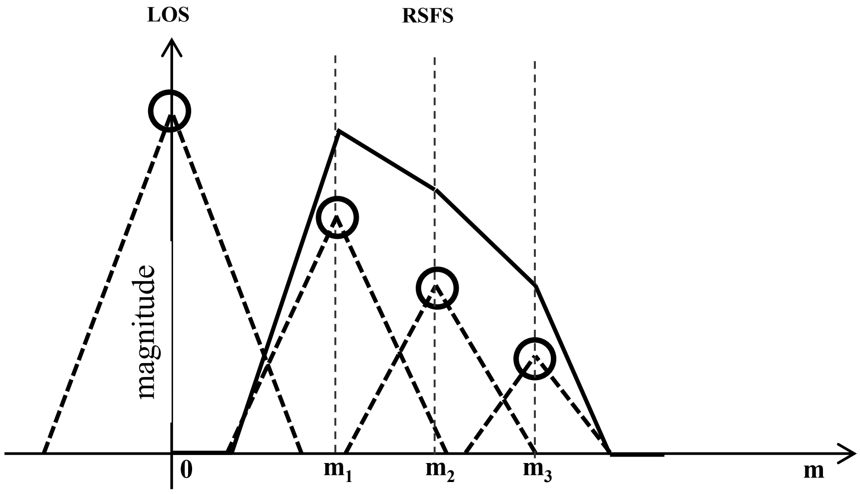

Figure 2-21 Correlator outputs.

2.4.1 Teager-Kaiser Energy Operator

The Teager-Kaiser energy operator [24, 25] is used to estimate the instantaneous energy of a digital signal. At first, the definitions of the continuous time TKEO and the discrete time TKEO are given by

$$\mathrm{TKEO}(t) = \dot{x}^2(t) - x(t)\ddot{x}(t) \tag{2.29}$$

and

$$\mathrm{TKEO}(n) = x^2(n) - x(n-1)x(n+1) \tag{2.30}$$

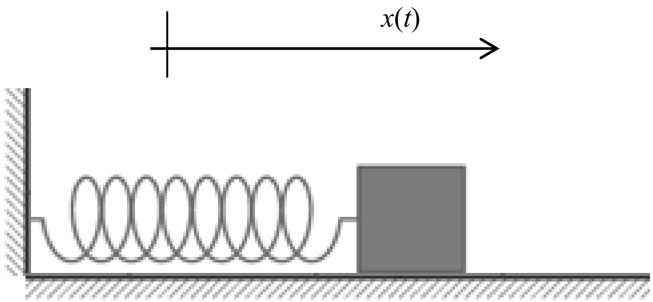

Figure 2-22 An undamped spring-mass system.

As an example, we consider an undamped spring-mass system in Figure 2-22. A mass m is suspended by a string with constant k. The periodic oscillation can is given by

$$x(t) = A\cos(\omega t + \varphi) \tag{2.31}$$

where A is the amplitude of the oscillation, $\omega = \sqrt{k/m}$ is the frequency of the oscillation and φ is the initial phase of the mass.

Therefore, the total energy E of the spring-mass system is the sum of the potential energy of the spring and the kinetic energy of the mass, given by

$$\mathrm{E} = \frac{1}{2}kx^2 + \frac{1}{2}mv^2 \tag{2.32}$$

where v=dx/dt is the speed of the mass. If the speed v(t) and position x(t) at time t are substituted, the energy E becomes

$$\mathrm{E} = \frac{1}{2}m\omega^2 A^2 \tag{2.33}$$

It is obvious that the total energy of the spring-mass system is proportional to the product of the squares of the frequency ω and the amplitude A.

Next, the total energy of the spring–mass system is computed with continuous TKEO and discrete TKEO respectively. The continuous TKEO is expressed with equation 2.29 and the equation of the periodic oscillation x(t) is known, therefore

$$\mathrm{TKEO(t)} = (\text{-A}\omega\sin(\omega t + \varphi))^2 - \mathrm{A}\omega\cos(\omega t + \varphi)(\text{-A}\omega^2\cos(\omega t + \varphi))$$

$$\mathrm{TKEO(t)} = \mathrm{A}^2\omega^2\sin^2(\omega t + \varphi) + \mathrm{A}^2\omega^2\cos^2(\omega t + \varphi) = \mathrm{A}^2\omega^2 \tag{2.34}$$

The continuous TKEO is just the product of the squares of the frequency ω and the amplitude A. As a result, the continuous TKEO can be used to express the total energy of the spring-mass system.

On the other hand, the total energy of the spring–mass system is computed with the discrete TKEO. The digital periodic oscillation of the spring-mass system is given by

$$x(n) = \mathrm{A}\cos(\Omega \mathrm{n} + \varphi) \tag{2.35}$$

Where Ω=2πf/fs=ω/fs is the digital frequency, and f and fs are the analog frequency and the sampling frequency respectively. According to the expression of the discrete TKEO, we need

$$x(n-1) = \mathrm{A}\cos(\Omega(\mathrm{n}-1)+\varphi) \tag{2.36}$$

$$x(n+1) = \mathrm{A}\cos(\Omega(\mathrm{n}+1)+\varphi) \tag{2.37}$$

The produce of the x(n-1) and x(n+1) is

$$x(n-1)x(n+1) = \mathrm{A}^2(\cos(\Omega(\mathrm{n}-1)+\varphi)\cos(\Omega(\mathrm{n}+1)+\varphi))$$

$$x(n-1)x(n+1) = \mathrm{A}^2\cos^2(\Omega n+\varphi) - \mathrm{A}^2\sin^2(\Omega)$$

$$x(n-1)x(n+1) = x^2(n) - \mathrm{A}^2\sin^2(\Omega)$$

$$\mathrm{A}^2\sin^2(\Omega) = x^2(n) - x(n-1)x(n+1) = TKEO(n) \tag{2.38}$$

If the digital frequency Ω small, then the $\sin(\Omega) \approx \Omega$, and the equation 2.38 can be written as

$$TKEO(n) = \mathrm{A}^2\Omega^2 \tag{2.39}$$

Hence we know that the discrete TKEO is proportional to the product of the squares of the frequency ω and the amplitude A. Consequently, we can conclude that both the continuous TKEO and the discrete can express the energy of the spring-mass system. Now an example of computing the energy of a frequency modulated signal.

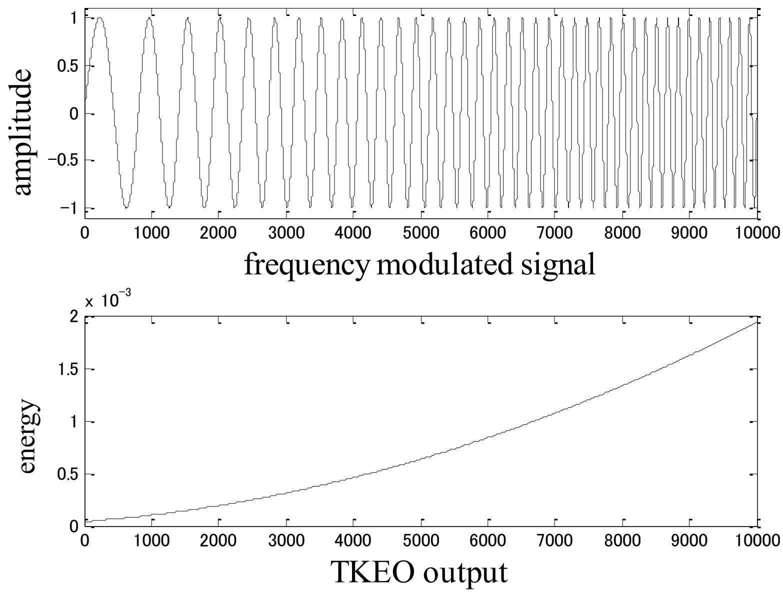

Figure 2-23 TKEO output for frequency modulated signal.

In Figure 2-23, the upper sub-figure shows a frequency modulated sinusoidal signal with amplitude of 1 and increasing frequency, and the lower sub-figure shows the TKEO output of the frequency modulated sinusoidal signal with an increasing trend. It implies that the TKEO can track the variation of the signal frequency. This result also shows that the TKEO can work as a high-pass filter.

In the ocean wave remote sensing system, the discrete TKEO is applied onto correlator output to identify RSFS. The discrete time Teager-Kaiser energy operator for the output of correlator is expressed as

$$TKEO(m) = (r^{kk}(m))^2 - r^{kk}(m-1)r^{kk}(m+1) \tag{2.40}$$

The TKEO is calculated for an equilateral triangle peak of the correlator output is

$$TKEO(m) = \begin{cases} 2r^{kk}(0)\delta - \delta^2 & m = 0 \\ \delta^2 & m \text{ at peak side} \\ 0 & m \text{ out of peak} \end{cases} \tag{2.41}$$

where δ is the magnitude of difference between two consecutive sampling instants on the correlation peak side, i.e. taken anywhere below the magnitude of the peak point. To compare TKEO values between peak point and peak side using

$$\frac{TKEO(0)}{\delta^2} = \frac{2r_{LOS}^{kk}(0)}{\delta} - 1 \tag{2.42}$$

a large value is usually yielded so that an obvious impulse appears.

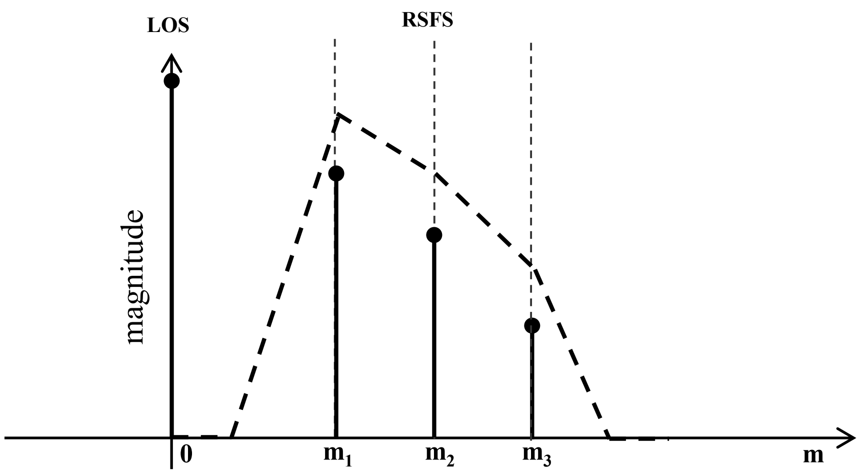

Figure 2-24 Teager output for each signals.

As an example, if the TKEO is resolved for the correlater outputs of the LOS signal and

RSFS, as shown in Figure 2-21, four outstanding peaks at 0, m_1, m_2 and m_3 are obtained, as shown in Figure 2-24.

But the relative time delay of each RSFS is not enough to estimate the wave characteristics. The magnitude of each peak in TKEO output is not constant but fluctuating because of the propagation of the ocean waves. The fluctuation of the magnitude is related to the wave period. Therefore, we try to estimate the wave period from the fluctuation of the magnitude of each peak in TKEO output.

2.4.2 Fourier Transform

The Fourier transform [26, 27] is an operation which translates a signal from the time domain to the frequency domain. Given a signal $x(t)$, its continuous Fourier transform and N-point discrete Fourier transform are given by

$$x(f) = \int_{-\infty}^{\infty} x(t) e^{-i2\pi ft} dt \tag{2.43}$$

$$x(k) = \sum_{n=0}^{N-1} x(n) e^{-i2\pi k \frac{n}{N}} \qquad K = 0,\ldots,N-1 \tag{2.44}$$

In practical, the Fast Fourier Transform is used to compute the discrete Fourier transform efficiently, and we can obtain the frequency characteristics composed of amplitude characteristics $|x(k)|$ and phase characteristics $\angle x(k)$.

Here an example of Fast Fourier Transform is given. The supposition is that there are two sinusoidal signals x1(t) and x2(t) with same frequency (f=0.1Hz). Their phases and amplitudes are different, as shown in Figure 2-25.

$$\mathrm{x1}(t) = \sin(2\pi ft + \pi/2) \text{ and } \mathrm{x2}(t) = 0.5\sin(2\pi ft + \pi/4)$$

With the Fourier transform, the amplitude characteristics and phase characteristics are shown in Figures 2-26 and 2-27. In Figure 2-26, the two peaks stand out at the same frequency of 0.1 Hz, and the phases of the two signals are π/2 and π/4 respectively in Figure 2-27. If these two signals denote the magnitude variations of two peaks in TKEO output, the wave period, wave speed and wave length can be estimated.

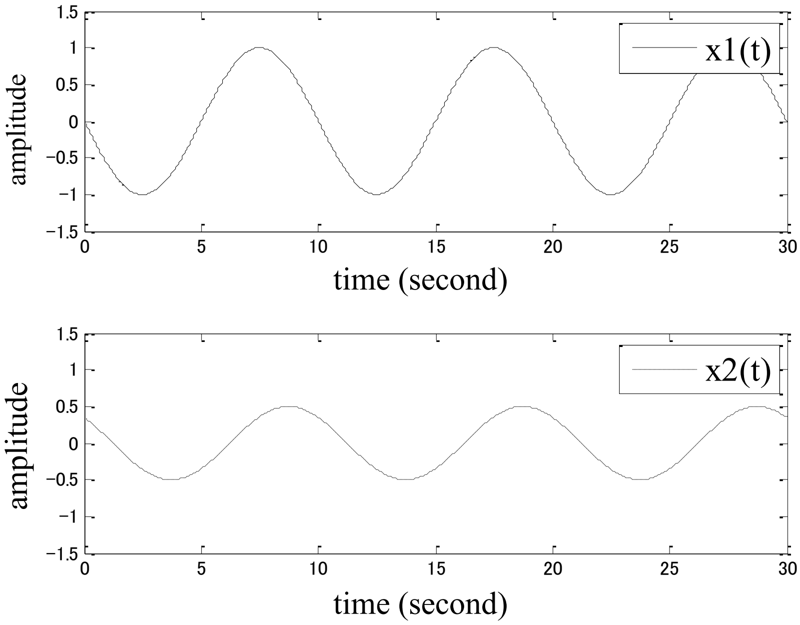

Figure 2-25 Two sinusoidal signals.

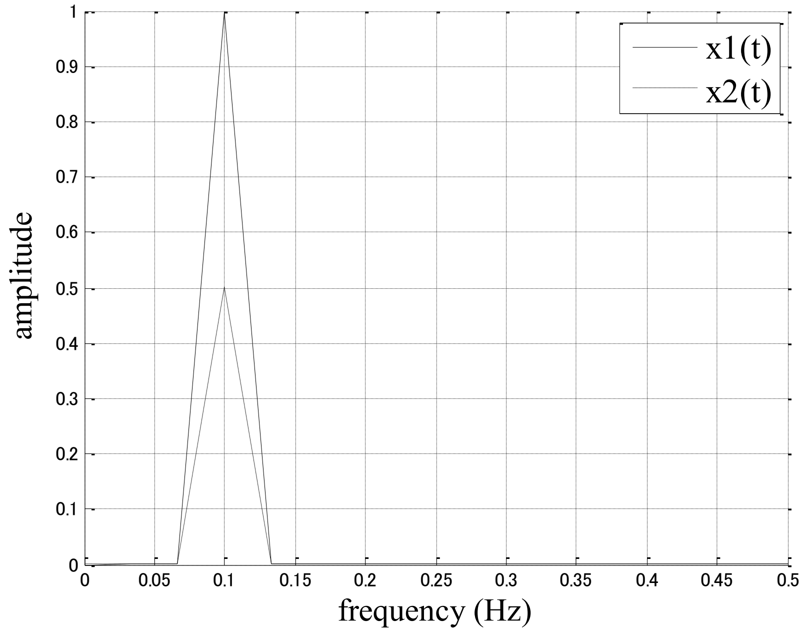

Figure 2-26 Amplitude characteristics.

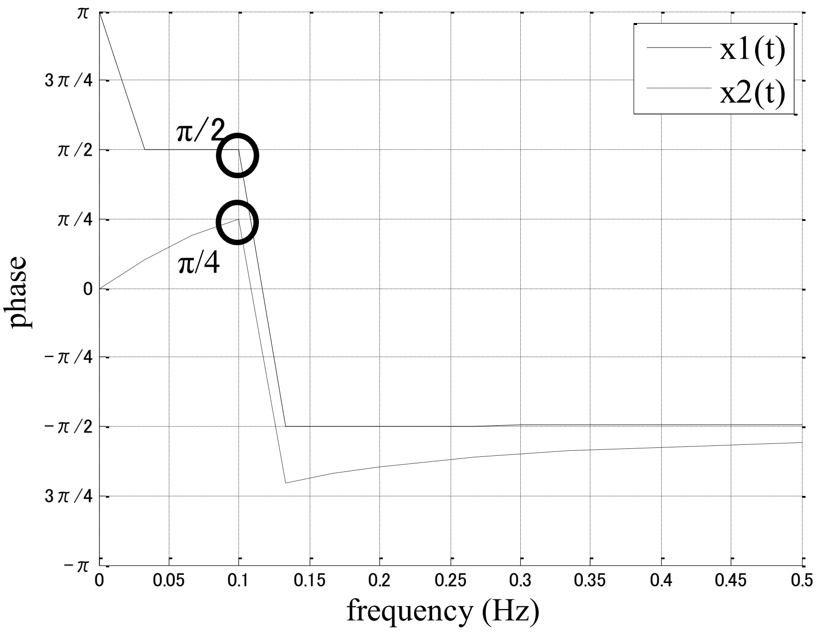

Figure 2-27 Phase characteristics.

Concerning the amplitude characteristics, the frequency indicated by the significant amplitudes is considered as the frequency of big ocean wave. Therefore the wave period (T_s) can be obtained as the reciprocal of the remarkable frequency. On the other hand, the wave speed (V_s) can be estimated with the phase difference $\Delta\varphi$ between the phase characteristics of two fluctuations of TKEO output. The propagation time Δt is proportional to phase difference ($\Delta t = T_s \times \Delta\varphi / 2\pi$) and the propagation distance Δd is the range between two reflection points. Therefore, the wave speed can be calculated as the $V_s = \Delta d / \Delta t$. Finally, the wave length (λ_S) is $\lambda_S = T_s \times V_s$.

2.4.3 Calculation of Wave Characteristics

In the ocean wave remote sensing system, the wave characteristic estimator is developed to estimate wave period, wave speed and wave length. Figure 2-28 shows the functional modules of the wave characteristic estimator.

The Doppler shift and the arrival times of the LOS signal are estimated with the software receiver. The arrival times of the LOS signal are then transferred to the wave characteristic estimator as a time reference to align the arrival times of reflected signals. The correlator resolves correlations for every millisecond RSFS according to the time

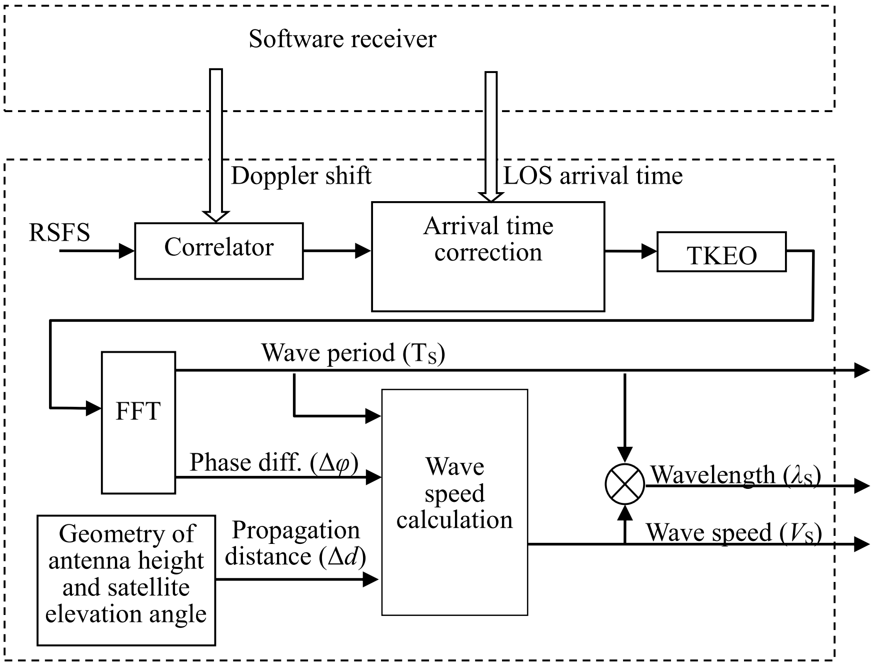

Figure 2-28 Functional modules of wave characteristic estimator.

reference. However the RSFS cannot be identified from a single correlator output because of the low level of carrier-to-noise ratio (C/N_0). After the arrival time correction, the averaging of correlator results can be used to reduce the noise. After that, the TKEO of the averaged correlator outputs are calculated to identify the RSFS. The Fourier transform is used to obtain the amplitude characteristics and phase characteristics. If sea swells exist, the fluctuation of the amplitude characteristics occurs and then the wave period (T_s) and phase difference ($\Delta\varphi$) can be estimated. Finally the wave speed (V_s) and wavelength (λ_S) are also resolved.

Another issue is how to select the objective satellite. Usually, during ocean wave measurement only one GPS satellite is selected, the one which is flying over the objective sea-surface. The satellite elevation impacts reflected signal intensity and measurement resolution. A higher satellite elevation results a lower reflected signal intensity and higher measurement resolution, on the other hand, a lower satellite elevation results a higher reflected signal intensity and lower measurement resolution.

2.5 True Wave Characteristics

The wave characteristics measured in one direction on the objective sea-surface cannot be considered as the true values because the array antenna direction is must not always be in the direction of ocean waves. The direction of ocean waves is even unknown during measurement. Figure 2-29 shows the measurement errors of wave characteristics. The two parallel lines denote the crests of two waves; the arrow perpendicular to these two waves shows the wave direction; and the other arrow is the antenna direction pointing to the array antenna. The included angle θ is equal to the difference angle between the wave direction and the antenna direction. Therefore the true wavelength is |PO| and the measured wavelength is |PA|, and

$$|PO| = |PA|\cos(\theta) \tag{2.45}$$

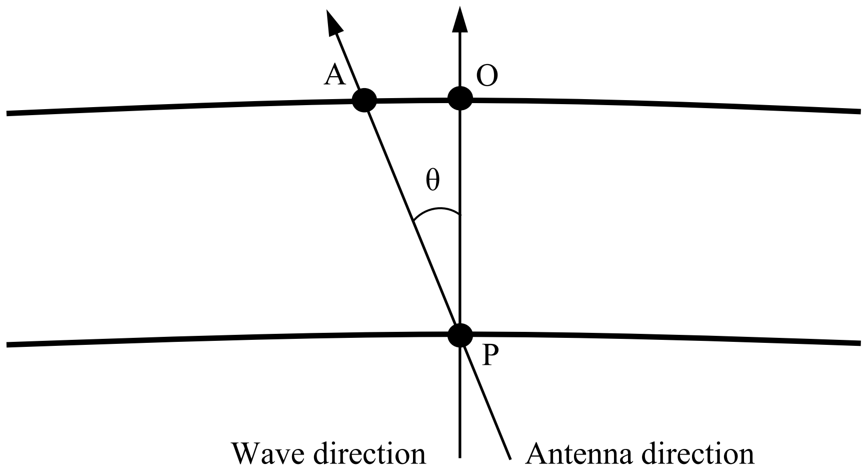

Figure 2-29 Measurement errors of wave characteristics.

Usually the difference angle is not zero so that the measurement error of wavelength is inevitable. It is obvious that the measured wavelength is longer than the true wavelength. Nevertheless, the measured wave period is almost the true wave period because the system observes the wave propagates from P to A during the wave propagates from P to O. As a result, the measured wave speed is not the true wave speed because the system observes the wave propagates a longer distance |PA| than |PO| in the same wave period, in other words the measured wave speed is larger than the true wave speed.

If the true wave direction is unknown, the difference angle θ cannot be determined. So the true wave speed and the true wave length cannot be estimated correctly. Hereon, two proposals are suggested to estimate the true values of wave characteristics. This first one uses two ocean wave remote sensing systems to measure the wave characteristics in two directions simultaneously, referred to as Double Systems Double Direction (DSDD); the second one uses only one system to measure wave characteristics in two directions separately, referred to as Single System Double Directions (SSDD). The detailed methods will be introduced in the following sub-sections.

2.5.1 Double Systems Double Directions

The Double Systems Double Directions is configured with two ocean wave remote sensing systems which have two intersecting bore sights on the objective sea-surface, as shown in Figure 2-30. Each array antenna denotes one ocean wave remote sensing system. P is the intersection point fixed by the bore sights. Although these two systems measure the identical sea-surface circled with a dashed line, the results of wavelength |PA| and |PB| are generally different because these two systems don't necessarily measure the true wave direction.

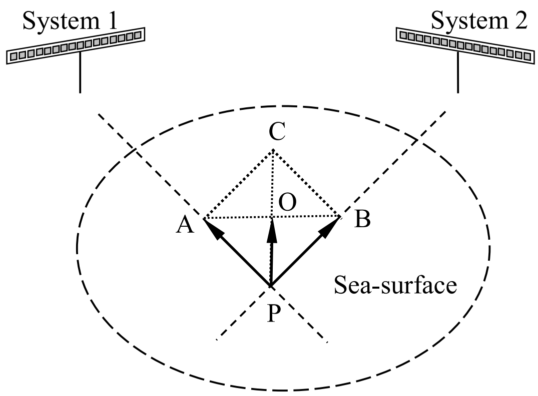

Figure 2-30 Double systems double directions.

If a parallelogram PACB is established on the sea-surface with two adjacent sides |PA| and |PB| and, its diagonal |PC| pointing to seashore just points to the true wave direction and a half-length of this diagonal, |PO|, is considered as the true wavelength. The two systems receive the RSFS from the identical objective sea-surface simultaneously and the true wavelength can be estimated with two resultant wavelengths. Similarly, the true wave speed can also be estimated with two resultant wave speeds using the relationship of the vectors as shown in Figure 2-30.

2.5.2 Single System Double Directions

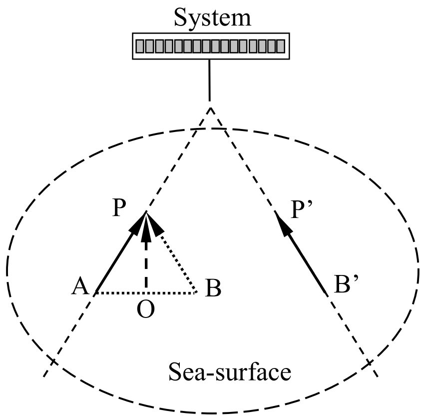

Figure 2-31 Single system double directions.

The Single System Double Directions uses one ocean wave remote sensing system to measure true values of wave characteristics, as shown in Figure 2-31. The system denoted by the array antenna measures two different wavelengths |AP| and |B'P'| in two directions on the objective sea-surface. A triangle APB is established by translating the vector B'P' until point P' and point P are combined. The perpendicular line |OP| points to the true wave direction and its length is the true wavelength. The single system can also measure the true wave speed if the relationship of the vectors in Figure 2-31 are used to the resultant wave speeds in two directions.

Each of these proposals has its advantages and disadvantages. The DSDD has to be made with two systems but the wavelengths are measured from the same ocean wave propagations because the data recording can be performed simultaneously; the SSDD can work with only one system but the wavelengths have to be measured from different ocean waves. Moreover, the data recording time will be almost double that of DSDD. However, in any proposals, two objective satellites over the objective sea-surface are need when the measurements are performed.

References

[1] R. S. Johnson, "A Modern introduction to the mathematical theory of water waves", Cambridge University Press, pp.62-64, 1997.

[2] S. R. Massel, "Ocean surface waves: their physics and prediction", World Scientific, pp.95-96, 1996.

[3] R. H. Stewart, "Introduction To Physical Oceanography", Orange Grove Books, pp.272-287, 2009.

[4] Ben Marcus, "The Surfing Handbook: Mastering the Waves for Beginning and Amateur Surfers", MVP Books, pp.108, 2010.

[5] S.L. Durden and J. F. Vesecky, "A physical radar cross-section model for a wind-driven sea with swell", IEEE Journal of Oceanic Engineering, Vol.10, pp.445-451, 1985.

[6] Richard E. Thomson, "Oceanography of the British Columbia coast", Dept. of Fisheries and Oceans, pp.119-123, 1981.

[7] Shuanggen Jin, Estel Cardellach, Feiqin Xie, "GNSS Remote sensing, Theory Methods and Applications", Springer, pp192-199, 2014.

[8] Arnaud Coatanhay, Ali Khenchaf, "Model of GPS signal from the ocean based on an electromagnetic scattering theory: a Two Scale Model (TSM) approach", IGARSS '05. Proceedings. 2005 IEEE International, Vol. 5, pp.3200-3203, July 2005.

[9] Leo H. Holthuijsen , "Waves in Oceanic and Coastal Waters", Cambridge University Press, pp11-23, 2007.

[10] Yunja Yoo, "Wave Direction Measurement Method Using GPS Buoy for Safety Navigation", Sept. 2007.

[11] Jonathan S. Bathgate, Malcolm L. Heron, and Arnstein Prytz, "A Method of Swell-Wave Parameter Extraction From HF Ocean Surface Radar Spectra", Oceanic Engineering, IEEE Journal of (Volume:31 , Issue: 4), pp.812-818. Oct. 2006.

[12] C. R. Jackson J. R. Apel, "Synthetic Aperture Radar Marine User's Manual", U.S.

Department of Commerce, National Oceanic and Atmospheric Administration, pp.9-10 and pp.140-141, Sept. 2004.

[13] U.S. Government Department of Defense, "Global Positioning System Standard Positioning Service Signal Specification", Second Edition, 1995.

[14] Tao Hu, "Controlled Indoor GPS Signal Simulation", Department of Geomatics Engineering, University of Calgary, pp.10-13 Jan. 2006.

[15] Rao, "Global Navigation Satellite Systems", Tata McGraw-Hill Education, pp.93-96, 2010.

[16] K. Borre, D. M. Akos, N. Bertelsen, P. Rinder, S. H. Jensen, "A software-defined GPS and galileo receiver: A single-frequency approach", Springer, pp.25-26, 2007.

[17] Bruce M. Hannah, "Modelling and Simulation of GPS Multipath Propagation", the cooperative research center for satellites system Queensland University of Technology, March 2001.

[18] S. Gopi, "Global Positioning System: Principles And Applications", Tata McGraw-Hill Education, pp.90-93, 2005.

[19] T. Edling, "Design of circular polarized dual band patch antenna", Uppsala university, 2012.

[20] J. M. Samper, R. B. Pérez, J. M. Lagunilla, "GPS & Galileo: Dual RF Front-end Receiver and Design, Fabrication, and Test", Communication Engineering, McGraw-Hill Professional, pp.61-122, 2008.

[21] F. Piazza, Q. Huang, "A 1.57-GHz RF Front-End for Triple Conversion GPS Receiver", IEEE Journal of Solid-State Circuits , Vol. 33, No. 2, pp.202-209, 1998.

[22] Tsui, "Fundamentals of global positioning system receivers: a software approach", vol.173 of Wiley Series in Microwave and Optical Eng., John Wiley & Sons, pp.330, 2005.

[23] NovAtel Inc., "Discussions on RF signal propagation and multipath", Calgary, Alberta, Canada, T2E 8S5, pp.9, Feb. 2000.

[24] K. Eivind, "Signal processing using the Teager Energy Operator and other nonlinear

operators", Candidatus Scient thesis, University of Oslo Department of Informatics, 2003.

[25] H. Ridha, R. Markku and H. Taneli, "Teager-Kaiser Operator Based Filtering", Tenth European Signal Processing Conference, EUSIPCO'-2000, Tampere, Finland, pp. 545-1548, 2000.

[26] K. Morita, "Applied Fourier Transform", John Wiley & Sons, pp.1-5, 1995.

[27] R. J. Beerends, "Fourier and Laplace Transforms", Cambridge University Press, pp.60-80, 2003.

CHAPTER 3

SYSTEM CONFIGURATION

The ocean wave remote sensing system estimates wave characteristics using two signal channels: LOS channel and multipath channel. The signals transmitted in these two channels are received simultaneously. As shown in Figure 1-3 in Chapter 1, the ocean wave remote sensing system contains two sub-systems to process these two signals. The sub-system processing the LOS signal includes the conventional antenna, the conventional GPS receiver and the software receiver. These three main components can be obtained from market. However the sub-system processing the RSFS has to be developed by ourselves because of the special characteristics of the array antenna and the RF front end, and the special processing steps of the wave characteristic estimator. Therefore, this chapter will focus on the configurations and developments of the array antenna, the RF front-end and the wave characteristic estimator.

Based on the development of these special equipment and software, we developed the prototype of the ocean wave remote sensing system. Then the ocean wave remote sensing system was evaluation with the numerical simulation and the experiments which will be introduced in next chapter.

3.1 Array Antenna

3.1.1 Directional Pattern

GPS antennae are usually considered as a part of GPS receivers. A conventional GPS antenna for positioning and navigation has a wide directional pattern to receive information from as many satellites as possible. In general, the antenna gain towards the zenith is high while it gradually decreases towards the horizon, and the peak gain can reach several dBi. That kind of antenna can receive not only the GPS signals transmitted directly from satellites but also the reflected signals, i.e. multipath propagations of GPS signals. In the proposed ocean wave remote sensing system, however, the desirable reflected signals should come from the objective sea-surface, that is to say, the reflected signals from other areas are undesired and should be removed or attenuated. Therefore, the array antenna [1, 2] which has a directional pattern has been decided to be utilized to receive signals from specified direction.

Here, we consider the Uniform Linear Array (ULA) in which the elements are identical and denoted with black points. They are aligned in a straight line with equal separations (*d*), as shown in Figure 3-1.

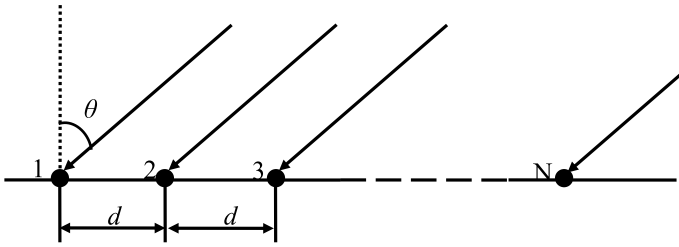

Figure 3-1 Configuration of uniform linear array antenna.

According to the antenna theory, the receiving pattern of the uniform linear array antenna is expressed by the array pattern multiplication property, i.e. the array pattern is the product of the antenna element pattern multiplied with an array factor.

$$F(\theta) = AF(\theta)\mathrm{R}(\theta) \tag{3.1}$$

where θ is the signal reception angle relative to the array. $F(\theta)$ is the receiving pattern of the array antenna, $AF(\theta)$ is the array factor and $R(\theta)$ is the radiation pattern of single antenna element. In addition, the radiation pattern of antenna has identical shape to its receiving pattern according to the reciprocity [3 ,4]. Here the array factor of the uniform linear array is

$$AF(\theta) = \frac{\sin(\frac{N}{2}kd\cos(\theta))}{\sin(\frac{1}{2}kd\cos(\theta))} \tag{3.2}$$

where $k = 2\pi/\lambda$, N is the number of the elements. If dipole patch antennae are used as the elements,

$$R(\theta) = \frac{\cos(\frac{\pi}{2}\cos(\theta))}{\sin(\theta)} \tag{3.3}$$

the antenna pattern can be described as follows,

$$F(\theta) = \frac{\cos(\frac{\pi}{2}\cos(\theta))}{\sin(\theta)} \frac{\sin(\frac{N}{2}kd\cos(\theta))}{\sin(\frac{1}{2}kd\cos(\theta))} \tag{3.4}$$

If the distance d is set to be half of wavelength of electromagnetic wave and 16 patch antennae are aligned, the antenna pattern becomes

$$F(\theta) = \frac{\cos(\frac{\pi}{2}\cos(\theta))}{\sin(\theta)} \frac{\sin(8\pi\cos(\theta))}{\sin(\frac{\pi}{2}\cos(\theta))} \tag{3.5}$$

Consequently, the ideal directional pattern of the array antenna is illustrated in Figure 3-2. The directional pattern has a narrow fan-beam on the broadside with which the signals from the broadside are enhanced and the others from side directions are diminished. The 3 dB beam width is about 10 degrees.

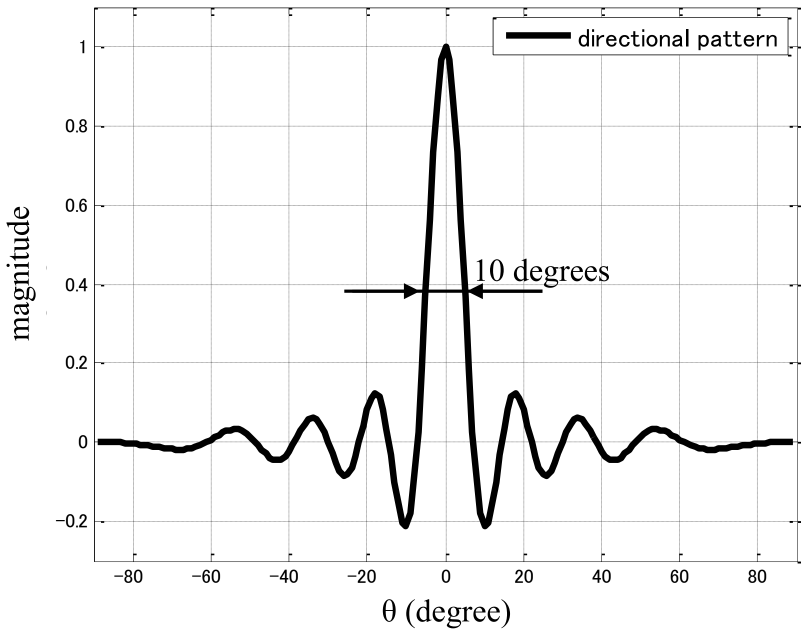

Figure 3-2 Ideal directional pattern of the array antenna.

3.1.2 Antenna Construction

The array antenna is designed and constructed to receive GPS signals reflected from the sea-surface. It is a uniform linear antenna array made up of 16 elements of LHCP GPS patch antennae spaced in half wavelengths (approximately 95.2 mm). Figure 3-3 shows the configuration details of the array antenna. The 16 patch antenna elements are fixed and aligned in a horizontal line.

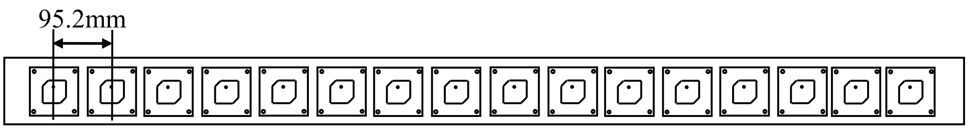

Figure 3-3 The construction of array antenna.

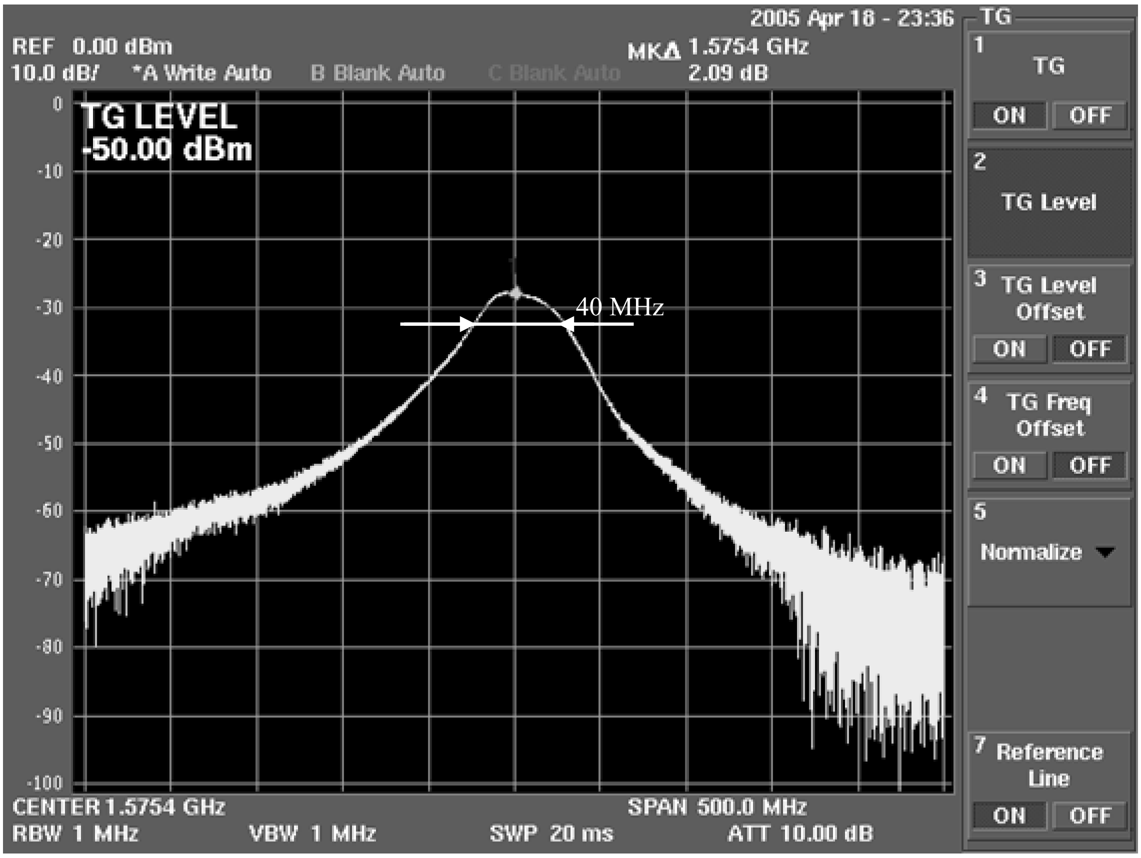

Figure 3-4 Frequency characteristics of the pre-amplifier.

Considering the line loss of long cables connected with a receiver and the weak signals reflected from far away, a high gain pre-amplifier is mounted as a part of the array antenna.

Figure 3-4 show the frequency characteristics of the pre-amplifier. The transmitter sends the signals with the level of -50 dBm. The intensity of the output signals of the pre-amplifier is -28 dBm. The total gain of the pre-amplifier is about 32.3 dBm if the 10.3 dBm loss of the testing system is considered.

The bandwidth of the pre-amplifier is estimated to be about 40 MHz. That means that the center frequency and the bandwidth of the output signal of the array antenna are 1575.42 MHz and 40 MHz respectively.

Figure 3-5 and Figure 3-6 show the photos of the front and the rear of the array antenna with two conventional antennae of the GPS compass on its sides. The array antenna is installed on a rotatable tower with which the direction of the array antenna can be changed 360 degrees in the horizontal direction and 90 degrees in the vertical direction. The direction of the array antenna should be adjusted smoothly according to the GPS compass when the azimuth of the objective satellite changes. The rear is covered with a piece of wire cloth to strengthen the electromagnetic shield and to mitigate reflected signals from its behind.

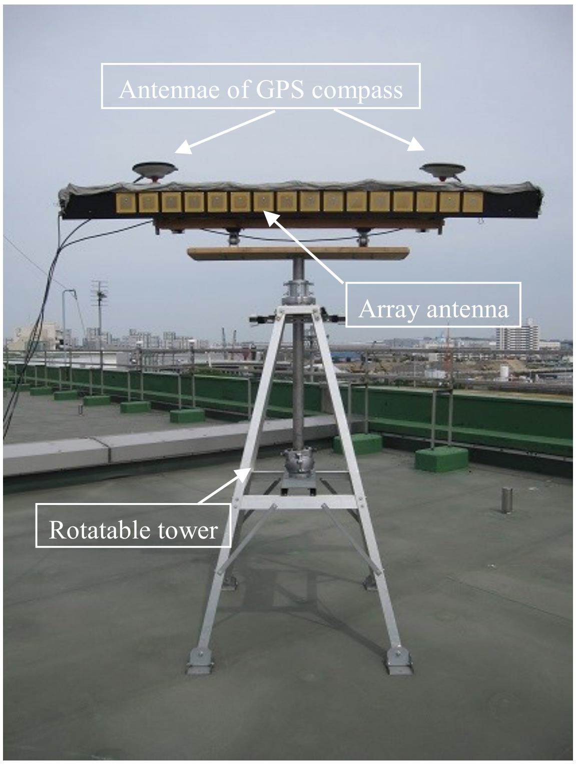

Figure 3-5 Front of the array antenna.

Figure 3-6 Rear of the array antenna.

3.1.3 Antenna Testing

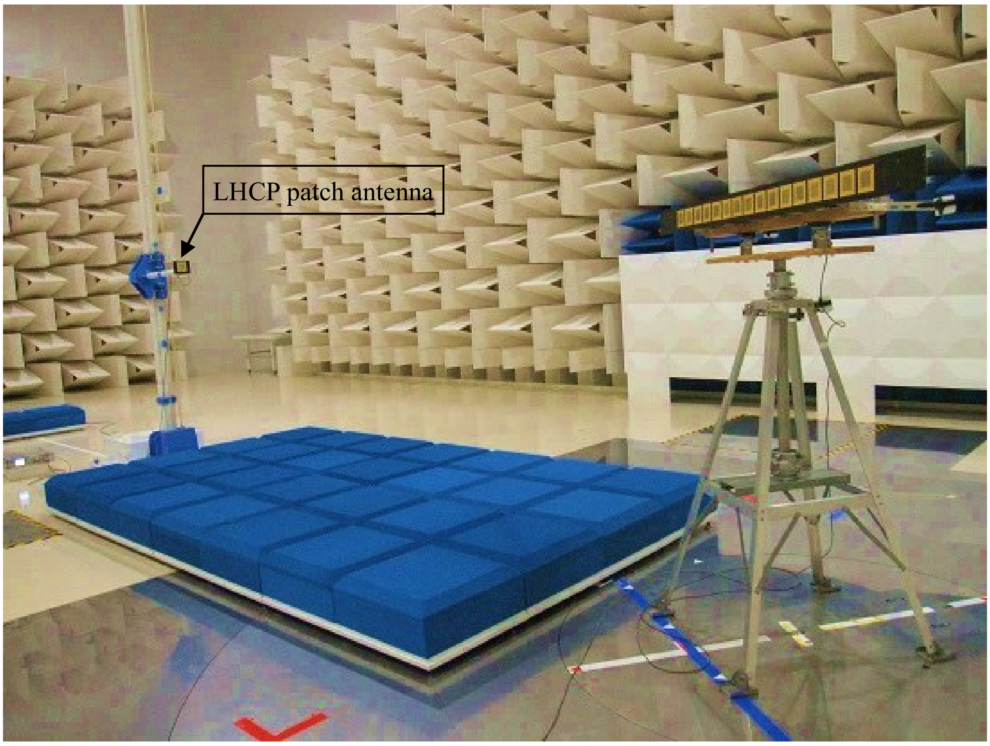

Figure 3-7 Array antenna test in the electromagnetic wave anechoic chamber.

The directional pattern of the array antenna was tested in the electromagnetic wave anechoic chamber at the Furuno Electric Company, as shown in the Figure 3-7. In the electromagnetic wave anechoic chamber, the one patch antenna transmitter emitted LHCP 110 dB (μV) 1575.5 MHz UHF signals. The array antenna was set 10 meters away from the transmitter. The walls of the room could absorb the reflections of electromagnetic waves completely. Therefore the signals received with the array antenna were considered as the signals transmitted by the patch antenna directly. During test, the array antenna turned 360 degrees slowly to generate the 360-degree directional pattern or antenna' gain (dB) with and without wire cloth.

The measurements of the antenna' gains (dB) of a single LHCP GPS patch antenna was also made in the electromagnetic wave anechoic chamber under the same condition. The patch antenna has a gain of about 5dBi. Therefore, the gain (dBi) of the array antenna relative to isotropic antenna can be obtained using the measured antenna' gains (dB) of the arrayed antenna and the patch antenna.

$$GA_{dBi} = GA_{dB} - GP_{dB} + 5_{\text{dB}} \quad (3.6)$$

where GA_{dBi} is the array antenna gain in dBi, GA_{dB} is the array antenna gain in dB, and GP_{dB} is the patch antenna gain in dB. It should be noted that the high gain of the array antenna is also contributed partially by the pre-amplfier mounted as a part of the antenna.

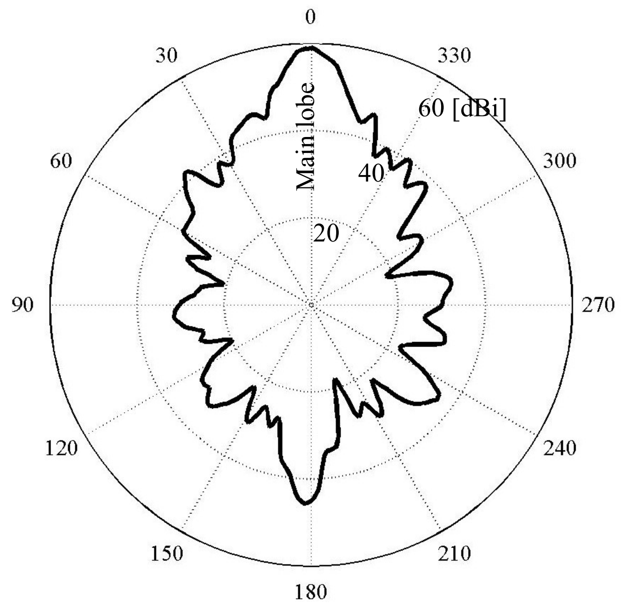

Figure 3-8 Directional pattern of array antenna (without wire cloth).

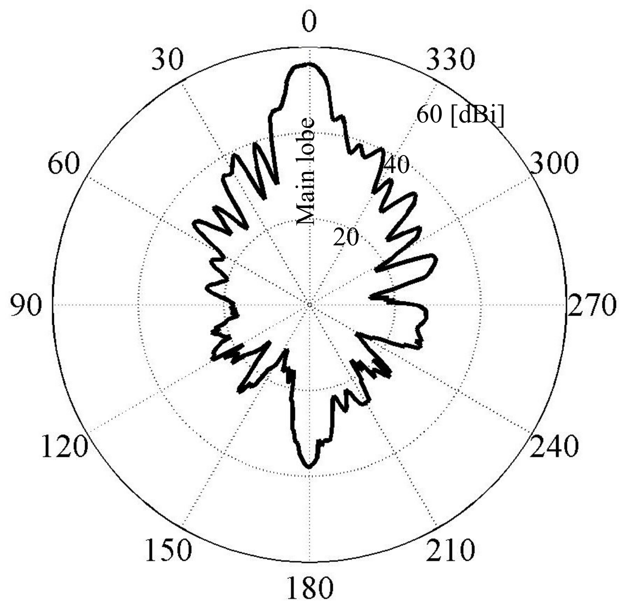

Figure 3-9 Directional pattern of array antenna (with wire cloth).

Figure 3-8 and 3-9 shows the directional patterns of the array antenna in horizontal plane by the dBi with and without wire cloth. By comparing these two figures, we found that the side lobes of the directional pattern are diminished if the wire cloth covered. In particular, the back lobe is cut off by 10 dB. Therefore, the wire cloth is necessary and effective in order to achieve a narrow fan beam directional pattern of the array antenna.

3.2 RF Front-end

3.2.1 Bandwidth Determination

In the GPS applications of positioning and navigation, the bandwidth of the IF signals in the conventional GPS receiver is consistent with the transmitted signal bandwidth set to 2 MHz to attenuate noise. However, a bandwidth of 2 MHz is not sufficient to identify each RSFS. We need to determine an appropriate bandwidth for RSFS detection. The bandwidth effects are shown in two aspects. One is the band-limited effects of the RF front-end, and the other is the band-limited effects of the TKEO. The former explains how the bandwidth deforms the output of RF front-end and the latter shows whether the TKEO is able to identify each RSFS or not.

The signal bandwidth is limited by the bandwidths of elements in the array antenna and the RF front-end. As the bandwidth of the array antenna is 40 MHz, 40 MHz can be selected as the maximum signal bandwidth.

Band-limited effects of RF front-end

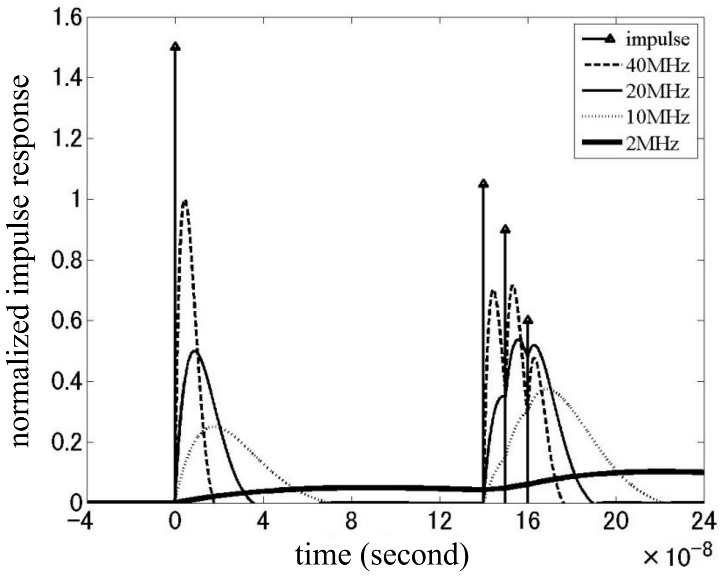

Figure 3-10 Band-limited effects of RF front-end

The band-limited effects of RF front-end are demonstrated with the impulse responses [5] of an impulse series. We suppose that the input signals of the RF front-end include the LOS signal and several RSFS, as shown in Figure 3-10. The LOS signal is received at 0 and three RSFS are received at 14, 15 and 16 microseconds respectively, namely the time interval of each RSFS is 0.01 microseconds which is consistent with sampling period in the ocean wave remote sensing system. The vertical straight lines denote the impulse signals and other curves are the impulse responses for different bandwidths.

Firstly, a 2 MHz bandwidth is used but the impulse responses (heavy line) does not show any shape coincident with the input impulse series. The signals cannot be distinguished at all. Secondly, the bandwidth is broadened to be 10 and 20 MHz respectively. The signals can hardly be separated from each other in the impulse responses (dot line and fine line). Finally, the total bandwidth of 40 MHz is evaluated and there are several peaks in its impulse responses (dash line) so that the each RSFS can be easily identified. Therefore, 40 MHz is chosen as the bandwidth of RF front-end.

The RSFS ought to be detected with TKEO but not the output signals of the RF front-end. However it is still unknown whether the TKEO can identify each RSFS with 40 MHz bandwidth or not. In the following discussions, the band-limited effects of TKEO are evaluated to show that 40 MHz is a proper bandwidth.

Band-limited effects of TKEO

Here the four GPS signals at each impulse position as shown in Figure 3-11 are used to examine the band-limited effects of TKEO. The Figure 3-11 (a) shows the series of GPS signals. Figure 3-11 (b) ~ (e) shows the calculated TKEO outputs with 2, 10, 20, and 40 MHz bandwidths respectively. The circles represent the TKEO outputs, and the black circles denote the TKEO outputs at signal positions.

In Figure 3-11 (b), there are no outstanding values because the TKEO outputs steadily increase. In Figure 3-11 (c) and (d), the black circles cannot be distinguished clearly from other while circles. In Figure 3-11 (e), the three outstanding black circles come out and can be identified from the white circles using 40 MHz bandwidth. Consequently, it is confirmed that the 40 MHz bandwidth is the appropriate selection for the RF front-end.

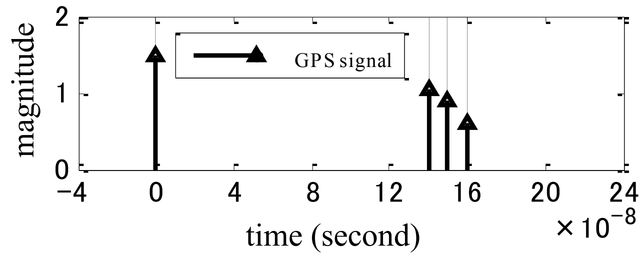

(a) A series of GPS signals.

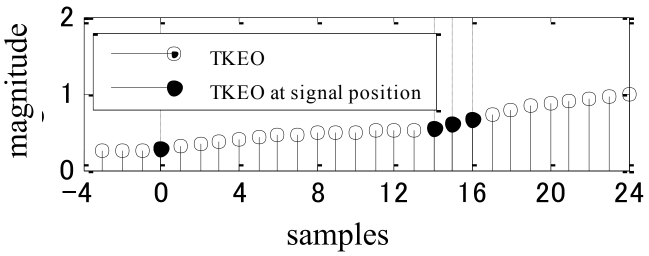

(b) TKEO outputs (BW=2MHz).

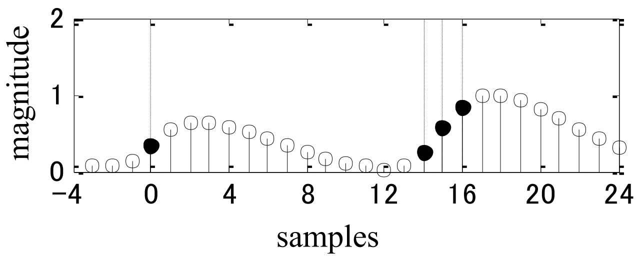

(c) TKEO outputs (BW=10MHz).

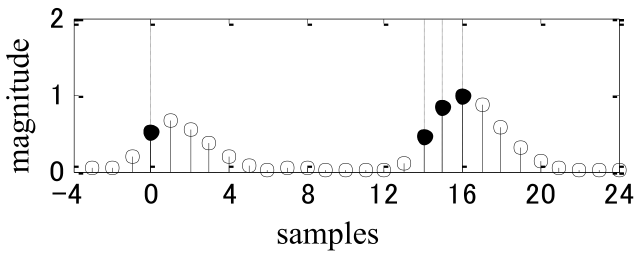

(d) TKEO outputs (BW=20MHz).

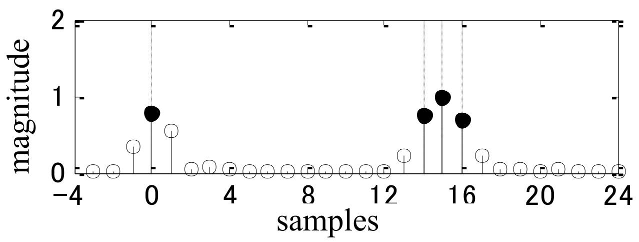

(e) TKEO outputs (BW=40MHz).

Figure 3-11 Band-limited effects of TKEO.

3.2.2 Design of RF front-end

The block diagram of RF front-end is shown in Figure 3-12. The incoming signal at the left side has the center frequency of 1575.42 MHz and the bandwidth of 40 MHz. The first component, an amplifier, is used to raise weak signals to an appropriate magnitude because the GPS signal power reflected from sea-surface is so weak that it is not strong enough to be processed by following components. The Voltage Controlled Oscillator (VCO) generates 1400MHz oscillator signals for mixer in which the signal is down-converted to an IF with the center frequency of a 175.42MHz. The Analog-to-digital converter has up to a 100 MHz sampling frequency.

The down-converted IF signal has 175.42 MHz center frequency larger than the 100 MHz sampling frequency, therefore the under-sampling frequency technique is utilized. The under-sampling [6] processing translates the all frequency components into the 1st Nyquist Zone from DC to 50 MHz (half of the sampling frequency) without aliasing, and the center frequency of the A/D converter output is translated from the 175.42 MHz to 24.58 MHz.

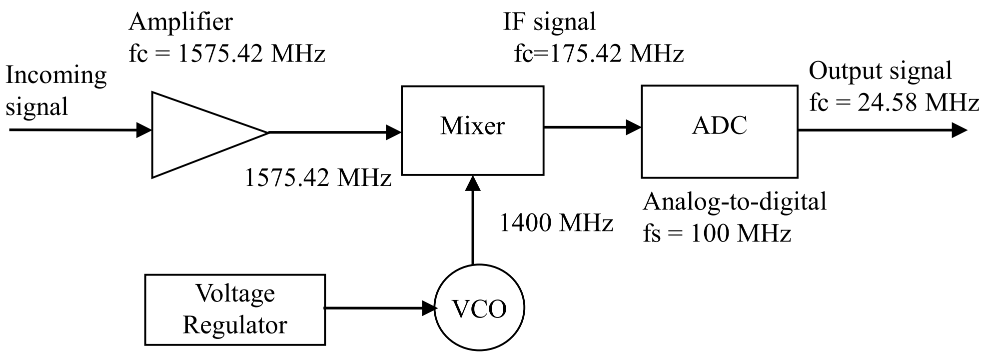

Figure 3-12 RF front-end.

3.2.3 GP2015 Based Front-end

Usual commercial front-end cannot satisfy the desired conditions of a 40MHz bandwidth. In the ocean wave remote sensing system, the RF front-end GP2015 [7] made by Zarlink Semiconductor Inc. is chosen to provide the crucial functional unit of the designed RF front-end.

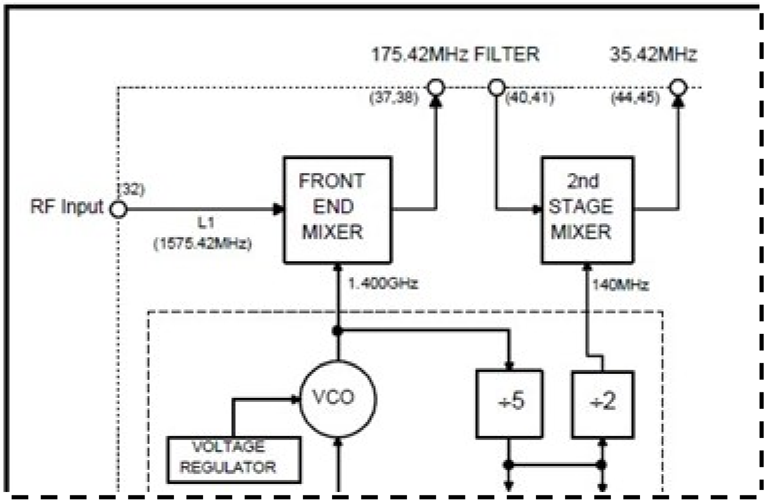

Figure 3-13 Part of the block diagram of GP2015.

Figure 3-13 shows a part of the block diagram of the RF front-end GP2015. The first down-conversion stage satisfies the design of our RF front-end. The 38^{th} pin provides the IF output with 175.42 MHz center frequency, especially the 40 MHz bandwidth of the incoming signal (RF input) is maintained.

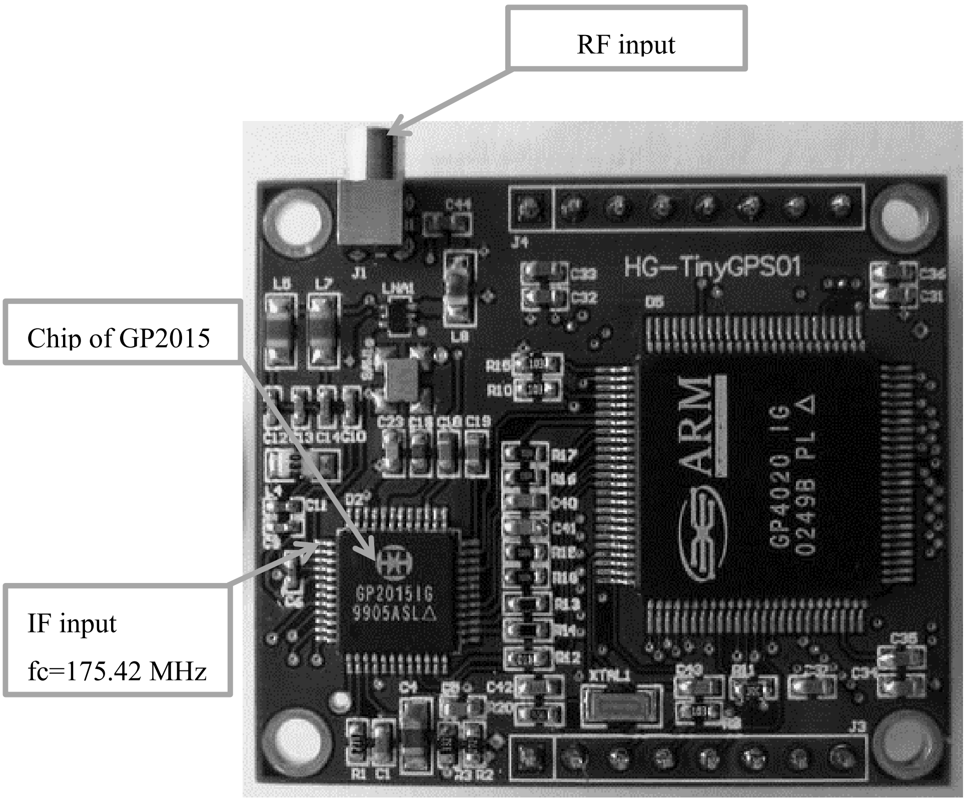

Figure 3-14 Evaluation board of GP2015

Figure 3-14 shows the evaluation board. This evaluation board is designed for common navigation applications so that that sampling frequency is low. Therefore, we have to connect the 38th pin with an external 100 MHz ADC. The NI PXI-5122 high-speed digitizers made by National Instruments converts the analog IF output of the mixer into digital signals with 100MHz sampling rate.

3.3 Wave Characteristic Estimator

Until now the configurations of the array antenna and the RF front-end have been described in this chapter. During ocean wave measurements, the LOS signal and the reflected signals transmitted by the objective satellite are recorded synchronously, and the digitalized signals are recorded by a hard disc drive and processed in the off-line mode with the wave characteristic estimator. The detailed processing methods are discussed in this section.

3.3.1 Processing of LOS signal

The necessary information extracted from the LOS signal is the Doppler shift and the arrival time of the LOS signal, while the azimuth and the elevation of the satellite are provided with a conventional GPS receiver. The Doppler shift is a relative change of the center frequency of GPS signal. Before processing the massive signals continuously the shifted center frequency has to be obtained to avoid searching the center frequency at any single correlation calculation, which always exists and has an almost constant value over a short term. The arrival time of the LOS signal is used as a time reference to align the calculation results of correlator. The arrival time of LOS cannot be estimated precisely from RSFS because of the severe fading of the RSFS. The Doppler shift [8] f_d is expressed as

$$f_d = \frac{\Delta v}{c} f_c \tag{3.7}$$

where Δv is the velocity of the satellite with respect to the receiver, f_c is the center frequency 1575.42 MHz and c is the velocity of light.

In practice, the Doppler shift f_d is not calculated with the above equation because the velocity which is Δv is unknown. The Doppler shift is estimated with correlation results calculated with different frequencies around f_c. If the signals of objective satellite are contained in the received signals, the correlation will yield a remarkable value when the precise shifted center frequency is used.

The arrival time of the LOS is estimated with the LOS channel. Generally the position of the maximum value of the correlation result in the time length of one C/A code (1 ms) indicates the arrival time of the LOS. But it is largely affected by the Doppler shift, unstable ionospheric delay and multipath so that a continuous series of arrival times of the LOS has an obvious decreasing or increasing trend caused by the Doppler shift and small disturbances caused by the ionospheric delay and multipath. Usually, the trend is corrected with the Least-Squares line method for a short term, and the small disturbances are removed with the Least-Squares higher degree polynomials.

3.3.2 Processing of RSFS

The calculation of correlation is the core function of the wave characteristic estimator. The estimations of the Doppler shift and the arrival time of the LOS are also based on the correlation results. For this reason, the calculation method of the correlator is introduced. There are several correlation algorithms we can choose. The processing of the efficient method referred to as Parallel Code Phase Search Acquisition [9] is chosen, as shown in Figure 3-15.

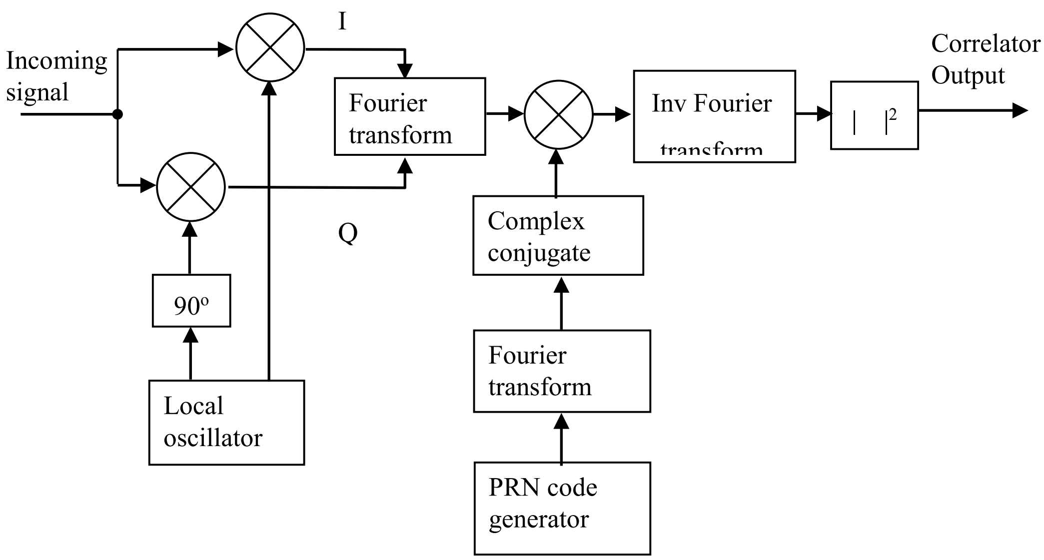

Figure 3-15 Block diagram of the correlator.

The incoming signal is the output of ADC with a 100 MHz sampling frequency and the correlator output is the circular cross-correlation between the incoming signal and the corresponding PRN code.

Let us suppose that the $x(n)$ is a finite sequence of the incoming signal, $y(n)$ is a finite sequence of the PRN code, $X(k)$ and $Y(k)$ are the discrete Fourier transform of $x(n)$ and $y(n)$ respectively, then the discrete Fourier transform $Z(k)$ of the circular cross-correlation $z(n)$ between $x(n)$ and $y(n)$ can be expressed simply as the following equation.

$$Z(k) = X^*(k)Y(k) \tag{3.8}$$

where * denotes complex conjugate. Consequently, the circular cross-correlation $z(n)$ can be obtained through inverse Fourier transform of $Z(k)$.

Before calculating the circular cross-correlation, the carrier wave of the incoming signal should be removed by the multiplication with the locally generated carrier signal. However not only the in-phase signal I but also the quadrature signal Q is necessary because the phase of the incoming signal is unknown. The I and Q signals are combined to become a complex signal and the discrete Fourier transform converts the complex signal into the frequency domain. The locally generated PRN code signal is also transformed into the frequency domain and complex conjugated. Consequently, the multiplication of equation 3.8 is calculated and the result is translated into time domain with the inverse Fourier transform, and the circular cross-correlation is generated as the absolute values of the output of the inverse Fourier transform. In order to identify RSFS, the TKEO should be calculated on the correlator output according to the TKEO algorithm introduced in Chapter 2. The TKEO is usually performed on the correlator output averaged over a certain time length.

Figure 3-16 shows an example of the correlator output and TKEO output of a composite signal. The composite signal contains two signals and the sample difference is 40 between the GPS signal at 0 and the GPS signal at 40. Applying the algorithm of Parallel Code Phase Search Acquisition, the correlator output is a curve with two obvious peaks, but it is difficult to tell the precise positions of the peaks. And it is also difficult to confirm whether any other peaks exist or not. However the two remarkable peaks at 0 and 40 illustrate the precise positions of the peaks. Consequently the relative time delay of the signal at 40 is estimated if the signal at 40 is considered as the RSFS.

Nevertheless, the wave characteristics cannot be estimated with only one result of the relative time delay. The relative time delay explains which area reflects the RSFS but does not contain the wave information. It is easy to understand that the intensities of the RSFS are varying because of the ocean wave propagation. If the TKEO outputs can show the variation of the intensities of the RSFS, the wave period and wave speed may be estimated. Therefore, we examine the performance of the TKEO to present the variation of the intensities of RSFS.

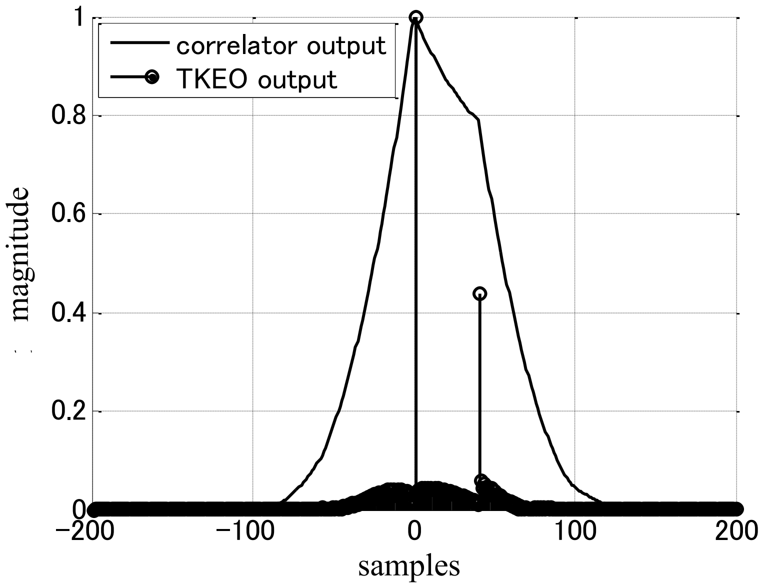

Figure 3-16 Example of outputs of correlator and TKEO.

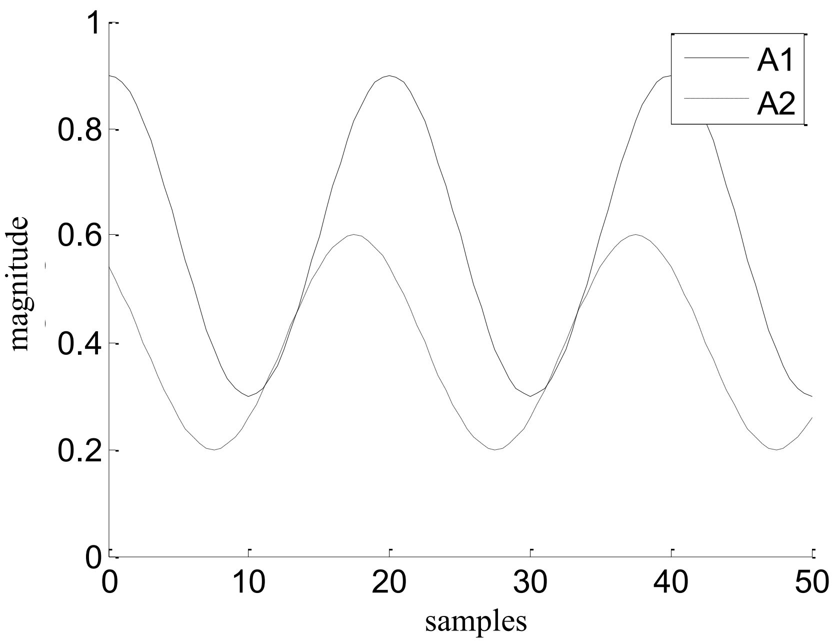

Figure 3-17 Amplitude variations of two RSFS.

Here, an example is given to demonstrate how to use the TKEO output to estimate the wave characteristics. The RF front-end outputs a composite signal containing one LOS signal and two RSFS (RSFS1 and RSFS2) without noise, and let the amplitude of the LOS be 1, and the amplitudes A1 and A2 of two RSFS are fluctuating as

$$\mathrm{A1} = 0.6 + 0.3\cos(2\pi \mathrm{f} t) \tag{3.9}$$

$$\mathrm{A2} = 0.4 + 0.2\cos(2\pi \mathrm{f} t - 3\pi/4) \tag{3.10}$$

where f = 0.05Hz, the frequency of the amplitude variation. The 3π/4 means the second amplitude variation of the RSFS has 17.5s = (3π/4) / (2πf) phase shift relative to the first RSFS. Figure 3-17 shows the amplitude variations of two RSFS. All the amplitudes of this two RSFS are less than the amplitude of the LOS signal.

Let the relative time delays of these two RSFS be 0.2μs and 0.25μs respectively. If the sampling frequency is 100MHz, the sample differences are 20 samples and 25 samples relative to the LOS signal. And we also consider the bandwidth of the composite signals to be 40MHz corresponding to the bandwidth of the RF front-end. One of correlator output and its TKEO output are shown in Figure 3-18.

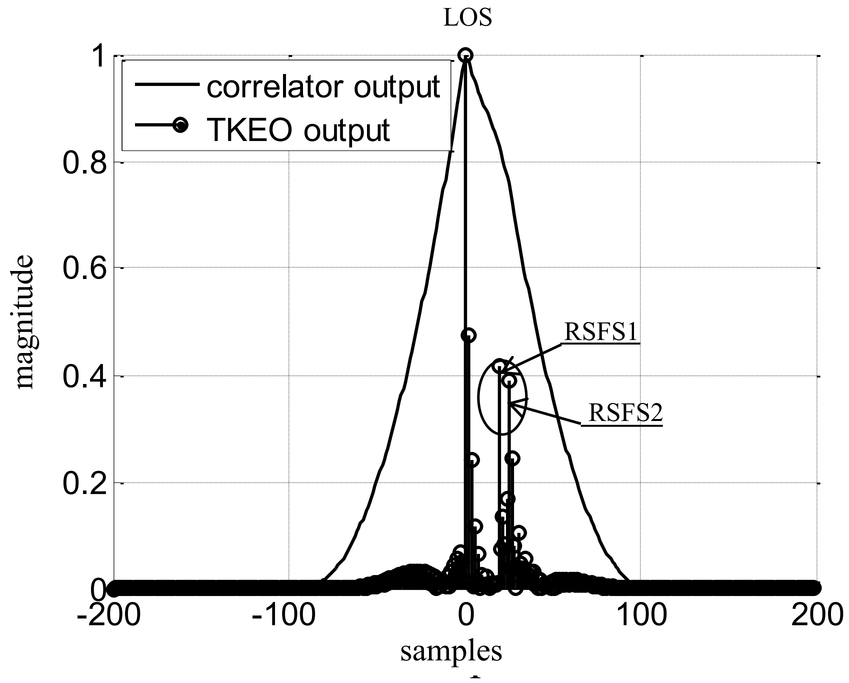

Figure 3-18 Correlator output and its TKEO output.

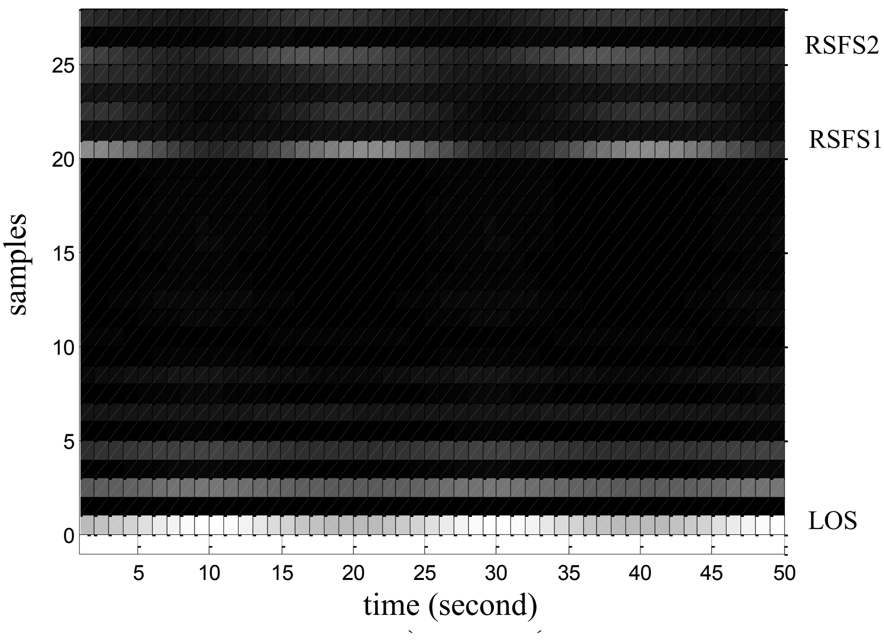

Figure 3-19 Top view of the aligned results of the TKEO output.

The correlator output is the total correlation of the composite signal, and the LOS signal can be identified from the correlator output but the two RSFS cannot be identified. However the two RSFS are identified obviously with two peaks at in the TKEO output. According to the amplitude variations of two RSFS shown in Figure 3-17, a series of TKEO out can be obtain, as shown in Figure 3-19.

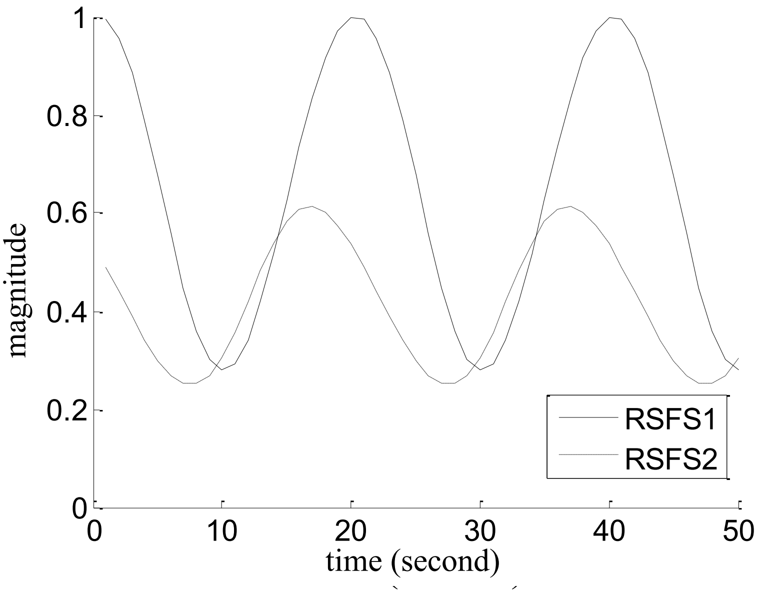

Figure 3-20 Magnitudes of two RSFS peaks.

Aligning all the results of the TKEO output using the reference position of the LOS peaks, we can obtain the top view of the aligned results of the TKEO output. The magnitude variations of the RSFS peaks can be seen and the magnitude of the LOS peak also varies slightly because of the signal fading. Figure 3-20 show the magnitudes of two RSFS peaks in the aligned results of the TKEO output. Comparing the Figure 3-20 with the Figure 3-17, it is found that the magnitudes of the RSFS peaks vary correspondingly with the amplitudes of the RSFS. Therefore, the magnitude variations of the RSFS peaks can reflect the intensity variations of the RSFS. Based on this, the wave period first can be estimated with FFT, and the wave speed can also be estimated if the phase difference between the two RSFS is calculated and the distance between two reflection areas is known.

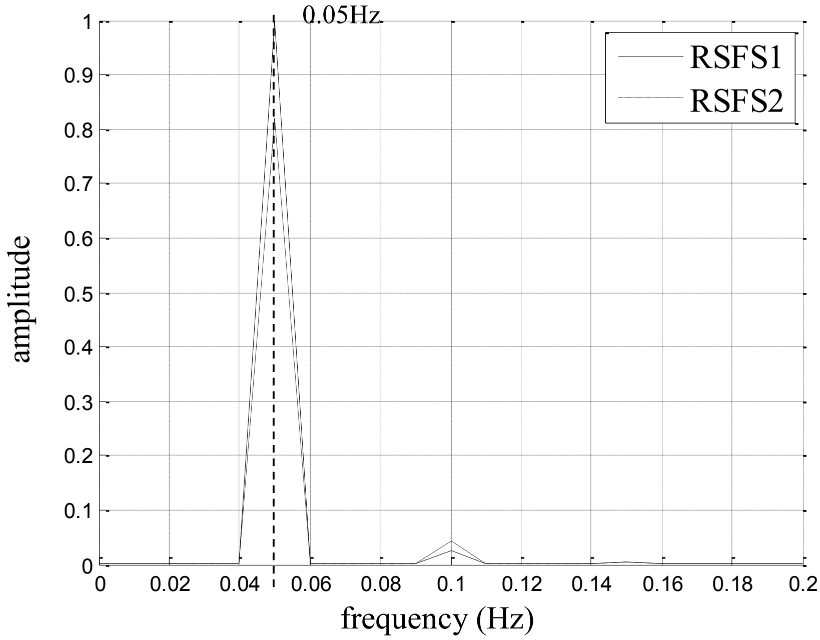

Figure 3-21 Amplitude characteristics.

Firstly, the wave period are estimated. Figure 3-21 and Figure 3-22 show the amplitude characteristics and the phase characteristics respectively. The variation frequency 0.05Hz is obtained from the outstanding peaks in the amplitude characteristics, and two phases 0 and $\pi/4$ are also estimated approximately. The variation frequency can be considered as the wave period. The propagation time between two RSFS can be calculated using the phase difference $3\pi/4 = (2\pi - \pi/4) - 0$ and the propagation distance can be calculated using the geometry of the antenna height and the satellite elevation angle. Therefore the wave speed is also resolved. Finally, wavelength is estimated as the multiplication of the estimated wave period and wave speed.

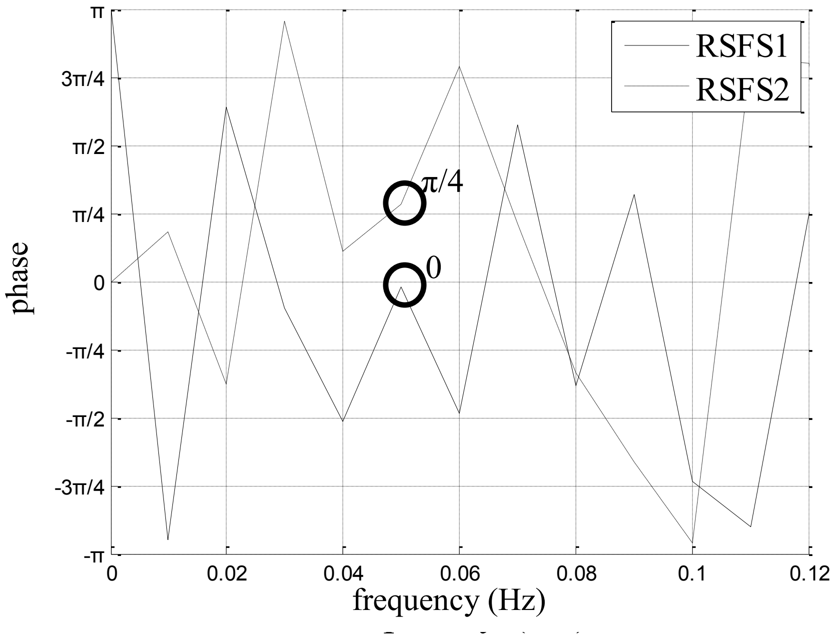

Figure 3-22 Phase characteristics.

In practice, the RSFS is complex and the noise is also a factor decreasing the estimation accuracy. The multipath fading is so severe that sometimes the magnitude variations of the RSFS peaks are not following the intensity variations of the RSFS. Therefore, long period measurement of the wave characteristics are necessary and averaging the TKEO output over a certain time period is considered as an available method to reduce the noise component and alleviate the effect of the multipath fading.

References

[1] Rajeswari Chatterjee, "Antenna theory and practice (second edition)", New Age International, pp.86-97, 1996.

[2] P. S. Naidu, "Sensor array signal processing", CRC Press, pp.75-105, 2000.

[3] A. W. Rudge, "The Handbook of Antenna Design", IET, pp.11-12, 1982.

[4] C.P. Narayan, "Antennas and Propagation", Technical Publications, pp.55-57 2007.

[5] R.Priemer, "Introductory Signal Processing", World Scientific, pp.67-76, 1991.

[6] Walter Allan Kester, "the Data Conversion Handbook", Newnes, pp.77-80, 2005.

[7] http://cesop.zarlink.com/zarlink/gp2015-datasheet-sept2007.pdf

[8] G. C. Xu, "GPS: Theory, Algorithms and Applications", Springer, pp41-43, 2007.

[9] K. Borre, D. M. Akos, N. Bertelsen, P. Rinder, S. H. Jensen, "A software-defined GPS and galileo receiver: A single-frequency approach", Springer, pp.81-84, 2007.

CHAPTER 4

SYSTEM EVALUATION

The prototype of the ocean wave remote sensing system has already been designed and constructed according to the methodology and the system configuration expatiated in chapter 2 and 3. After that we tried to evaluate the performance of the prototype system with numerical simulation and coastal experiments. In this chapter, the numerical simulation and costal experiments will be introduced.

In the numerical simulation, we configure the simulation conditions based on the practical conditions of the system applications. Concerning the objective satellite, the elevation angle is set to be 25 degrees with which the proper intensities of the RSFS are able to be received and the distance resolution on the sea-surface is about 50 meters; the wave period is also selected according to sea swell which is destructive and frequently occurs near coasts. With the numerical simulation, we evaluate the prototype system and we can conclude that the measurement methods are reasonable and practical.

The numerical simulation is not sufficient to confirm that the whole system can work well to measure the characteristics of ocean waves. Therefore the experimental evaluation became the necessary way to measure ocean waves in a real environment where big waves are coming from the open sea. The processing of system evolution is also introduced. Thereby, we can understand how the design of the system was improved gradually and how the prototype system came out. With the prototype system, the wave characteristics of sea swell were measured successfully. Before the experiments, the 3rd typhoon named “MAWAR” developed on the west pacific near the Philippines on June 1st and then it moved toward Japan and slowing dissipated to the southeast of Japan in early morning of June 6th. Therefore the sea-surface was almost smooth during the morning of June 6th but the sea swells occurred in the afternoon on that day. So we were able to measure the ocean waves with two types of sea-states on the same objective sea-surface in one day. Also we were able to compare the measurement results from two types of sea-state and further confirm the measurement performance of the prototype system.

4.1 Simulation

4.1.1 Simulation Processing

The numerical simulation mainly processes three parts, GPS satellites, ocean wave and the ocean wave remote sensing system. In the first part, GPS signals transmitted from the objective satellites are generated. The generated GPS signals will be received with the conventional antenna, and they will also be reflected from sea-surface and received with the array antenna. In the second part, ocean waves with given wavelength and period are generated near the ocean wave remote sensing system. The sea-surface with propagation of the generated ocean waves reflects the GPS signals generated in the first part. In the last part, the LOS signal and the RSFS are received and processed with the ocean wave remote sensing system. At last the characteristics of the generated ocean waves are estimated. Through comparing the estimated characteristic and the given characteristics, we can evaluate the measurement methods we proposed. Figure 4-1 shows the main functional models of the simulation processing. According to the sequence of the simulation processing, the main functional models are listed from top to bottom in the figure. The three parts of the processing are also shown. The arrows in the figure only denote the sequence order.

The upper functional model is to set simulation conditions which include the satellite status, the GPS signal parameters, the characteristics of ocean waves, and the installation of array antenna and so on. The L1 GPS signals are generated and the white noise is added in because the thermal noise of the environment exists. And here we only consider the C/A code and the carrier wave, and we ignore the navigation data. The powers of the signals and the noise are determined with the usual values on the Earth's surface.

On the objective sea-surface, three things should be considered, i.e. wave form on the sea-surface, the intensities of the RSFS and the relative time delay of the RSFS. We use a spectrum model of sea swell to generate ocean waves on the sea-surface with certain wavelength and significant wave height. If we have the sea-surface with sea swell, the intensities of the RSFS are calculated with the scattering pattern of the reflection point, and the relative time delays of the RSFS are calculated with the geometrical relationship of the satellites, the reflection points and the array antenna.

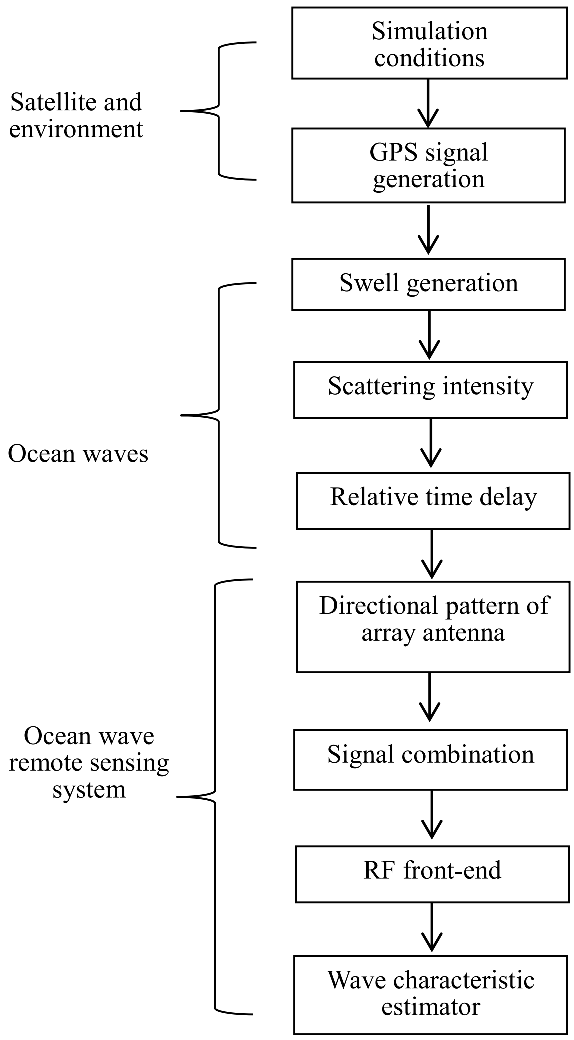

Figure 4-1 Functional models of simulation processing.

Until now, the RSFS of any space point over the objective sea-surface can be produced with the reflected intensity and the relative time delay of each RSFS and the distance from reflection point. Consequently, the RSFS arriving at the array antenna is also determinate. However, the received RSFS with the array antenna is affected by the directional pattern of the array antenna. With the narrow fan beam directional pattern, the signals coming from the front side of the array antenna are received and others are suppressed. All the received FSFS are added up to produce the received signals in the array antenna. The received signals will be amplified, down-converted and sampled in RF front-end. The sampled IF signals are processed with the wave characteristic estimator.

In the following sections, signal generation and processing will be introduced. The output of the wave characteristic estimator indicates that the proposed ocean wave remote sensing system is possible to measure wavelength and wave period theoretically.

4.1.2 Simulation Conditions

Table 4-1 Simulation conditions.

	Characteristic	Value
Simulation time	resolution	0.25 ns
Sea-surface	facet	1 m^2
GPS satellite	elevation	25 deg.
	azimuth	180 deg.
Ocean wave (Sea swell)	water depth	10 m
	period	20 s
	length	200 m
	significant height	2 m
	direction	0 deg.
Array antenna	antenna height	50 m
	direction	face to satellite

Table 4-1 shows the conditions of the numerical simulation, such as the status of satellites, the characteristics of ocean wave, and the installation of the antenna. The ocean wave characteristics are selected from a relatively long period sea swell [1]. The relationship of water depth, period and length can be validated using the dispersion relation mentioned in section 2.1.1.

According to the Nyquist sampling theorem, the representative frequency of the GPS signals is set to be 4 GHz (simulation time = 0.25 ns) more than twice the frequency L1 is 1575.42. Higher representative frequency can also be used to generate GPS signals but the final estimation results are almost same because the RSFS will be resampled with frequency 100MHz. The size of the grid on the sea-surface is 1 square meter which is much shorter than the wave length. Meanwhile, it is easy to calculate the intensity because the unit of the signal intensity is watt per square meter. The 25-degree satellite elevation is reasonable to ensure the enough intensity of the RSFS and about 33-meter distance resolution on sea-surface when the array antenna is installed 50-meter height over the sea-surface. The array antenna is facing the objective satellite because the 180-degree satellite azimuth and the 0-degree direction of the array antenna. The wave period of the sea swell is set to be 20 seconds because usually the periods of sea swell ranges from 10 seconds to 30 seconds.

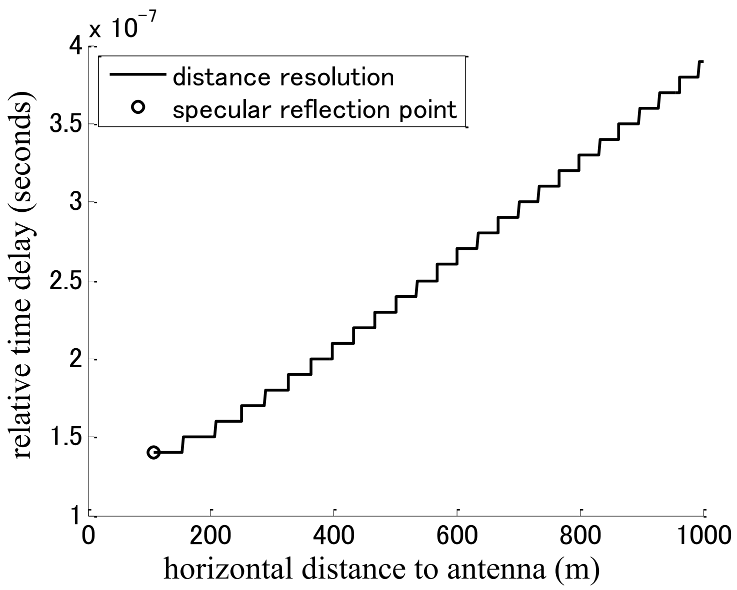

Figure 4-2 Distance resolution.

The distance resolution on the objective sea-surface should be considered. With the conditions of the GPS satellite and the array antenna, the distribution of the relative time delays of RSFS in the direction of the array antenna is calculated. We hereby obtain the distance resolution on the objective sea-surface away from the specular reflection point, as shown in Figure 4-2. The small circle is the specular reflection point and about 107 meters away from the array antenna. The reflected signals from the farther sea-surface have the longer relative time delays. The distribution has a step shape because some RSFS have same relative time delay in the view of the prototype system in which the sampling frequency is 100 MHz. Therefore, the distance resolution of 33-meter can be obtained from the step-shape. And we also know that the resolution is not uniform.

4.1.3 Signal generation

The generation of GPS signal is the multiplication of the C/A code and the carrier wave. Usually 1ms signal is enough because the C/A code repeats in 1ms. The representative frequencies of the C/A code and the carrier wave should be consistent, i.e. 4GHz.

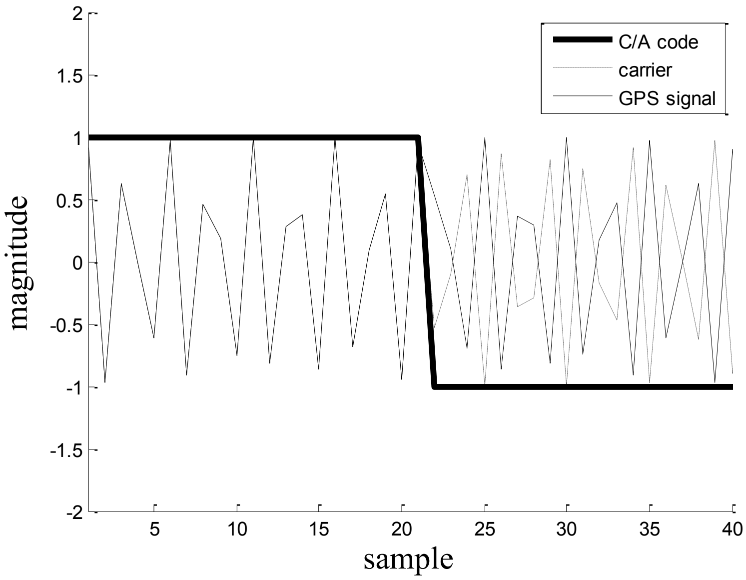

Figure 4-3 GPS signal generation.

Figure 4-3 shows a 0.01μs segment of GPS signal. The bold line is C/A and it jumps from 1 to -1 at the 22th sample. It is also found that the phase of the carrier is shifted by 180 degrees at the same position.

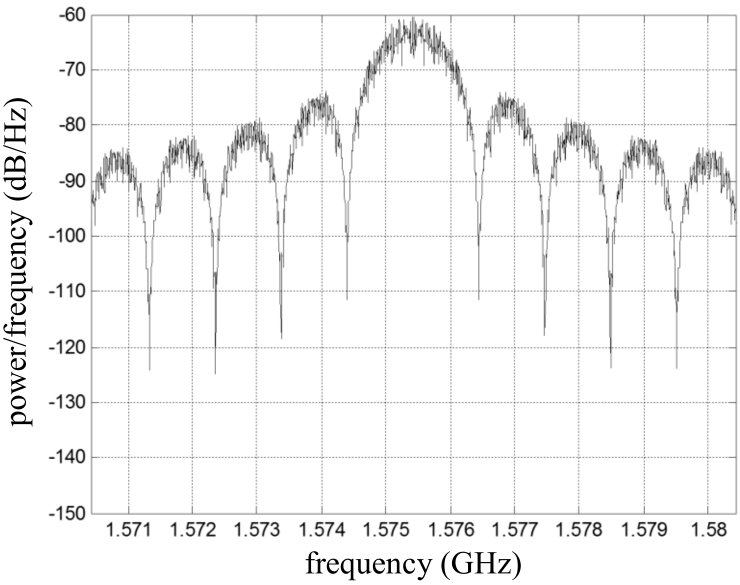

Figure 4-4 Frequency spectrum of the generated noise-free GPS signal.

Figure 4-4 shows the frequency spectrum of the generated GPS signal without noise component. The center frequency is 1.57542GHz and the main lobe bandwidth is about 2MHz.

The thermal noise is indispensable in a practical measurement environment. Therefore, the intensity of the RSFS should be strong enough otherwise the correlator cannot detect any signals. The intensity of GPS signals is descripted with the carrier to noise ratio. In the numerical simulation, the C/N_0 should be determined since it varies due to channel conditions. Here, the C/N_0 is calculated as follows,

$$C/N_0 = 10\log_{10}(\frac{P_s}{P_n}) \tag{4.1}$$

where P_s and P_n are the RSFS power received by the array antenna and the noise power respectively. Usually -160 dBW carrier power at the Earth's surface [2] and -204 dBW noise power are used to generate GPS signals and white Gaussian noise [3]. The value of the C/N0 is not constant because of the fading of the RSFS.

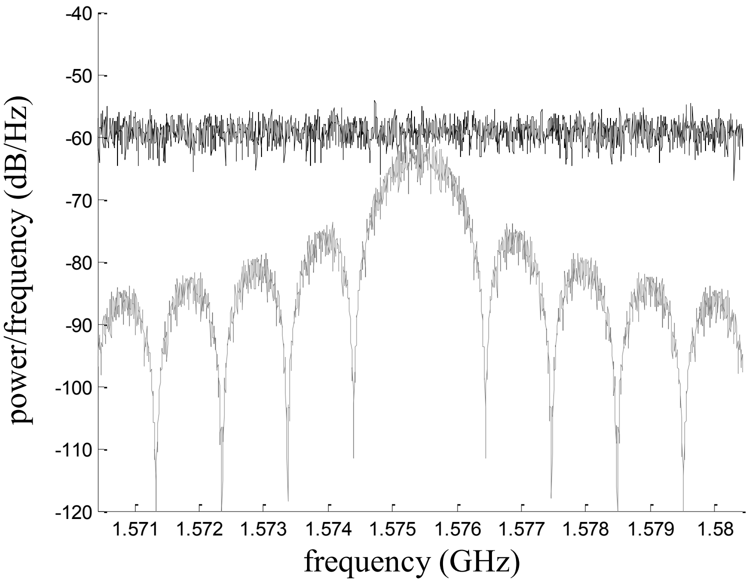

Figure 4-5 Noise spectrum and signal spectrum.

In the simulation, the amplitude of the carrier is set to be 1 and the intensity of the white noise is 1/40 which is originated from the relative power difference between the thermal noise and the signal. After the generated white noise is added up to the GPS signals, the signal will be below the noise level. Figure 4-5 shows the spectrums of noise and signals.

4.1.4 Wave Model

As introduced in section 2.1.1, the sea-surface ocean wave can be descripted with various wave spectrums. Here, the wave spectrum model of sea swell is calculated using the following spectrum [4, 5],

$$F(k) = \frac{H_s^2}{16\sqrt{2\pi}\sigma_l} \exp\left[-\frac{1}{2} \left(\frac{k - k_{peak}}{\sigma_l} \right)^2 \right] \tag{4.2}$$

where H_s is a significant wave height, k_{peak} is the wave number of the spectral peak and σ_l is the spectrum width.

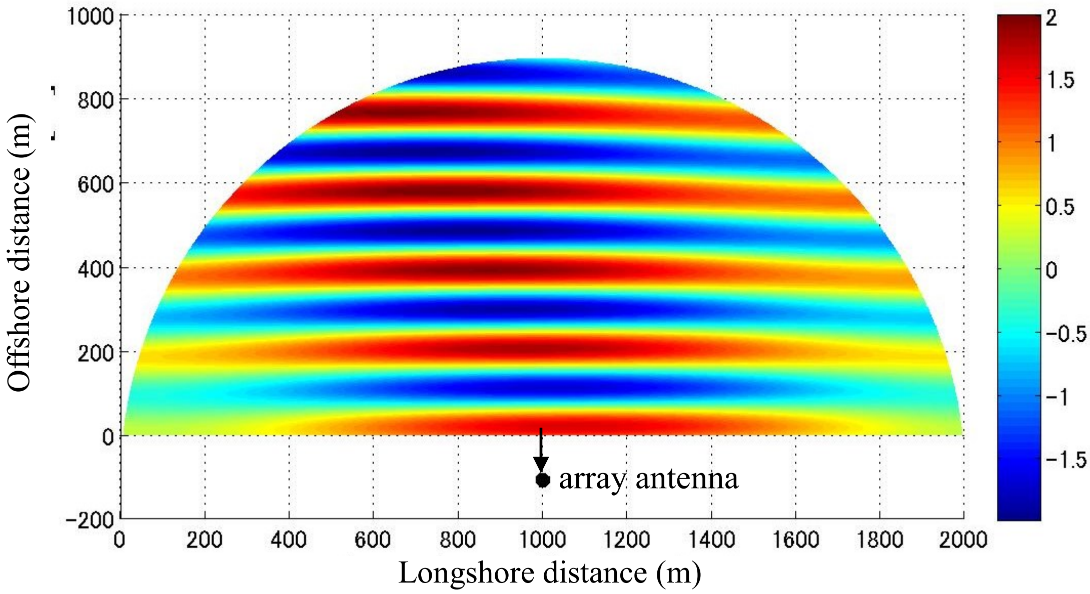

Figure 4-6 The modeled objective sea-surface.

Figure 4-6 shows the calculated sea-surface according to the wave spectrum and the wave conditions in Table 1. This sea-surface model is defined by an arc from a 1,000 meters radius circle centered at the position of the array antenna, with the area below, a straight line (parallel to the array antenna) passing through the specular reflection area, removed. The range of 1,000 meters is a reasonable scope on the sea-surface because five waveforms can be included and the intensities of RSFS are strong enough for receiving and processing.

In this sea-surface area, four waves of sea swell are generated completely. The warm color areas are the crests of the sea swells and the cool color areas are the troughs of the sea swells. The shapes of the sea swells are regular. As a result, we can image that the stronger reflection areas also distribute regularly and are moving towards the array antenna. The arrow indicates the wave direction and the black point mark is the position of the array antenna. The signals reflected from the area between the specular reflection point and the array antenna are masked because they have the same relative time delays as the signals reflected from the modeled sea-surface.

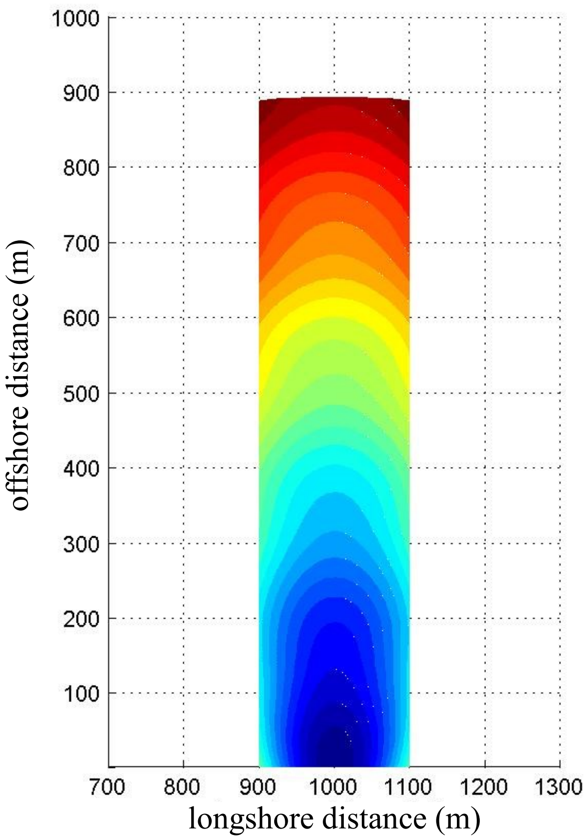

Figure 4-7 Relative time delay distribution of the objective sea-surface.

With the generated sea-surface with big waves, the relative time delays of all points on the sea-surface can be calculated according to the geometrical relationships. Figure 4-7 shows the relative time delay distribution of the sea-surface in front of array antenna. The size of the sea-surface is about 200m × 900m, where is the main reflection area for the array antenna. The warm color areas have longer relative time delays than the cool color areas.

We can find three facts about the relative time delay distribution. Firstly, the relative time delays increase with the increase of the distances away from the array antenna. Secondly, a series of ring-shaped areas exist, in which the relative time delays are homogeneous. It also means that all the signals reflected from the same ring-shaped areas will be regarded as one RSFS. Meanwhile, the distance resolution on the objective sea-surface is also demonstrated obviously. Finally, the boundaries of each ring-shaped area are not circle because the existence of big wave has redistributed the relative time delays.

4.1.5 Scattering Pattern

Only parts of RSFS can reach the array antenna. The amount of the RSFS reaching the array antenna is related to the scattering pattern of the modeled objective sea surface because the scattering pattern determines the signal intensity reflected from the modeled sea-surface in any scattering direction. According to the practical remote sensing environment on a rough sea-surface, a scattering pattern is defined by the bi-directional reflectance distribution function as follows [6].

$$R \propto (\cos\theta_0 \cos\theta_1)^{k-1} \frac{1-g^2}{(1+2g\cos\Theta + g^2)^{3/2}} \tag{4.3}$$

where, $\cos\Theta = \cos\theta_0 \cos\theta_1 + \sin\theta_0 \sin\theta_1 \cos(\phi_1 - \phi_0)$, and

θ_0: incidence angle, $[0,\pi/2]$;

θ_1: scattering angle, $[0,\pi/2]$;

k: factor of intensity along normal direction, $[1,\infty]$;

g: anisotropy factor, $(-1, 1)$;

Θ: scattering phase angle;

φ_0: azimuth angle of satellite, $[0,\pi]$;

φ_1: azimuth angle of reflection, $[0,\pi]$.

Figure 4-8 shows a scattering pattern from the reflected point P. The scattering pattern calculated with equation 4.3 is shown by dashed lines which are set by setting the coefficients "*k*" and "*g*" to be 2 and 0.7, $\varphi_1 - \varphi_0$ and θ_0 to be π and 7π/18 respectively. The incidence signal is "I", the normal direction of the scattering surface is "N", the direction to the antenna point is "S". These three vectors locate in the same plane which is perpendicular to the sea-surface. We suppose that the energy of incidence signals is totally scattered into the air. The scattering coefficient "R" is decided by the magnitude of the scattering pattern from point "P" on the sea-surface. The magnitude is scaled with the length between point "p" and each point of the scattering pattern, and it is found that the scattering magnitude in the specular reflection direction obtain its maximum.

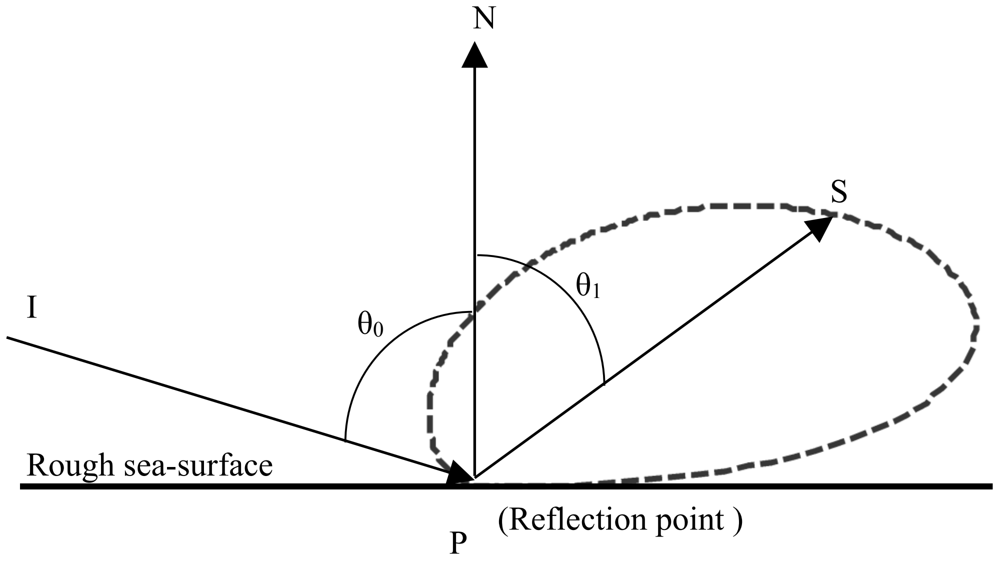

Figure 4-8 Scattering pattern.

4.1.6 Received Signals

Three characteristics of the signals received by the array antenna should be considered, signal intensities, relative time delays and polarization. The received signal intensities are determined by the distance between the refection points and the array antenna, the scattering pattern of the sea-surface and the directional pattern of the antenna; the relative time delay can be calculated using the geometrical relationship of reflection introduced in section 2.2.4.

After each RSFS with a relative time delay has been generated, the received signal at the array antenna is calculated according to the next equation [7]. Let (*i*, *j*) be the coordinates of the reflected point on the sea-surface.

$$x_{i,j}(t)=\frac{1}{\sqrt{2\pi}d_{i,j}(t)}R_{i,j}(t)E_{i,j}(t)RSFS(t-\tau_{i,j}) \tag{4.4}$$

where attenuation factors $d_{i,j}(t)$ is the distance from the reflection point coordinate (i, j) to the array antenna, $R_{i,j}(t)$ is the scattering coefficient at the reflection point, and $E_{i,j}(t)$ is the electric field intensity of the incident wave at the array antenna from the coordinate (i, j). $\tau_{i,j}$ is a time delay, and $RSFS(t - \tau_{i,j})$ is the reflected signal from the sea surface with time delay $\tau_{i,j}$.

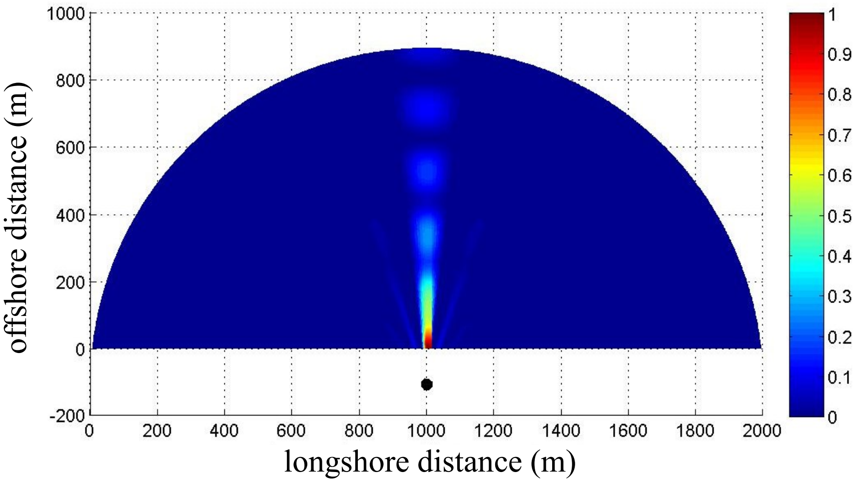

Figure 4-9 Normalized reflected signal intensities.

The normalized intensities of the received signal calculated with equation 4-4 without time delay $\tau_{i,j}$ can be illustrated on the modeled sea-surface in Figure 4-9. From this figure, the bright areas (glistening zones) and the dark areas indicate respectively the received signals with strong intensities and those with weak intensities. The distribution of the strong and weak received signals is consistent with the significant wavelengths of the simulated sea swell. The scattering toward the array antenna is produced mostly by specular reflections from a statistical ensemble of large-sale slopes of the sea-surface and the strongest scattered signals come only from the center of the glistening zone near [8]. The scattered signals with same relative time delay will produce one correlation peak in the correlator output. Through measuring and identifying the stronger received RSFS, the wavelengths of the modeled sea swell in the direction of the received antenna can be measured. Note that the received signal at the array antenna should be calculated by considering the relative time delay of the reflected signal.

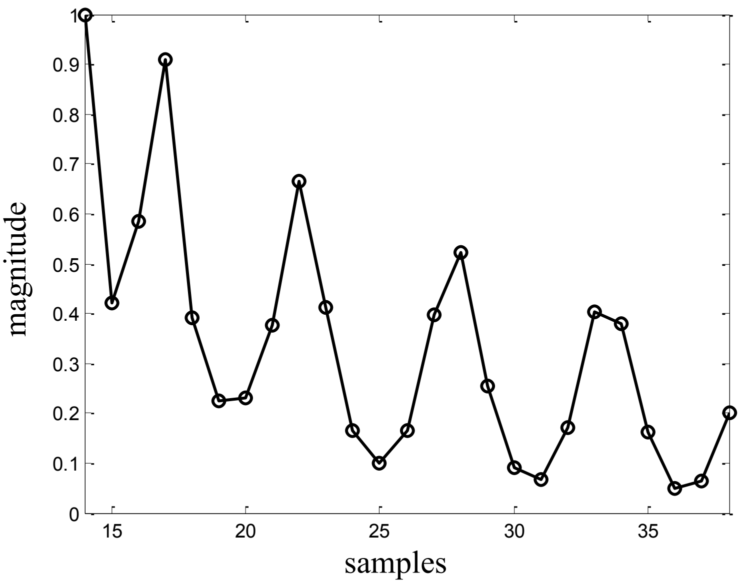

Figure 4-10 Normalized intensities of RSFS from ring-shaped areas.

According to the ring-shaped areas in the relative time distribution shown in Figure 4-7, the RSFS reflected from same ring-shape can be regarded as one signal. The intensities of received signals reflected from the series of ring-shaped areas can be illustrated in Figure 4-10. We can find that the fluctuation of the intensity is corresponding to the wave forms of the generated sea swell in Figure 4-6. With the propagation of the sea swell, the received signal intensity in a ring-shaped area is varying, and the distance between the stronger intensity areas is approaching to the wavelength.

Now, we have obtained the received GPS signals of only one millisecond. Accordingly, one correlator output and TKEO output can be computed. However it is not enough to estimate the characteristics of the sea swell. Here are three reasons. Firstly, the correlator outputs include so much noise that averaging the correltor outputs over a certain time length become necessary; secondly, sometimes the RSFS cannot be detected because of the signal fading, this is to say, sometime the RSFS is detectable and sometime not so that long time signals are necessary; thirdly, the wave period calculation with FFT needs a series of continuous signals of TKEO outputs.

4.1.7 Simulation Results

The wave characteristic estimator is used to estimate the wavelength, the wave period and the wave speed of waves moving in the direction of the antenna array. In the numerical simulation, the computation of the Doppler shift of RSFS and that of the arrival time correction are not necessary because the Doppler shift and the arrival time of the RSFS are given.

50-second received signals are generated and input into the correlator. The time length is over twice the wave period of the sea-swell and the waves will be propagating 500 meters towards the array antenna. The correlations between the received signals and the locally generated C/A code are calculated and the TKEO outputs are also calculated. Figure 4-11 show one correlator output averaged over 1 second and its TKEO output. In the TKEO output, some remarkable peaks can be found to be corresponding to waveforms of the sea swell. The averaged TKEO for the 50-second received signals is shown in Figure 4-12. The warm color areas denote remarkable peaks in TKEO outputs. The traces of these remarkable peaks are descending gradually alone with time. This implies that the stronger reflection areas are propagating to the array antenna because of movements of sea swells. This is the reason why the movements of ocean waves can be measured by means of the measurements of the variations of the RSFS.

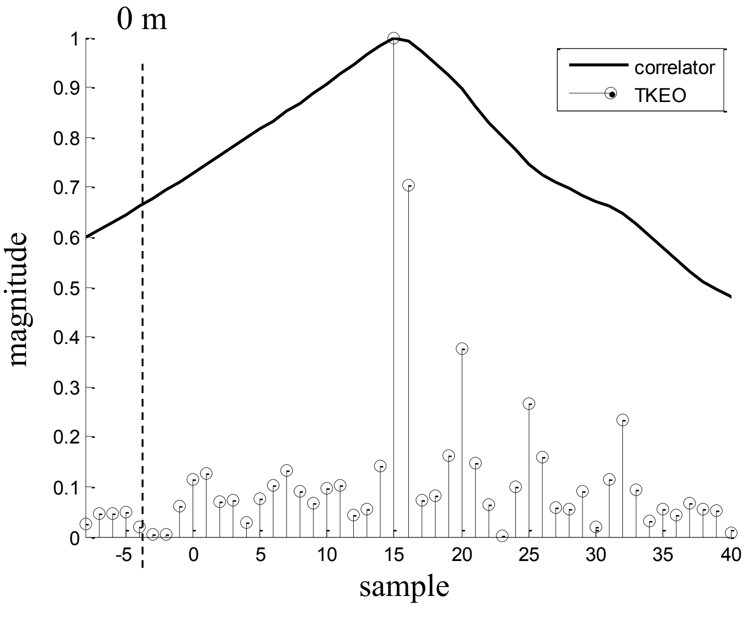

Figure 4-11 Correlator and TKEO output signals.

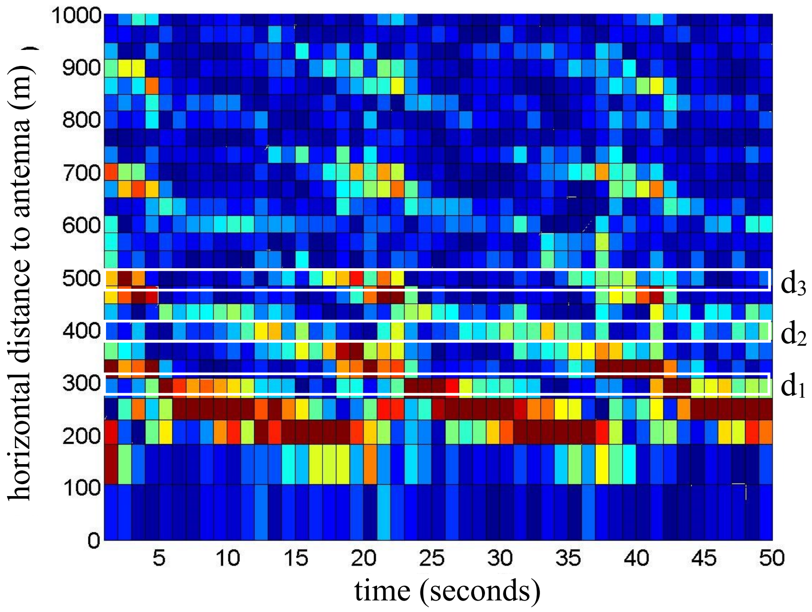

Figure 4-12　Top view of aligned results of averaged TKEO.

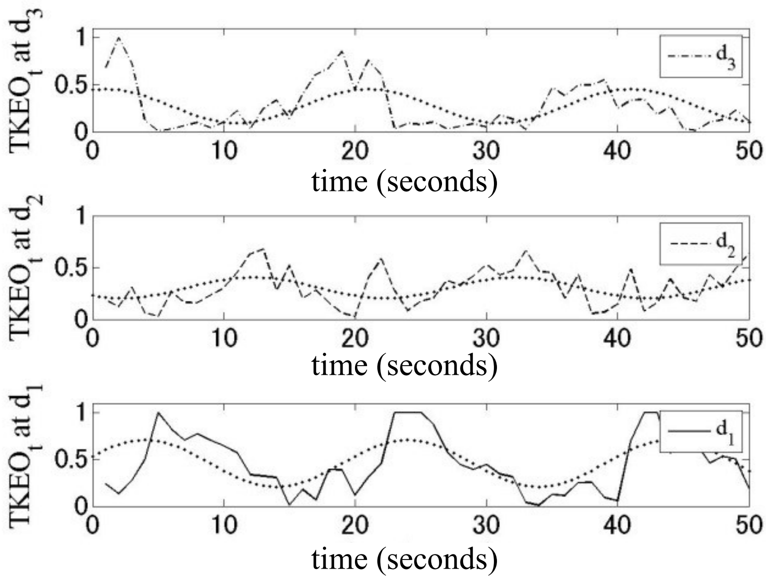

Figure 4-13　Variations of three TKEO time signals.

Now, we firstly measure the wave period of the sea swell, and then calculate the wave speed. Accordingly, the wavelength is the product of the resultant wave period and speed. The wave period is measured using the quantitative method, i.e. Fourier transform. We take out a series of TKEO outputs along the time axis to estimate the wave period, which has the same horizontal distance from the array antenna. In other words, the selected TKEO outputs represent the RSFS which have the same relative time delay. These TKEO outputs are referred to as TKEO time signals ($TKEO_t$). Here several $TKEO_t$ are selected to estimate the wave period. If the sea swells exist, the remarkable frequency component is considered as the wave period of the sea swells.

In Figure 4-12 three horizontal distances to the array antenna (d_1=307.0, d_2=415.0 d_3=518.0 meter on the vertical axis) are selected to estimate the wave period at first. Figure 4-13 shows three variations of three $TKEO_t$ along the horizontal axis. It is easy to find the wave period of the three $TKEO_t$ using the Fourier transform. Firstly, the wave period near the reflected sea surface is estimated using the amplitude characteristics of the Fourier transform, and after that the wave speed is estimated using the phase characteristics of the Fourier transform.

Figure 4-14 and Figure 4-15 show the amplitude characteristics and the phase characteristics of the three $TKEO_t$. In Figure 4-14, the amplitude characteristics of the three $TKEO_t$ have remarkable frequency component at same frequency. The remarkable frequency component with the maximum amplitude of the three $TKEO_t$ is obtained at 0.05 Hz (f_s), and the significant period of the wave is reciprocal of the frequency, 20.0 seconds (T_s).

In Figure 4-15, three phase values (φ_{d1}, φ_{d2} and φ_{d3}) of the three $TKEO_t$ on the remarkable frequency 0.05Hz are shown. One wavelength (λ_s) of the signal at 0.05 Hz corresponds to 2π radians and 20.0 seconds, therefore the phase difference ($\Delta\varphi_{d1,d2}$) between two adjacent phases of the $TKEO_t$ is equivalent to the propagation time (t_s) that the ocean wave moves the distance from d_1 to d_2 (Δd). Figure 4-16 shows the phase change of the three $TKEO_t$. The wave speed can be estimated with the phase change.

In Figure 4-16, the vertical axis is the horizontal distance from the array antenna. The upper horizontal axis is the phase value (φ) of the $TKEO_t$, and the lower horizontal axis is the propagation time (t) of the sea swells. There are three points for the phase values of the three $TKEO_t$. The heavy line in this figure is the regression line of the three phase values, and the gradient of this line shows the wave speed (V_s=9.1 m/s) near the reflected surface. The relationship between wave speed (V_s), wave period (T_s) and wavelength (λ_s) is shown by the equation, $\lambda_s = V_s \times T_s = 9.1 \times 20.0 = 182.0$ meters, thus the wavelength is obtained. From the simulation results, it is clear that the wave characteristics estimator is functioning well.

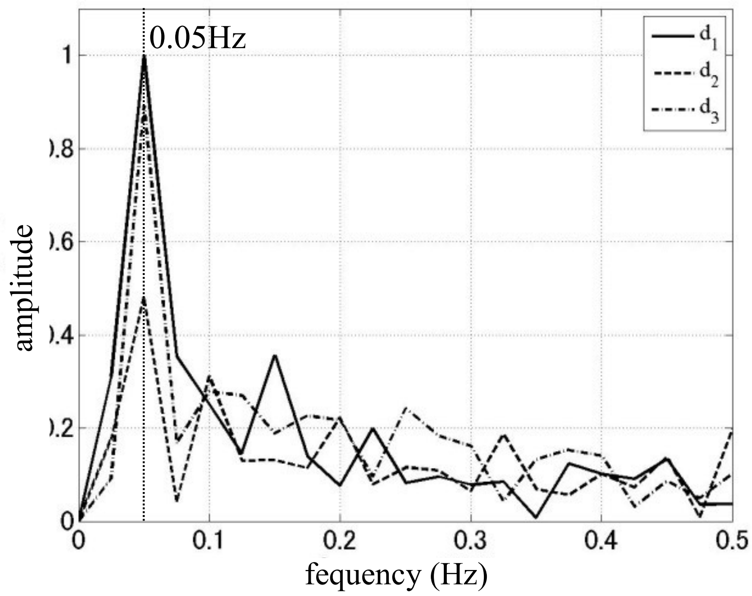

Figure 4-14 Amplitude characteristics of TKEO time signals.

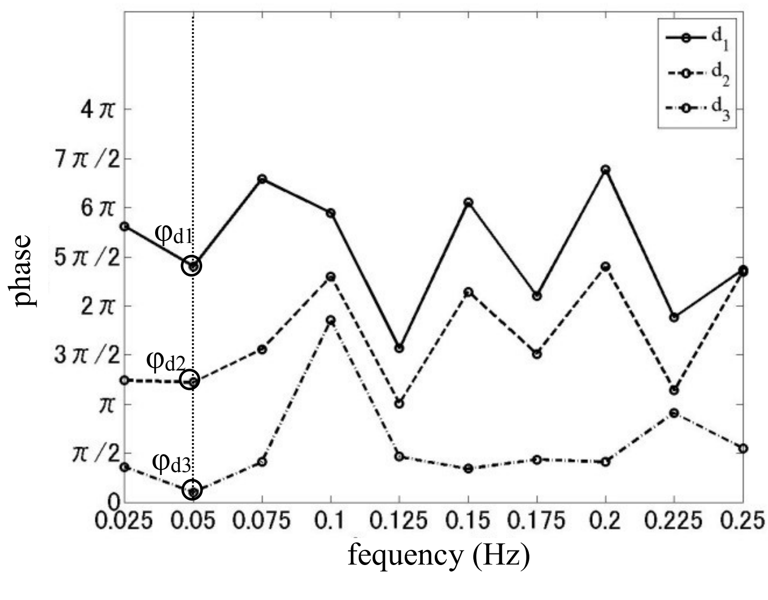

Figure 4-15 Phase characteristics of TKEO time signals.

Table 4-2 shows the wave conditions and estimation results. The wave period is measured exactly. But the wave speed and the wavelength are estimated with some errors.

There are several reasons affecting the accuracy. The main reason is that the generated sea-surface contains a lot of frequency components which also affects the reflection of RSFS. The waveforms of sea swells cannot be generated with same wave height and same wavelength.

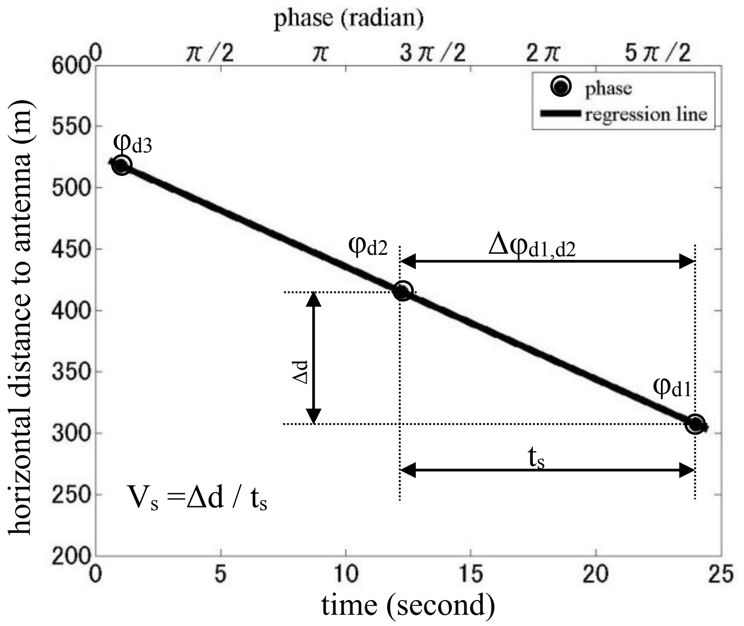

Figure 4-16 Phase change at three points of TKEO time signals.

Table 4-2 Simulation conditions and results

Characteristics	Set value	Estimated value
Wave period [s]	20.0	20.0
Wavelength [m]	200.0	182.0
Wave speed [m/s]	10.0	9.1

4.2 Experiments

4.2.1 System Evolution

The current ocean wave remote sensing system was not built in a short term but went through a long evolution. The whole system was improved gradually through practicing with various testing and experiments. These testing or experiments deepened our understanding of the theories and techniques of ocean wave remote sensing. Wide bandwidth signal was needed to identify RSFS in the correlator output; the GPS compass was equipped to adjust the array antenna to aim at the objective satellite and the wire cloth was cover the back of the array antenna to cut off the reflected signals from behind; the array antenna was set to look up slightly to avoid the undesired signals from the area between the array antenna and the specular reflection point; TKEO was applied to identify RSFS in the correlator output. FFT was used in the wave characteristic estimator to calculate wave period and speed quantitatively. In this sub-section, some testing and experiments will be introduced to show the evolution process of the ocean wave remote sensing system.

Initial design of the ocean wave remote sensing system

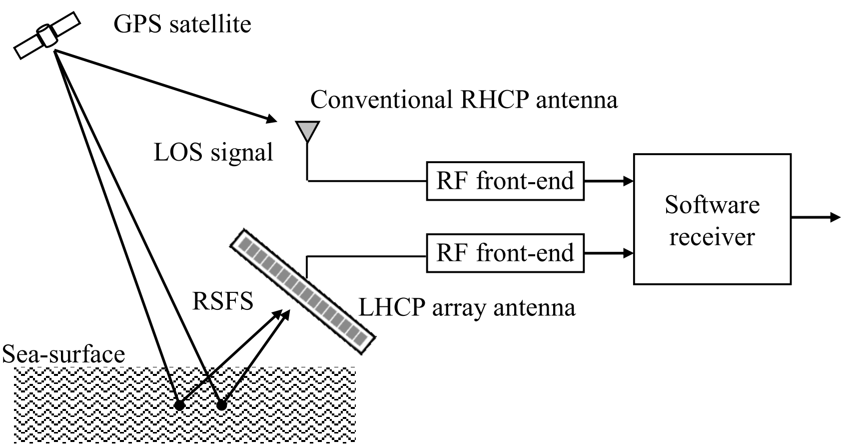

Figure 4-17 Initial design of the ocean wave remote sensing system.

Figure 4-17 shows the initial design of the ocean wave remote sensing system [9]. There were two sub-systems. The upper one had a conventional RHCP antenna for receiving the LOS signal and the lower one had a LHCP array antenna for receiving the RSFS. The two sub-systems had the same type of RF front-ends to sample GPS data simultaneously. The software receiver was used to calculate correlation. We expected the RSFS could be identified in the correlator output, and the wavelength could be estimated with single correlator output.

We built up the whole system through constructing the array antenna, selecting the RF front-end and programming the correlator in software receiver. And then some testing and experiments were conducted to validate the system and measurement method.

Front

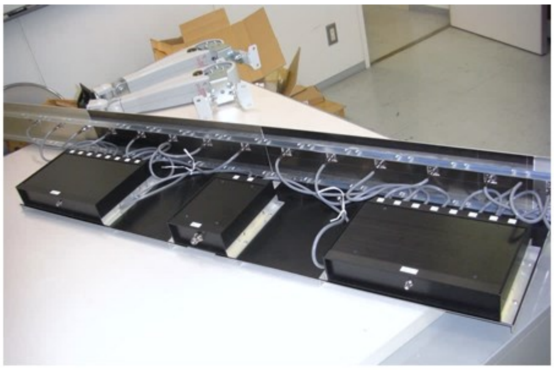

Rear

Figure 4-18 Front and rear of the array antenna.

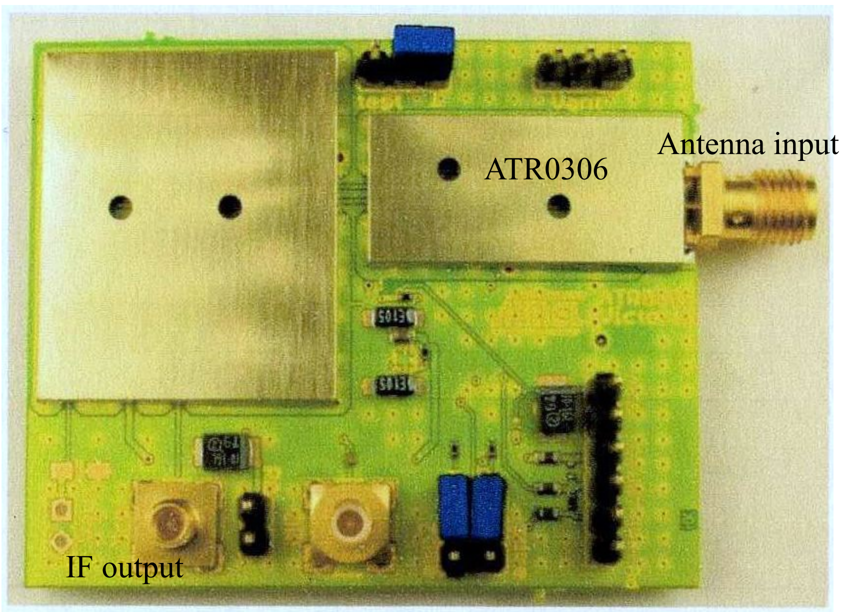

Figure 4-19 Evaluation board of GPS front-end chip set ATR0603.

Figure 4-18 shows the front and the rear of the array antenna. The uniform linear array is composed of 16 LHCP patch antennae and the center black box in the rear contains the pre-amplifier. The output of the pre-amplifier is passed to the RF front-end which is an evaluation board of GPS front-end chip set ATR0603. Figure 4-19 is the photo of theevaluation board. The array antenna is connected to the port in the right side of the board with a long cable and the analogue IF signals have the center frequency of 102.32997MHz. The analogue signals are under-sampled with 100MHz sampling frequency. The center frequency of the digital IF signals becomes 2.32997MHz (102.32997MHz – 100MHz). The bandwidth of the digital IF signal is 2MHz.

System testing

We did a testing of the array antenna and the front-end evaluation board. This testing was done on the roof of a tall building and the array antenna looked down to the ground, as shown in Figure 4-20. The height of the array antenna was about 14 meters over the ground and the depression angle of the array antenna was set to be 60 degrees to receive the signals

Figure 4-20 Installation of the array antenna and the reflection ground.

reflected from the ground. The elevation angle of the objective satellite was 45 degrees. The 60-degree depression angle of the array antenna and the 45-degree elevation angle of the satellite could eliminate more energy of the LOS signals.

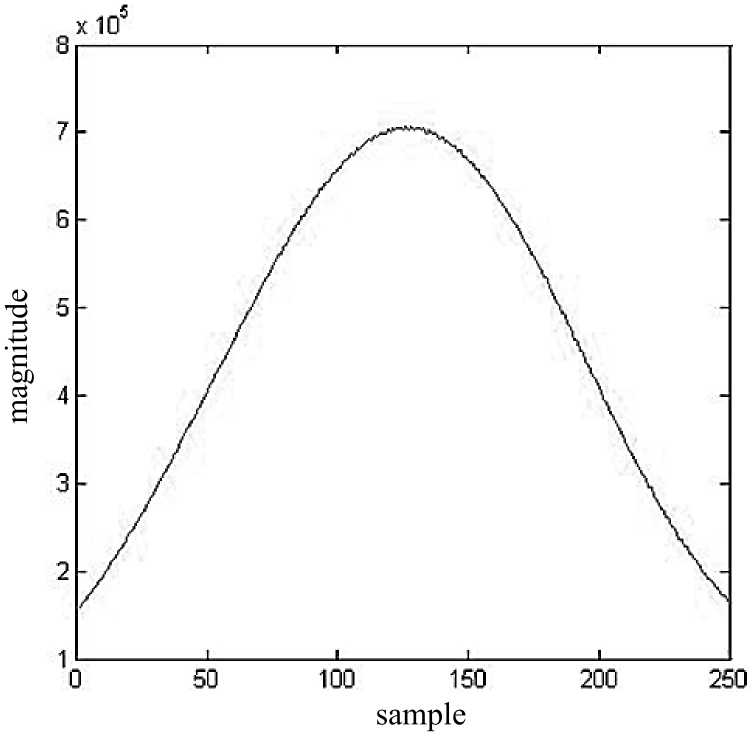

Figure 4-21 The correlation peak of the correlator output.

Figure 4-21 illustrates the correlation peak of the correlator output. It implies that the reflected signals of the objective satellites had been received successfully with the array antenna.

First sea-side experiment

After the testing on the roof, a sea-side experiment was conducted at Awajishima, Hyogo Prefecture of Japan. Figure 4-22 shows the wave conditions on the objective sea-surface and Figure 4-23 shows the array antenna installed on a tall building, about 25 meters over sea level. The depression angle was adjusted to be 20 degrees. The direction of the array antenna was measured with a magnetic compass. The objective satellite was search with a conventional GPS receiver. The azimuth and elevation of the satellite were 210 degrees and 27 degrees respectively.

Figure 4-22 wave condition on the objective sea-surface.

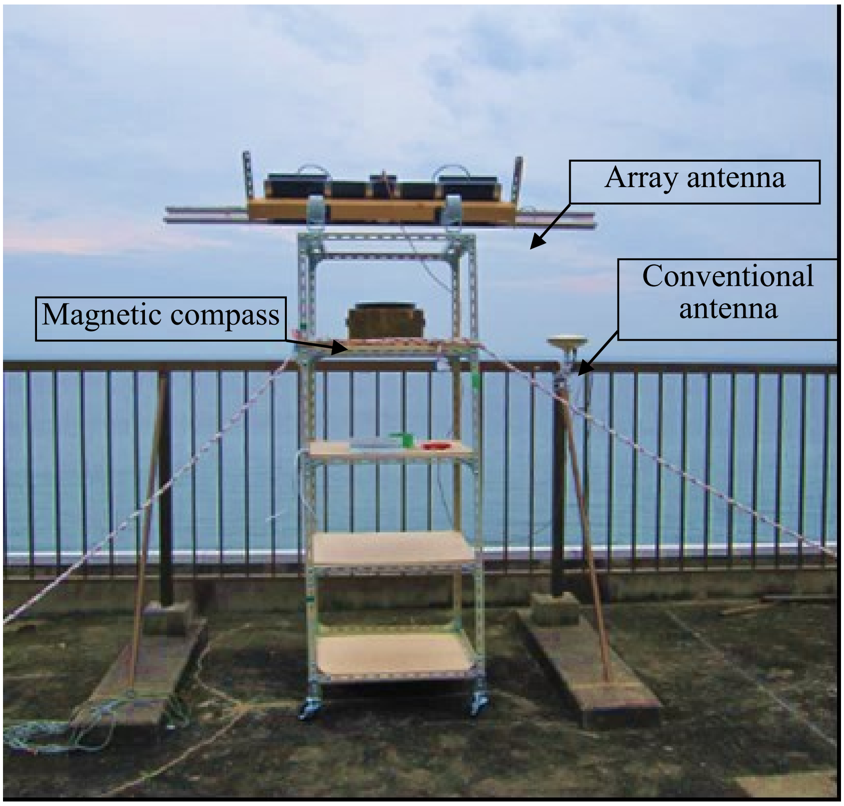

Figure 4-23 Installation of the antennae.

The correlation peak of the correlator output had almost same smooth curve as shown in Figure 4-21. This experiment validated that the GPS signals reflected from sea-surface could be received with the array antenna and detected with the correlator. However any

RSFS could not be identified from the correlation peak at all, and we even could not tell how much the correlation peak represented the RSFS because the array antenna also received LOS signal possibly with the 20-degree depression angle of the array antenna and the 27-degree elevation angle of the objective satellite. According to the experiment conditions, the relative time delay of the RSFS of the specular reflection area was about 0.08μs. We believed that the RSFS could not be separated from LOS signal in the correlator output because of the short relative time delay. Therefore, we were prepared to conduct next experiment in a height site.

Sea-side experiment in a high site

A wave measurement experiment was conducted near the seaside of Japanese sea area of Kyotango, Kyoto, Japan. Figure 4-24 shows the wave conditions and Figure 4-25 shows the installation of the array antenna. The height of the array antenna was about 80 meters above the sea level. The elevation angle of the objective satellite was 27 degree. According to the geometrical relationship, the relative time delay of the RSFS of the specular reflection area was about 0.24μs. The position of the maximum value of the correlator output was 1.26μs in Figure 4-26. Comparing the correlator output in Figure 4-21, another peak near 1.50μs could also be detected [10]. Therefore we could confirm that the array antenna received a composite signal which included the LOS signal and the RSFS of the specular reflection area. The high experiment site lengthened the relative time delay of the RSFS.

Figure 4-24 Wave condition on the objective sea-surface.

Figure 4-25 Installation of the array antenna.

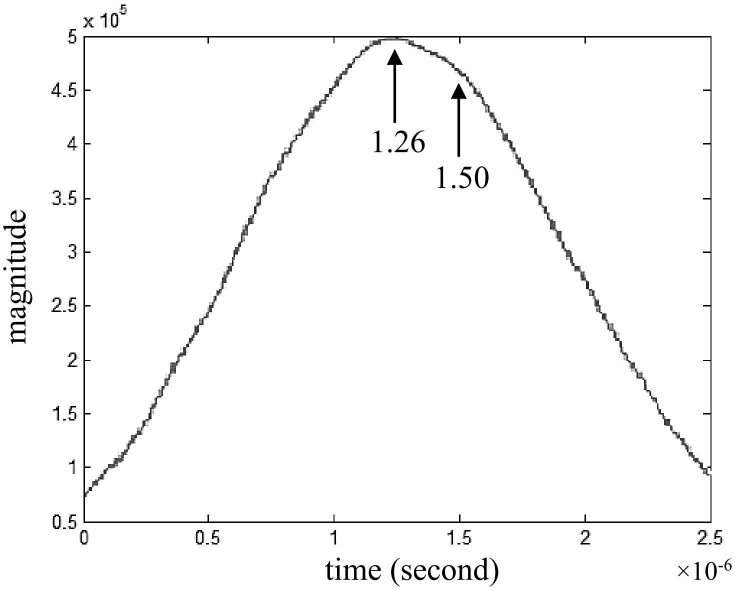

Figure 4-26 The correlation peak of the correlator output.

With the system testing and the sea-side experiments, we realized some constraints of the system. Firstly, the correlator output was seemed to be smooth because of the narrow bandwidth of the digital IF output of the RF front-end. More sharp peaks in the correlator output could be obtained using adequate bandwidth of the RF front-end. Secondly, the peak near 1.50μs might represent the RSFS or the reflected signals from the back side of the array antenna. Thirdly, the signals reflected from the area between the array antenna and the specular reflection point should be mitigated because this area not only reflected strong signals but also they had same relative time delays with the signals reflected from the sea-surface far away from the specular reflection area. Additionally, the array antenna direction measured with the magnetic compass was not precise to aim at the objective satellite.

Experiment with the improved system

We made some improvements on the system and the experiments. A new RF front-end was used (Figure 3-13 and Figure 3-14), which could output wide bandwidth IF output to obtain sharp correlation peaks; the back side of the array antenna was shielded with a wire cloth to cut off the reflected signals from behind (Figure 3-6); the array antenna was adjusted to look up slightly to avoid the undesired signals when receiving the RSFS in experiments; A GPS compass was used to measure the array antenna direction precisely to receive more RSFS from objective satellite (Figure 3-5). Figure 4-27 shows an averaged correlator output over 1 second with the improved system. There were several sharp peaks in the correlator output. Roughly the LOS signals and the RSFS could be identified. However it is impossible to pick out the LOS signal and separate one RSFS from the others.

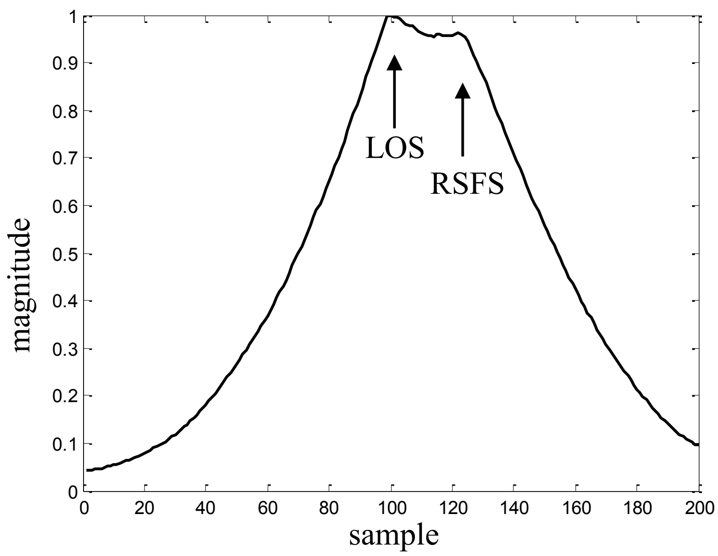

Figure 4-27 Correlator output.

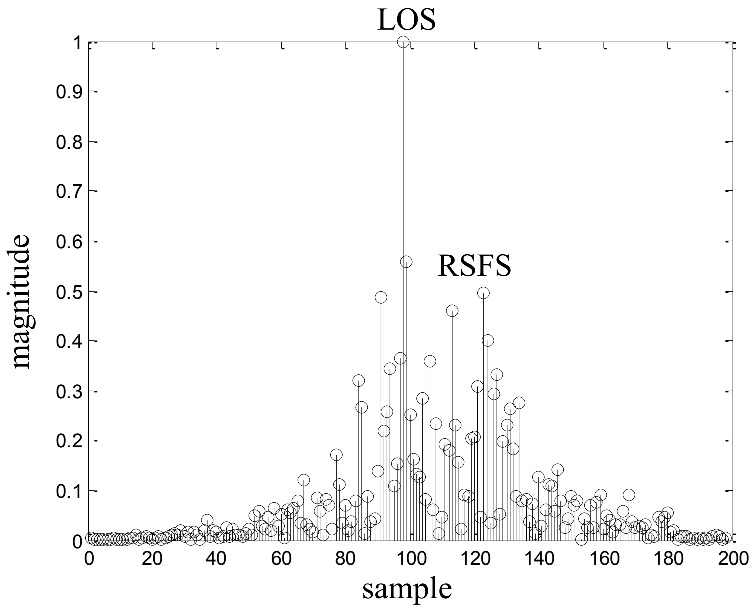

Figure 4-28 TKEO output.

Finally the TKEO introduced in section 2.4.1 was used to identify each RSFS [11, 12] and the 40MHz bandwidth of the RF front-end was also determined using the band-limited effects of TKEO. The LOS signal could be identified but the RSFS were a group of peaks with which the wave characteristics could not be estimated because of the noise, as shown in Figure 4-28. Moreover, the peak for the LOS signal did not always appear because of the severe signal fading.

Consequently, we took two measures. On the one hand, the LOS signal was received with a 2MHz bandwidth RF front-end and processed with software receiver to calculate the precise arrival time of the LOS signals. On the other hand, the LOS signal and the RSFS were sampled simultaneously and the time length of the sampling was extended from 1 second to 24 seconds. The FFT was also applied to analyze the 24-second TKEO output and estimate the characteristics of ocean wave. Finally, we designed the wave characteristic estimator to execute the correlator, TKEO, FFT and the calculations of wave characteristic.

4.2.2 Experimental Evaluation

The current system is demonstrated in Figure 1-3, composed of the array antenna, the 40MHz bandwidth RF front-end, the wave characteristic estimator, the GPS compass conventional receiver, the software receiver and so on. When the prototype of the whole system was built completely, an experimental evaluation was carried out.

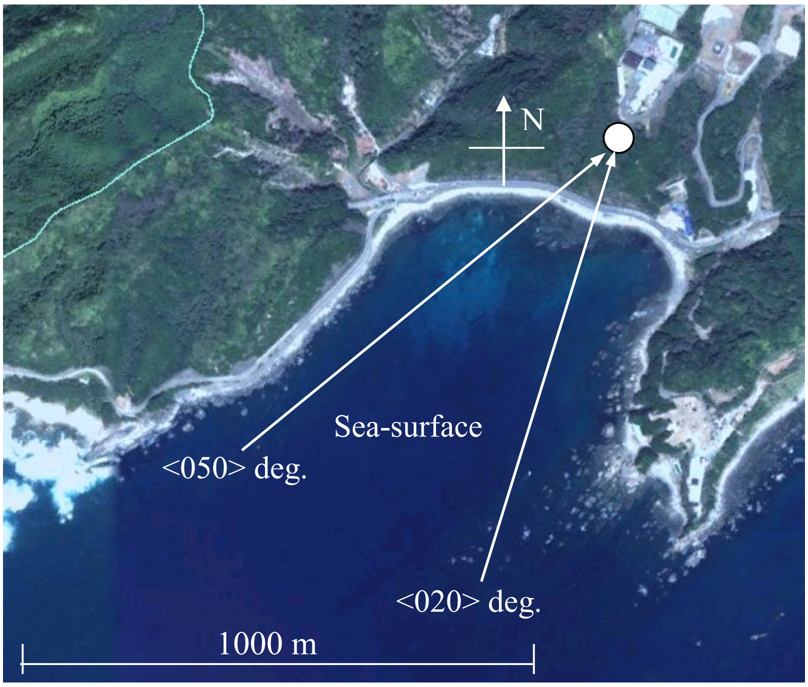

Figure 4-29 Experiment site located on SUSAMI-coast. [Google Earth V7.0.3.8542. (March 28 2011). SUSAMI, WAKAYAMA Japan. 33°33’3.22”N, 135°28’39.15”E, Eye alt 2.5 km.].

Experimental conditions

The experiment was carried out on June 6th, 2012 with adequate wind and wave propagation from an approaching typhoon. Figure 4-29 shows the experiment site located on the SUSAMI-coast of WAKAYAMA Prefecture in Japan. The ocean waves come from the open sea into the objective sea-surface. The measurable direction of the antenna ranges from 20 to 50 degrees. The depth of the reflected sea area is about 10 meters. The ocean wave remote sensing system was set on the hillside 110 meters above sea level, which is marked by the white circle.

Figure 4-30 shows the distance resolution away from the specular reflection point. The small circle is the specular reflection point about 302 meters from the array antenna. We can know that the distance resolution was about 100 meters near the specular reflection point. During experiment, the array antenna was adjusted to look up slight to avoid the area between the array antenna and the specular reflection area. Theoretically, each step in the step-shape distance resolution had the RSFS with same relative time delay, which would be one peak in the TKEO output.

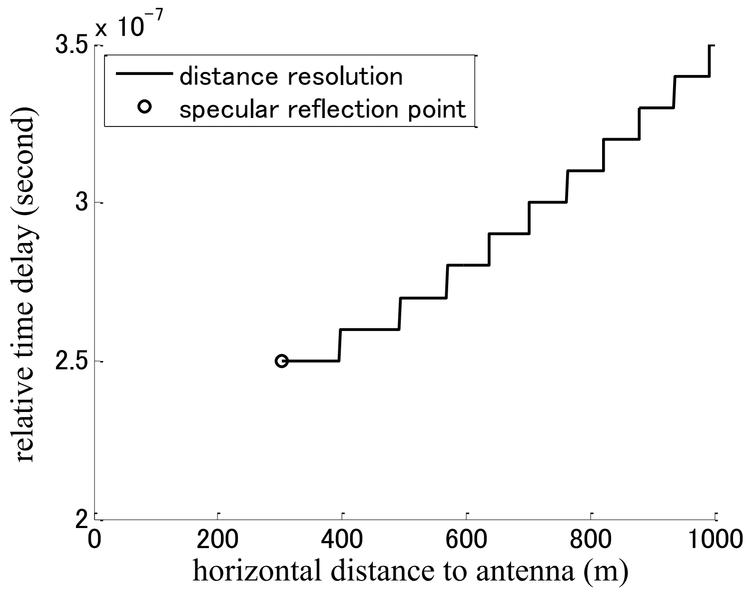

Figure 4-30 Distance resolution.

Figure 4-31 shows the installation of the antennae. The upper photo (a) illustrates that the conventional antenna receiving the LOS signals was tilted toward the objective satellite to achieve high CN0 and located near to the array antenna. Its signals would be processed with a software receiver to estimate the arrival time of LOS signal which was used to align the arrival time of the RSFS. In the lower photo (b), the array antenna was also looking up slightly to avoid the reflected signals from near sea-surface and the hillside because they had the same relative time delays with the RSFS away from the specular reflection point.

(a) Tilted conventional antenna near to array antenna.

(b) Looking-up array antenna.

Figure 4-31 Photos of installation of the antennae.

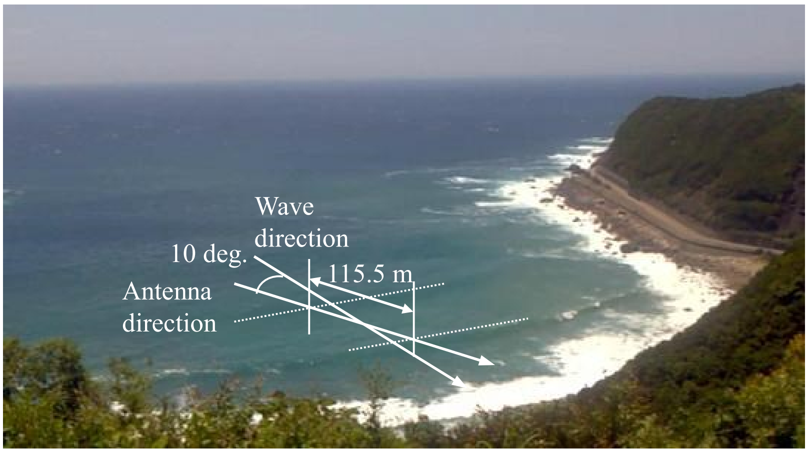

Figure 4-32 Moderate wave condition near the objective sea-surface.

In the morning, there was a smooth sea but it became a moderate sea because the sea swells generated by the 3rd typhoon "MAWAR" came into the objective sea-surface. Figure 4-32 shows the wave conditions of moderate sea state on the objective sea-surface. Some big waves can be seen. The sea states were very different in the morning and in the afternoon. Therefore, three experiments, one in the morning on smooth sea-surface, and two in the afternoon on moderate sea-surface were carried out using different satellites.

The conditions of the satellites and the ocean waves are shown in Table 4-3. The first wave conditions were smooth, but in the second experiment the wave heights were 1.5

meters, as estimated by sight, and the wave period of 11.5 seconds and the wavelength of 13.7 meters were measured from an image grab from the video footage of the experiment. The wavelength in the direction of the antenna was calculated using the difference angle between wave propagation and the direction of the antenna. The wavelength in the antenna direction was calculated to be 115.5 meters according to the cosine relation as 115.5 = 113.7 ÷ cos(10) because of the 10- degree difference angle. The direction of the array antenna was measured with the GPS compass and adjusted to the objective satellite. In the experiments, 20-degree satellites were used to receive strong RSFS. The output signals from the front-end were sampled and recorded for 24 seconds. Next the wave characteristics were estimated with the wave characteristic estimator.

Table 4-3 Experimental conditions

	experimental No.	1	2	3
time	recording time [s]	24	24	24
data	No. of samples [$\times 10^9$]	2.4	2.4	2.4
satelite	SV No.	21	22	22
	azimuth [deg.]	223	202	203
	elevation [deg.]	20	20	20
sea	state	smooth	moderate	moderate
	height [m]	-	1.5	1.5
	period [s]	-	11.5	11.5

Estimation of wave characteristics

The LOS signals and the RSFS were sampled with 100MHz sampling frequency simultaneously. The sampled data of the LOS signals and the RSFS were stored in the mass-storage Hard Disk Diver (HDD). The data type of the samples was 8-bit integer. Because of the 100 MHz sampling frequency, 200 MB data per second have to be saved in the HDD for two sampling channels.

The sampled data were stored with individual files for every observation. The file was named with sampling time and some basic information of the objective satellite and array antenna. For example, 2012_06_06_15_20_05_SV01_EL20_AZ215_HI110_DG10.bin was the name of one data file. The number series at the beginning was the time when the sampling was started. The number, elevation and azimuth of the objective satellite and the height and degree of the array antenna were also recorded in the name of the data file. It was a convenient method for programs to read the satellite conditions. The recorded data was processed with the functional modules of the wave characteristic estimator shown in Figure 2-22. The correlations were computed with the correlator, and then the arrival times of the RSFS were corrected with the arrival time of LOS estimated by the software receiver.

However the arrival time of the LOS signals are not able to align the RSFS directly because it includes two much uncertain results of the arrival times, as shown in the upper sub-figure in Figure 4-33. The vertical axis is the code phase of the LOS signals with unit of sample, which can be converted into arrival times. The horizontal axis is the 24-second recording time. There is a descending trend and some arrival times are displaced from the trend line. The descending trend originates from the Doppler shift, and the displaced points occur because of the noise and multipath disturbance. The lost arrival time should be removed and an estimated value should be given. The lower sub-figure shows the estimated arrival times of LOS signals in 24 seconds with a straight descending trend line.

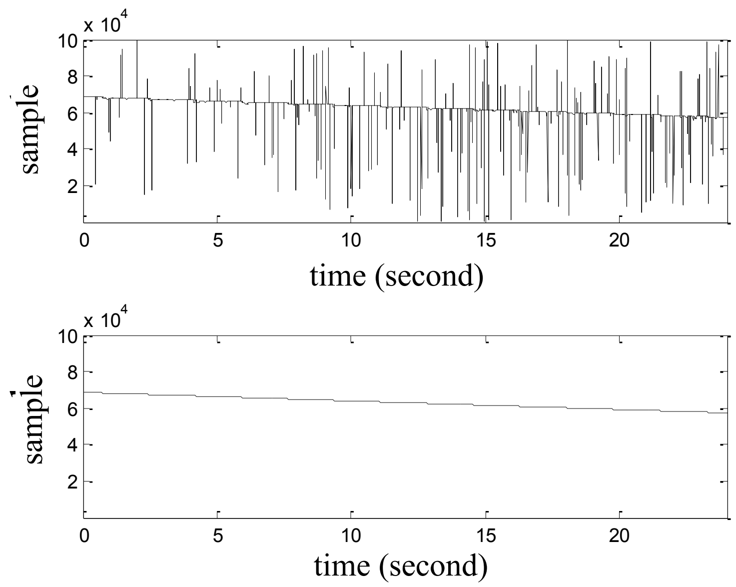

Figure 4-33 Estimation of the arrival time of the LOS signals.

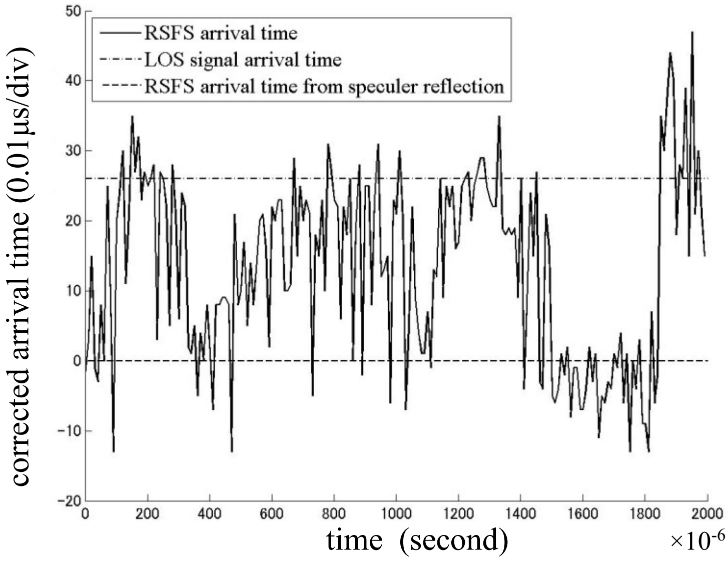

Figure 4-34 arrival time correction of the RSFS.

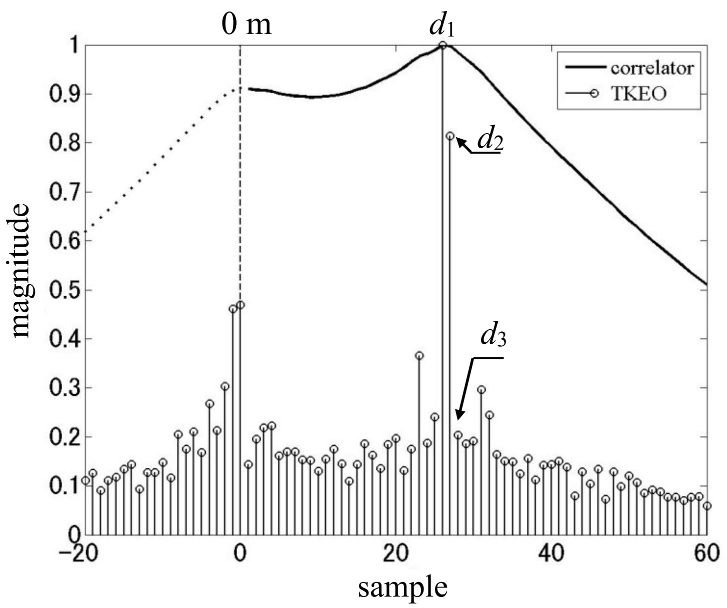

Figure 4-35 Correlator and TKEO output signals (smooth).

The estimated arrival time of the LOS signals is used as a reference time to correct the arrival time of the signals received with the array antenna. A 2-second segment of the arrival time correction of the RSFS is shown in Figure 4-34. Some corrected arrival time goes near to 0 because the LOS signal could not be eliminated completely and the arrival time was severely fluctuating because the RSFS and LOS signals interfered with each other.

After arrival time correction of all the correlator outputs for RSFS, the TKEO were executed. Following that, the wave characteristics were estimated for the smooth sea state and the moderate sea state respectively. Figure 4-35 shows the correlator and TKEO outputs of smooth sea state. The strong TKEO signal near the zero sample point of the vertical axis is the LOS signal, and the next strong TKEO signal near the 26th and 27th sample points are the RSFS.

Figure 4-36 shows the top view of the aligned results of the averaged TKEO. In order to analyze the TKEO signals more fully, the signals at the 28th sample point is also considered. The horizontal distances at the 26th, 27th and 28th sample points are $d_1 = 348.0$, $d_2 = 444.0$ and $d_3 = 531.0$ meters from the array antenna position.

Figure 4-37 shows three variations of each TKEO_t along the horizontal axis for the smooth sea state. Figure 4-38 shows the amplitude characteristics of the TKEO_t by the Fourier transform. In this figure, since there is no significant component, we cannot find the remarkable wave period from these experimental results. Therefore, the wave speed and wavelength cannot be estimated.

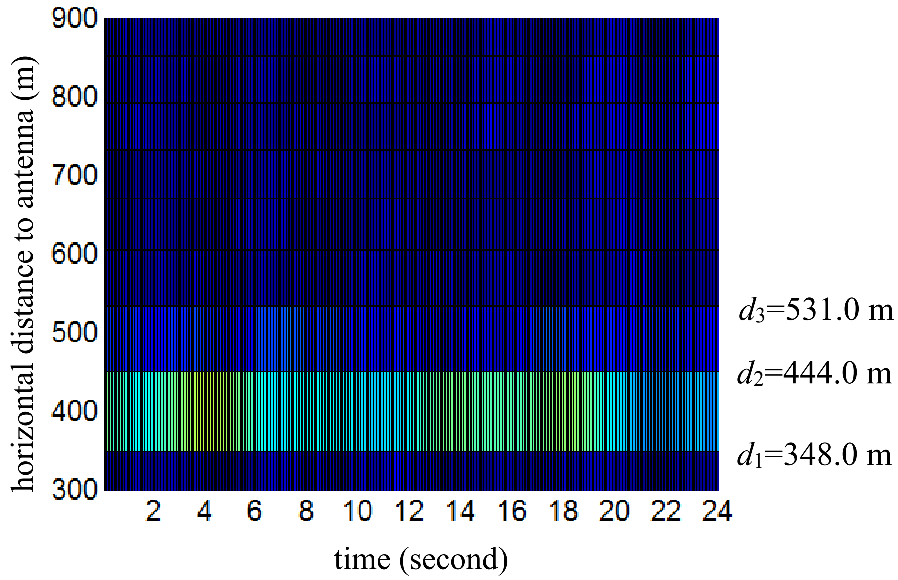

Figure 4-36 Top view of the aligned results of averaged TKEO (smooth).

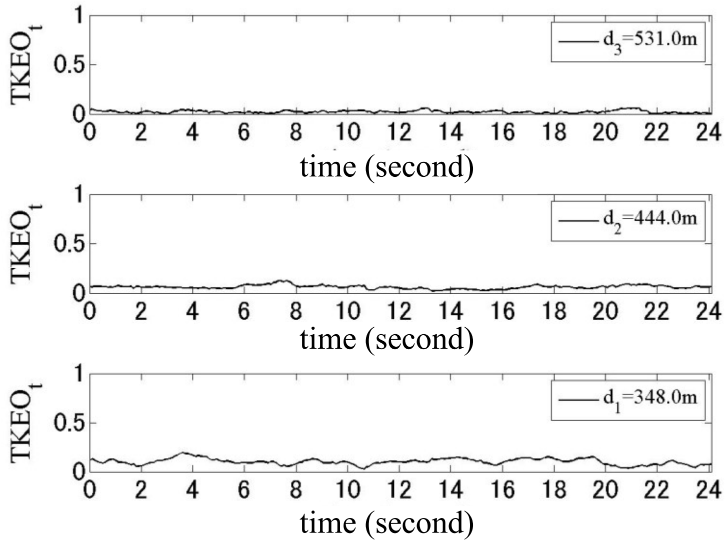

Figure 4-37 Time variations of TKEOt (smooth).

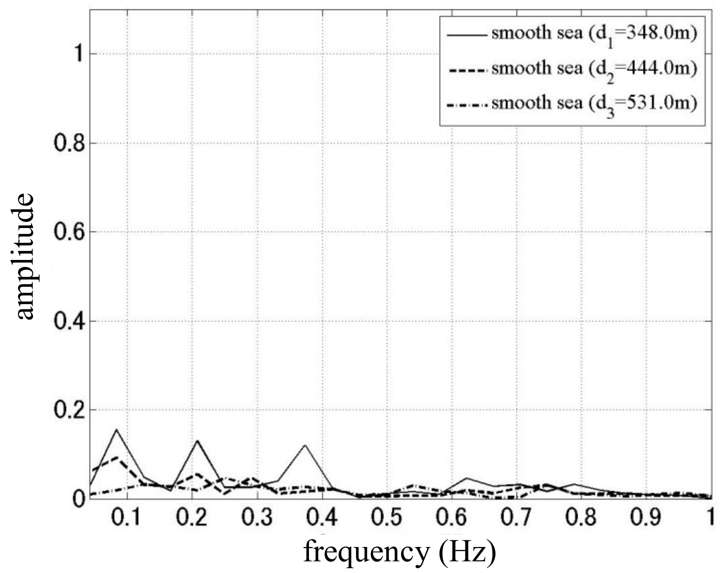

Figure 4-38 Amplitude characteristics of TKEOt (smooth).

On the other hand, the correlator and TKEO output signals for the moderate sea condition are calculated and shown in Figure 4-39. Figure 4-40 shows the top view of the aligned results of the averaged TKEO. In these figures, three horizontal distances to the antenna (vertical axis: d_1 = 348.0, d_2 =444.0 and d_3 = 531.0 meters) are selected to estimate the wave characteristics

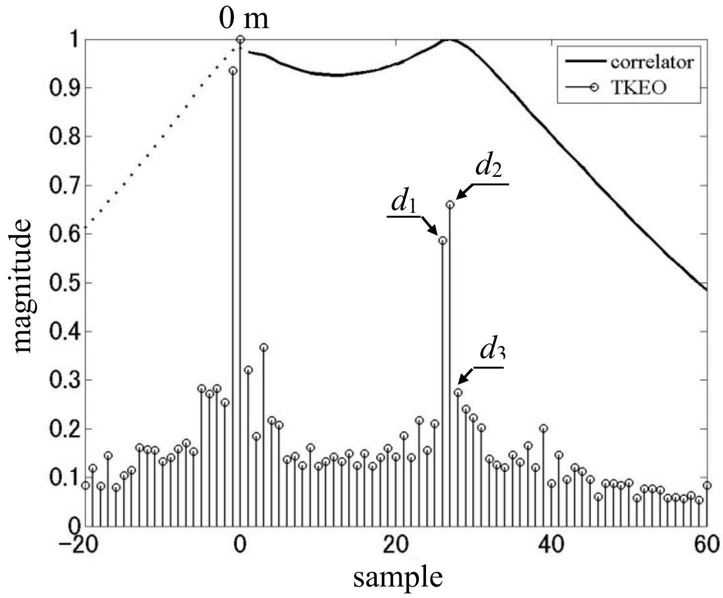

Figure 4-39 Correlator and TKEO output signals (moderate).

.

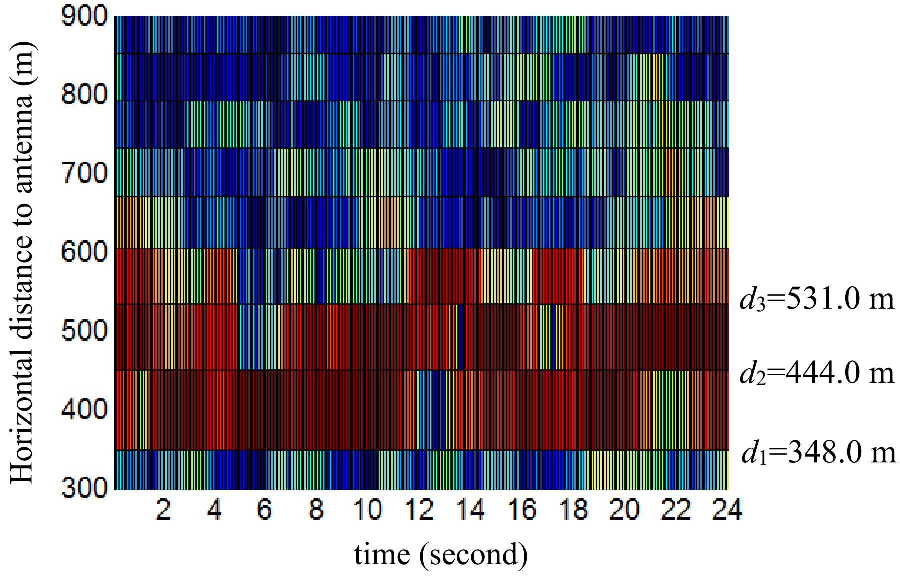

Figure 4-40 Top view of the aligned results of averaged TKEO (moderate).

Figure 4-41 shows three variation of each $TKEO_t$ along the horizontal axis in moderate sea conditions, after that the variations of three $TKEO_t$ are analyzed using the Fourier transform. Figure 4-42 shows the amplitude characteristics of the $TKEO_t$, and the remarkable frequency of the wave is f_0 = 0.083 Hz (wave period is T_S = 12.0 seconds). Figure 4-43 shows the phase characteristics of the $TKEO_t$.

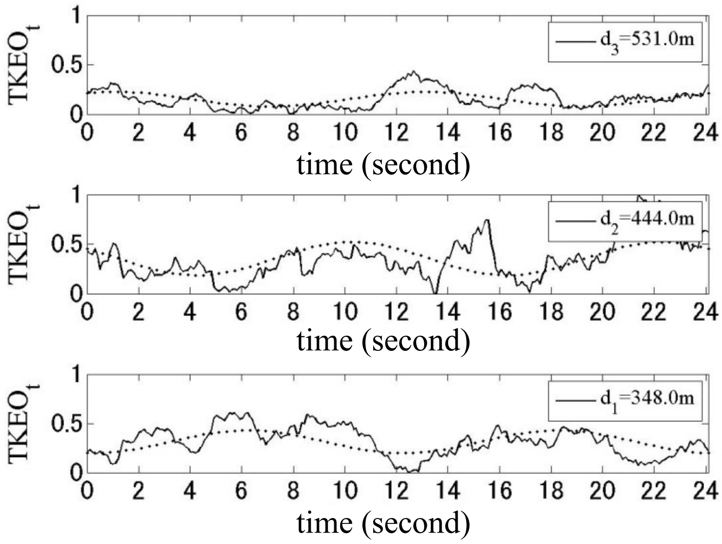

Figure 4-41 Time variations of TKEOt (moderate).

Figure 4-44 shows the phase change at three points of TKEO$_t$. In this figure, the three phase values of the TKEO$_t$ of the remarkable frequency (f_0 = 0.083Hz) are drawn with three dots and the solid line is the regression line of the three points. The gradient of this line is the wave speed (V_s = 10.6 m/s). The wavelength (λ_S) is estimated to be 127.2 meters (λ_S = 10.6 × 12.0). Moreover, the 12.0-second wave period and 114.1-meter wavelength were also calculated for the third experiment.

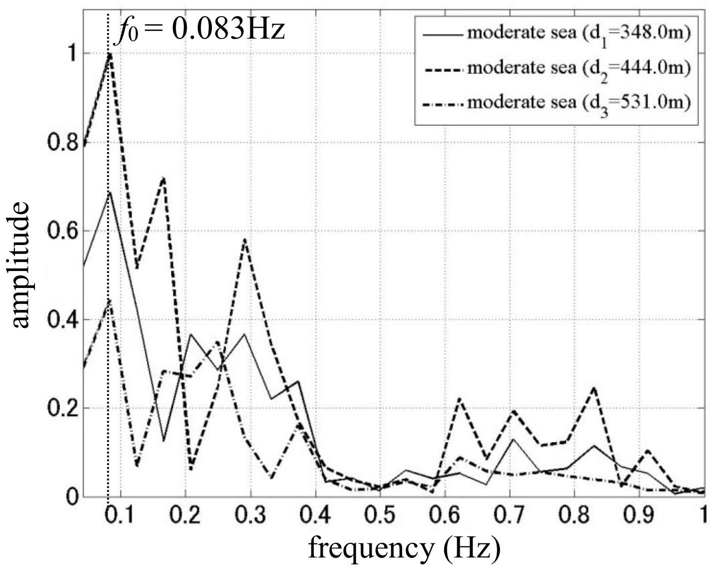

Figure 4-42 Amplitude characteristics of TKEOt (moderate).

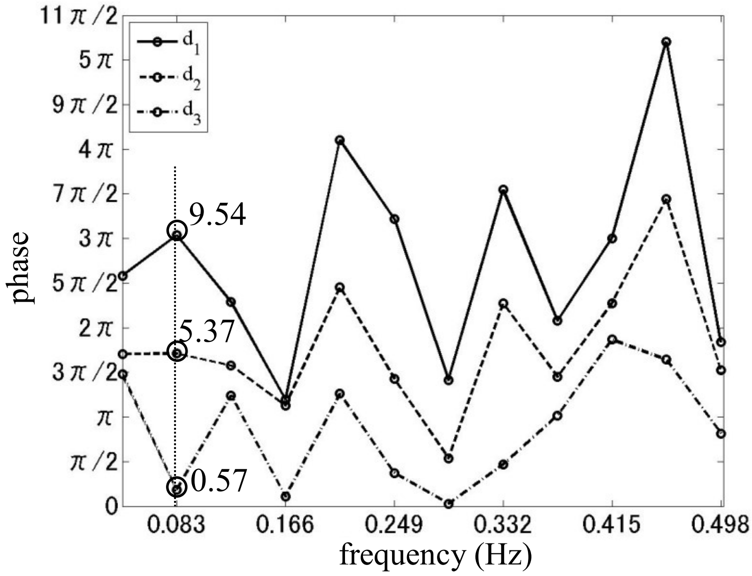

Figure 4-43 Phase characteristics of TKEOt (moderate).

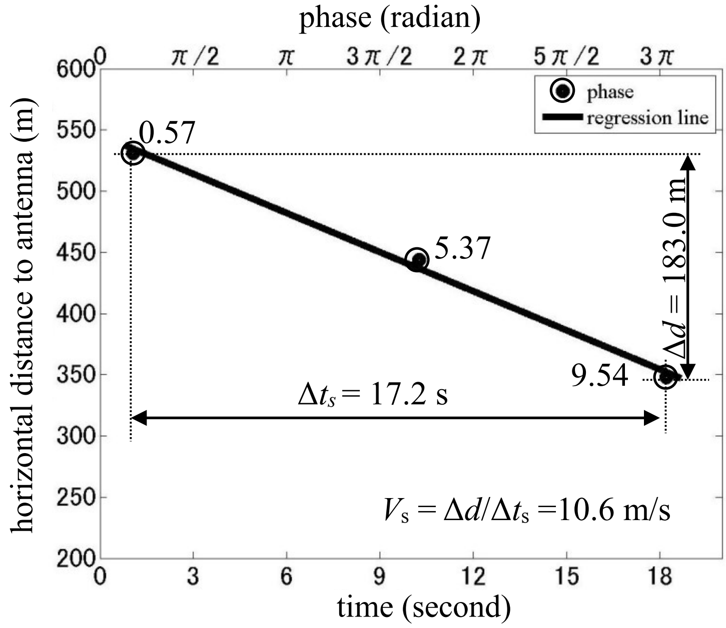

Figure 4-44 Phase change at three points of TKEOt (moderate).

On the other hand from the dispersion relation, the wave speed and wavelength can be calculated using the wave period and the depth of water. The depth of the reflected sea area is about 10 meters. Hence in the experimental results, another estimation value of the wave speed and the wavelength can be calculated from the dispersion relation. From the wave period (T_S = 12.0 seconds) and the water depth (z =10.0 meters), the wave speed (V_S) is 9.4 m/s and the wavelength (λ_S) becomes 113.2 meters.

Table 4-4 shows the experimental results for the moderate sea state. In this table, the measurement values were obtained from the video grab, the estimation values were estimated by the prototype system and the calculation values were obtained from the dispersion equation.

The prototype system estimated the wave period, wavelength and speed in values virtually consistent with the measurement values and calculation values. The measurement values are not precise enough to analyze the estimation error, but the purpose of our research was to evaluate the usefulness of the prototype system and compare it with previous simulation results. From the experimental results, it is clear that our prototype system can be used to estimate ocean wave characteristics.

Next some factors affecting the estimation values are considered. The recording time of the experiments was too short to estimate the wave period precisely; as ocean waves have a lot of frequency components, the interference between the RSFS caused errors in the measurement phase; and as the signals from the specular reflection point to the array antenna had the same relative time delays of the RSFS, the signals having the same relative time delay, interfered with each other.

Table 4-4 Experimental results for moderate sea state

Wave characteristics	Measurement from video grab	Estimation by prototype system		Calculation from dispersion relation
Experimental No.	-	2	3	-
Period [s]	11.5	12.0	12.0	-
Wavelength [m]	115.5	127.2	114.1	113.2
Speed [m/s]	10.0	10.6	9.5	9.4

References

[1] H. Mitsuyasu, "Physics of Ocean Waves", Iwanami-Shoten, 1995.

[2] U.S. Government Department of Defense, "Global Positioning System Standard Positioning Service Signal Specification", Second Edition, June 2, pp.9, 1995.

[3] R.B. Langley, "GPS Receiver System Noise", GPS World, Vol.8, No.6, April, pp.40-45, 1997.

[4] S.L. Durden and J. F. Vesecky, "A physical radar cross-section model for a wind-driven sea with swell", IEEE Journal of Oceanic Engineering, Vol.10, pp. 445-451, 1985.

[5] D. Hauser, E. Soussi, E. Thouvenot and L. Rey, "SWIMSAT: A Real-Aperture Radar to Measure Directional Spectra of Ocean Waves from Space - Main Characteristics and Performance Simulation", Atmospheric and Oceanic Technology, Vol.18, pp.421-437, 2001.

[6] H. Kuze, Y. Likuza, S.T. Akeuchi and H. Yoshimori, "Physical Principles of Remote Sensing, Second Edition", Cambridge University Press, pp.46–48, 2005.

[7] J.G. Proakis, "Digital Communications, Third Edition", McGraw-Hill Inc, 1995.

[8] Scott Gleason, Demoz G. Egziabher, "GNSS Applications and Methods", Artech House, pp.410-411, 2009.

[9] Jian Cui, Nobuyoshi Kouguchi, Shigeyuki Okuda, Yasuo Arai, "Wave Measurement System using GPS Signal", Proceedings of Asia Navigation Conference 2009.

[10] Jian Cui, Nobuyoshi Kouguchi, Akihiro Ikawa, Shigeyuki Okuda, Yasuo Arai, "Wave Remote Sensing System by GPS", Proceedings of OCEANS 2010 IEEE – Sydney, May 2010.

[11] Jian Cui, Nobuyoshi Kouguchi, "Ocean Wave Observation by GPS Signal", Proceedings of OCEANS, 2011 IEEE – Spain, Jun. 2011.

[12] Jian Cui, Nobuyoshi Kouguchi, "Evaluation Test of Local Area Remote Sensing System", Proceedings of ION GNSS 2012 – Nashville, pp.2022-2028, Sep. 2012.

CHAPTER 5

CONCLUSIONS

The ocean wave remote sensing system using the GPS signals reflected from the sea-surface was proposed in this dissertation. Its prototype was constructed and then evaluated with the numerical simulation and the coastal experiments. From the researches on the designs, constructions and evaluations of the ocean wave remote sensing system, we can draw some of the following conclusions.

The ocean wave remote sensing system was designed to make use of the RSFS to measure the characteristics of ocean wave. The system is mainly composed of the array antenna, RF front-end and wave characteristic estimator. The array antenna is utilized because it can only receive the GPS signals reflected from the objective sea-surface and suppresses others from side directions, which would become interference with same relative time delays. In the prototype system, a uniform linear array antenna with 16 patch antenna elements was constructed and its narrow fan beam directional pattern was realized. The narrow fan beam ensures that the received signals come from the objective sea-surface and the signals from side directions can be reduced greatly. In addition, the wire cloth covered on the back of the array antenna cuts off the intensity of signals from behind by about 10dB. As a necessary part of the array antenna, the pre-amplifier was mounted to improve the signal intensity to a proper level for the components of the following RF front-end.

The RF front-end converts the analogue RF signals into the IF digital ones. The band-limited effects of the RF front-end were also evaluated and then 40 MHz was chosen as the bandwidth of the RF front-end. Furthermore, 40MHz was also proven to be an appropriate bandwidth for the TKEO to identify each RSFS. For this reason, a 100 MHz ADC was used to sample the 40 MHz bandwidth signals. The 40 MHz bandwidth RF front-end is implemented with the first down-conversion stage on the chip of GP2015. The mixer outputs the signals with the center frequency of 175.42 MHz, and the digital output of the ADC has the center frequency of 24.58 MHz because of the under-sampling that occurs without any aliasing.

The modules of the wave characteristic estimator were also developed to estimate wave period, wave speed and wave length through the algorithmic combination of the correlator and TKEO. The correlator calculates the correlation between the output signal of the RF front-end and the locally generated C/A code to indicate the RSFS, and the TKEO is applied to the output of the correlator to identify each RSFS clearly. The Doppler shift of the objective satellite and the precise arrival time of LOS provided by the software receiver are the information necessary to calculate the correlation efficiently and accumulate the correlator outputs along the correct reference time respectively. The wave period is estimated from the amplitude characteristics of the TKEO time signal and the wave speed is estimated from its phase characteristics, which are processed with the FFT quantitatively.

The prototype system is evaluated with the numerical simulation and the costal experiments. The numerical simulation showed the reasonableness of the ocean wave remote sensing system system and its measurement method, and the estimation results of the costal experiments showed that the prototype could receive the RSFS and estimated the wave period and wavelength in the direction of the array antenna. The measurement from video grab, the estimation by prototype system and the calculation from dispersion relation are fairly consistent with each other. It should be emphasized that the experiments can be performed under conditions of bad weather and low visibility.

In the experimental evaluations, we were able to apply the constructed prototype system to estimate the wave period, wave speed and wavelength of sea swells successfully. The successful measurements also provide the possibility to measure the characteristics of long period gravity wave. And furthermore, the performance of the ocean wave remote sensing system can be improved if some considerations and proposals are implemented in the future research; these are described as follows:

(1) Distance resolution

The distance resolution on the objective sea-surface is related to the sampling frequency of RF front-end. This means that the propagation distance between two adjacent TKEO time signals is shortened if the sampling frequency is increased. Therefore, the resolution of the distance scale of the ocean wave remote sensing system is increased by broadening the bandwidths of the array antenna pre-amplifier and the RF front-end amplifier, and then by raising the sampling frequency of the A/D converter in RF front-end.

(2) Time resolution

The continuous outputs of TKEO have to be averaged over a certain time to increase the CN0. The averaging time is equal to the time resolution. If the CN0 is increased by using a more suitable amplifier, correspondingly the averaging time will be reduced so that the resolution of time scale can be increased.

(3) Frequency resolution

In the experimental evaluations of the prototype system, as the recording time was set to 24 seconds, the resolution of frequency scale was limited to 1/24 Hz. Accordingly by making the recording time 60 seconds, the resolution of frequency scale can be improved up to 1/60 Hz.

(4) Undesired signal

At the same distance from the border of the specular reflection point, the close range area and the long range area have the same delay time to the LOS signal. The reflected signals from the close range area contaminate the reflected signals from the long rage area. If the reflected signals from the close range area can be attenuated or removed, the interference from the close range area will be reduced greatly. In the future, the undesired signals reflected from close range area could be suppressed by connecting several sets of array antennae vertically to reduce the vertical beam-width.

(5) Wave height

The wave height isn't discussed in this dissertation. In the next step, wave height will be obtained using the amplitude frequency characteristics of the TKEO from pre-simulation and comparing the pre-simulation results with the experimental results. In order to compare the estimated wave height with the actual wave height more precise measurements will be required.

(6) Comparative wave characteristics

Because the comparative wave characteristics were measured by means of a video grab taken near the coast, the accuracy of them was less than perfect. In the near future, the GPS buoys will be used to measure more accurately the wave characteristics, and the accuracy of the comparative wave characteristics will be dramatically improved. The performance of the ocean wave remote sensing system can be verified by comparing it with the measurement results of GPS buoy system.

(7) True wave characteristics

The measurement of true wave characteristics will be conducted in a future study. According to the methods discussed in chapter 2, the true wave characteristics can be measured with double systems double directions or single system double directions. In particularly, the true values of the wave length and the wave speed can be obtained.